

# **Development of Fabrication Process Using Suspension and Solution Plasma Spray for Titanium Oxide Photovoltaic Device**

Hsain Sagr

A Thesis

in

Information Science and Manufacturing Engineering,  
Graduate School of Engineering

Presented in Partial Fulfilment of the Requirements for the  
Degree of Doctor of Philosophy at Ashikaga University  
Japan

March 2019

## **Abstract**

The following study, using four experiments, examines new ways for coating efficiency specifically concerning cost-effectiveness. The first experiment involved the deposition of photocatalytic TiO<sub>2</sub> film with low power atmospheric suspension plasma spraying using Ar/N<sub>2</sub> working gas. As the photocatalytic titanium oxide film deposition process, thermal spray is hoped to be utilized practically since it is relatively easy to deposit anatase rich films. However, because of its high equipment and feedstock power costs, it is very difficult to introduce thermal spray equipment into small companies. In this study, to develop a low cost thermal spray system, what is examined is low power atmospheric suspension plasma spray equipment using titanium hydroxide suspension created by hydrolysis of titanium tetra iso butoxide using Ar, N<sub>2</sub> as working gas. For avoiding sedimentation of the hydroxide particles in the suspension, mechanical milling of the suspension was conducted (to create colloidal suspension) before using it as feedstock. Moreover, the new designed ultrasonic wave container was used to keep the suspension particles moving while the spray process was conducted after the film deposition, as for the coating, anatase rich TiO<sub>2</sub> film could be obtained. For characterization of the film, microstructure observation by an optical microscope, and X-ray diffraction was carried out. Consequently, by creation of colloidal suspension, deposition could be conducted without sedimentation of the hydroxide particle in the suspension during operation. It was proved the film had enough photocatalytic property to decolor methylene-blue droplet. The second experiment looked at the design and optimization of an ultrasonic atomization plasma spray system for coating photocatalytic TiO<sub>2</sub> thin films. Ultrasonic atomization plasma spray system (UAPSS) was designed to provide a systematic and cost-effective mechanism which is capable of depositing nanoparticles and TiO<sub>2</sub> thin films

with consistent crystalline structure and stoichiometry. The common atomization techniques for feedstock feeding, which use pressure in order to generate feedstock mist, generally produce drops over 100 times more than the atomization technique using ultrasonic. UAPSS seeks to fulfill the need for more precise control of structural, morphological, and optical properties of TiO<sub>2</sub> thin films. In the experiment, an ultrasonic atomizer set to a frequency of 1.7MHz was used to atomize the starting material, ethanol titanium tetrabutoxide. The carrier gas was Ar and its flow rate was 1.6 L/min. The working gas was Argon, and its flow rate was 5 L/min. Deposition distance was varied from 20 to 100 mm and spray time was 15 minutes. TiO<sub>2</sub> thin film included rutile and anatase was deposited. Methylene blue decolorization testing suggests that the deposited TiO<sub>2</sub> film has effective photo-catalytic properties. The third experiment looked at the deposition of photocatalytic TiO<sub>2</sub> film with a new design of ultrasonic atomization plasma spray using Ar working and carrier gas. In the experiment, an ultrasonic atomizer set to a frequency of 1.7MHz was used to atomize the starting material, ethanol titanium tetrabutoxide. The carrier gas was Ar and its flow rate was 1.6 L/min. The working gas was Argon, and its flow rate was 3.4 L/min. Deposition distance was varied from 20 to 100 mm and spray time was 15 minutes. TiO<sub>2</sub> thin film included rutile and anatase was deposited. Methylene blue decolorization testing suggests that the deposited TiO<sub>2</sub> film has effective photo-catalytic properties. The deposited films featured a columnar structural morphology. The final experiment looked at the disposition of photocatalytic TiO<sub>2</sub> film with a new design of ultrasonic atomization plasma spray using Ar working and N<sub>2</sub> carrier gas. In the fourth experiment, an ultrasonic atomizer set to a frequency of 1.7MHz was used to atomize the starting material, ethanol titanium tetrabutoxide. The carrier gas was N<sub>2</sub>, and its flow rate was 1 L/min. The working gas was Argon, and its flow rate was 5 L/min. Deposition distance was varied from 20 to 150 mm and spray time was 20 minutes. TiO<sub>2</sub> thin film included

rutile and anatase was deposited. Methylene blue decolorization testing suggests that the deposited TiO<sub>2</sub> film has effective photo-catalytic properties. In the second, third, and fourth studies, the deposited films featured a columnar, porous structural morphology. From these results in all three studies, the newly designed ultrasonic atomization plasma spray system seems to be highly promising for the rapid fabrication of functional thin films. All show photo-catalytic properties are present. The use of these new coating efficiencies prove to be a sustainable and cost-effective measure.

*To my devoted mother and the eternal soul of my father*

## **ACKNOWLEDGEMENTS**

Foremost, I thank Almighty Allah for bringing me this far in my education. This project would not have been possible without Him.

I would also like to express my special appreciation to my Supervisor, Professor Dr. Yasutaka Ando for guiding me. His patience, advice and motivation have been very helpful to me.

My Sincere gratitude also goes to Professor Dr. Sakurai Yasuo who offered valuable suggestions.

Last but not least, my deepest thanks go to my father, mother, wife, siblings and children who have played wonderful roles in my life.

## Table of Contents

<i>Abstract</i>	<i>i</i>
<b>ACKNOWLEDGEMENTS</b>	<b>v</b>
<b>CHAPTER 1 Introduction</b>	<b>1</b>
1.1. Background of this study	1
1.2. Motivation for thesis work	5
1.3 Literature Review	7
1.3.1 <i>Suspension plasma spray (SPS)</i>	7
1.3.2 <i>Solution Precursor Plasma Spray (SPPS)</i>	8
1.3.3 <i>Photovoltaic device</i>	8
1.3.4 <i>Atmospheric plasma spray</i>	10
<b>CHAPTER 2 Design of Suspension and Solution Plasma Spray feedstock feeder parameters</b>	<b>13</b>
2.1 SPS Design Parameters	13
2.1.1 <i>Introduction</i>	13
2.1.2 <i>The Mechanism of The SPS Feeder</i>	15
2.1.3 <i>SPS Feeder Design Concept and Sketch</i>	19
2.1.4 <i>Mechanical Components Drawing and Dimensions</i>	23
2.2 Ultrasonic Atomization Plasma Spray System UAPSS Design Parameters	31
2.2.1 <i>Introduction</i>	31
2.2.3 <i>The Mechanism of The UAPSS Feeder</i>	34
2.3 Design analysis parameters	35
2.3.1 <i>Inlet carrier gas flow parameters</i>	35
2.3.2 <i>The output of inlet carrier gas</i>	40
2.3.3 <i>The flow between station A and station B for design</i>	43
2.3.4 <i>Characteristics of flow in the UAPSS and gases mixing point</i>	52
2.4 UAPSS Feeder Mechanical Components Drawing and Dimensions	54
<b>CHAPTER 3 Development of a Fabrication Process Using Suspension Plasma Spray for Titanium Oxide Photovoltaic Device</b>	<b>71</b>
3.1 Introduction	71
3.2 Experimental Procedure	72
3.2.1 <i>Method</i>	72
3.2.2 <i>plasma spray parameter</i>	76

3.2.3 <i>Suspension Preparation</i>	77
3.2.4 <i>Injection Method</i>	78
3.3 Results and Discussion	79
3.3.1 <i>SPS Titanium Oxide Film</i>	79
3.3.2 <i>Photocatalytic Activity of TiO<sub>2</sub> Coating</i>	82
3.4 Conclusions	84
<b>CHAPTER 4 Deposition of photo-catalytic TiO<sub>2</sub> film by low power atmospheric suspension plasma spray using Ar/N<sub>2</sub> working gas</b>	<b>85</b>
4.1 Introduction	85
4.2 Materials and Methods	86
4.3 Results	91
4.4 Conclusions	96
<b>CHAPTER 5 Design and Optimization of Ultrasonic Atomization Plasma Spray System for Coating Photo-Catalytic TiO<sub>2</sub> Thin Films</b>	<b>97</b>
5.1 Introduction	97
5.2 Experimental	99
5.3 Conclusion	109
<b>CHAPTER 6 Summary and Conclusion</b>	<b>110</b>
<b>References</b>	<b>112</b>

# CHAPTER 1:

## State of the Question and Literary Review

### 1. Introduction

#### 1.1 Background of this study

Within recent years, nanostructured materials have been an important consideration in the development of various engineering applications, leading to targeted development of materials with desirable mechanical properties such as strength and hardness. Nanostructured materials are chiefly created using a fine microstructure, created by depositing small melted particles onto a substrate. Cobalt ferrites, with particle size less than 10 nm, are of interest due to their magnetic and structural properties [1].

Research has shown that many of the unique material properties of nanostructured materials are based in the large volume ratio of internal surfaces. Several methods are used to produce nanoscale coatings (thickness less than 2  $\mu\text{m}$ ) beginning with a gas phase, including reactive magnetron sputtering [2], chemical vapor deposition (CVD) [3], plasma-assisted thermal CVD [4], and hypersonic plasma particle deposition [5]. For thick coatings (thickness greater than 100  $\mu\text{m}$ ), many studies have documented the thermal spray deposition of agglomerated nanoparticles. These particles are in a mushy state at impact [6] or are made of materials with different melting points such as  $\text{TiO}_2$ , and  $\text{Al}_2\text{O}_3$  [7]. The mechanical techniques of spraying, spinning, dipping and draining, flow coating, roller coating, pressure-curtain coating, brushing, and offset printing of reagent solutions [8] are used for depositing coatings from liquid media that are subsequently reacted chemically to form the inorganic thin film product. Chemical reaction of the coating residue, often by thermal oxidation, hydrolysis, or pyrolysis (in the case of

metalorganics) produces the desired solid film. Spin-on deposition of film-forming solutions is widely used in solid-state technology. Liquid spray coating is probably the most versatile mechanical coating technique of the deposition techniques noted, and it is particularly well-suited for high-speed automated mass production. Deposition of very thin films is possible by judicious selection and optimization of spray machine parameters for forming “atomized” droplets and the reagent and solvent systems used to formulate the spray liquid [9]. Suspension and solution thermal spraying technology, an attractive technique in coating technology, has been used for depositing nanostructured coatings. It is technically difficult to feed powders of particle size less than 10 – 5 um due to the effect of surface forces on powder flow. In the newly developed suspension plasma spray (SPS) process, nanosized particles are suspended in a liquid before being injected into the plasma plume, thus circumventing the normal feeding methods, similarly, the solution precursor plasma spray (SPPS) process deposits melted feedstock onto a substrate as splats. The difference between SPPS and SPS processes is the nature of the feedstock material. The SPPS and SPS methods combine the simplicity and high throughput of the plasma spray process with the versatility and economics of the spray pyrolysis process to produce the desired nanostructured materials [10]. In the SPPS process, metal salt complexes are dissolved in a water / organic solvent to form a liquid solution, whereas in the SPS process, metal powders are dispersed in a water / organic solvent to form a powder suspension. Moreover, in SPPS, the coating is produced directly from a solution precursor and all physical and chemical reactions, such as evaporation, decomposition, crystallization and coating formation, occur in a single step [11]. The coating is built up by the overlapping and stacking of layers deposited in each pass of the plasma torch.

Photovoltaic and dye-sensitized solar technology both need the application of liquids and coatings during the manufacturing process. As most of these substances are very expensive, any

losses due to over-spray or quality control are minimized with the use in this study of new designed ultrasonic feeding system. In efforts to reduce the manufacturing costs of solar cell, control only a few millimeters of expensive catalyst material (flow rate range) The mist resulting from ultrasonic treatment is most commonly used in fuel cell coating application, highly porous and homogeneous coating, efficient combustion and particles heating, control of drop size, and control of particle velocities. In addition to using air, it is possible to use various carrier gasses. Moreover, the air atomizing spray method has disadvantages such as agglomerates of catalyst in air spray droplets, Fig.1, the nanoparticles remain agglomerated, and difficulty of control expensive catalyst material.

The morphology, crystalline structure, structural properties, optical properties, electronic properties, and stoichiometry of TiO<sub>2</sub> NPs and TFs have very sensitive deposition conditions. This is an inherent disadvantage for many physical vapor deposition methods [11, 12] such as laser ablation, where there are large variations in the optical and structural properties of the synthesized NPs and TFs [13]. These variations in NPs properties arise from small changes in the deposition conditions, which are a key challenge in the development of techniques for the production of TiO<sub>2</sub> NPs and TFs at a large industrial scale. The newly-designed ultrasonic plasma sprayer offers a way to keep the deposition system as simple as possible while keeping costs at a minimum and maximizing throughput. The conventional deposition method of titanium oxide thin film for the photocatalytic application (anatase-TiO<sub>2</sub>, etc.) can be deposited by various deposition techniques such as sputtering, CVD, MOCVD, spray pyrolysis, and sol-gel process. However, there are several engineering problems associated with these deposition processes such as low deposition rate, high deposition time, and requirement of special and costly equipment, such as vacuum equipment. The sol-gel process is further hampered by the difficulty of thick film deposition due to break down by internal stress occurring during deposition. One approach to improving the cost

and deposition time, low deposition rate, high starting material powder cost, and ability to control film's structure and makeup is to use suspension plasma spray to deposit titanium oxide film. Moreover, produce a design work with the suspension, precursor plasma spray equipment. The Photovoltaic and dye-sensitized solar technology both require the application of liquids and coatings during the manufacturing process. With most of these substances being very expensive, any losses due to over-spray or quality control problems are minimized with the use of this newly designed ultrasonic feeding system. In an effort to reduce the manufacturing costs of solar cells, by controlling as little as a few millimeters of expensive catalyst material (flow rate range), the mist resulting from ultrasonic vibration can be most commonly used in fuel cell coating applications. It provides highly porous and homogeneous coating, efficient combustion and particle heating, controllable drop size, controllable particle velocities and the possibility of using several different gases instead of air as carrier Gas. On the other hand, the air atomizing spray method has disadvantages such as agglomerates of the catalyst in spray droplets. Nanoparticles remain agglomerated, and there is difficulty controlling the expensive catalyst material. Plasma spraying has been widely used as high rate thick film deposition process in the atmosphere environment. In the plasma spraying, feedstock powders are melted and accelerated by a plasma jet towards a substrate. Upon impact with the substrate, the molten particles flatten and solidify to form "splats". However, development of a high rate film deposition method using simple equipment such as suspension plasma spray. Hence, photocatalytic titanium oxide film deposition by atmospheric suspension plasma spray using titanium tetra iso butoxide (TTIB,  $\text{Ti}(\text{OC}_4\text{H}_9)_4$ ) as feedstock was carried out. On the other hand, high starting material powder cost such as use ethanol as a diluted titanium butoxide to raise the temperature of the combustion flame to use it as a liquid feedstock for this deposition processes the high ingredient powder cost need to be solved in this

study.

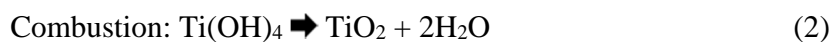
## **1.2 Motivation for thesis work**

Titanium oxide thin film for photocatalytic application (anatase-TiO<sub>2</sub>, etc.) [14] is typically deposited using several deposition techniques such as sputtering, CVD, MOCVD, spray pyrolysis, and sol-gel process. However, there are several engineering problems associated with these deposition processes such as low deposition rate, deposition time, and requirement of special and costly equipment, such as vacuum equipment [15]. The sol-gel process is further hampered by the difficulty of thick film deposition due to break down by internal stress occurring during deposition [16]. One approach to improve the cost, deposition time, low deposition rate, high starting material powder cost, and ability to control the film's structure and makeup is to use various spraying techniques that are more compatible with the data and can better address the engineering problems. The creation of outputs that correspond to the problems of sedimentation for suspend particles in case of suspension and the precise control of the stoichiometry of precursor's solutions prepared by wet chemistry method need to be investigate , Moreover need for precise control of structural, morphological, and optical properties methods for depositing titanium dioxide, as a thin films, and the control only a few millimeters of expensive catalyst material (flow rate range) during the deposition process. In addition, reduce cost of equipment that used to deposition materials by spray plasma need for deposited TiO<sub>2</sub> thin films that produced in a single-step route without the need for laborious, expensive purification and excessive annealing procedures. On the other hand, need for full and accurate control of the deposition process.

Plasma spraying has been widely used as a high rate thick film deposition process in atmospheric environment [17], difficulty of film component and structure control and high

ingredient powder or/and solution precursor cost need to be solved in this study.

In the plasma spraying, feedstock powders are melted and accelerated by a plasma jet towards a substrate. Upon impact on the substrate, the molten particles flatten and solidify to form “splats”. However, development of high rate film deposition method using simple equipment such as suspension plasma spray, solution precursor plasma spray (SPPS). Hence, photocatalytic titanium oxide film deposition by atmospheric suspension plasma spray, solution precursor plasma spray, using TTIB as feedstock was carried out. On the other hand, high starting material powder cost such as use ethanol as a diluted TTIB to raise the temperature of the combustion flame to use it as a Liquid Feedstock for this deposition processes, the high ingredient powder cost needs to be solved in this study [18]. Though, ethanol has solvent properties is a versatile solvent, miscible with water and with TTIB. In order to solve the problem is to use a starting material without ethanol and use only distilled water. In this process, the reaction between the alkoxide precursor and the desired amount of water occurred in an anhydrous alcohol medium. The hydrolysis and condensation reactions can be summarized as follows:



However, the liquid feedstock starting material ( $\text{Ti(OH)}_4$  hydroxide) preparation was difficult to make it distribution mixture because its particles is un-dispersant, therefore if the particles are large enough, then their dynamic behavior in any given period of time in suspension would be governed by forces of gravity and sedimentation. Therefore, resulting in difficulty atomization and then deposition. Consequently, Was conducted Mixing process using simple equipment In order to distribute the material in the mixture and reduce the particles size has been

successfully done, and it can be deposited on the substrate using suspension plasma spray, and different spray parameter.

To the authors` knowledge, no studies on the deposition of TiO<sub>2</sub> which starting material Ti(OH)<sub>4</sub> hydroxide by suspension plasma spray have been reported in the literature. These observations and requirements motivate the work presented in this thesis.

## **1.3 Literature Review**

### **1.3.1 Suspension plasma spray (SPS)**

SPS consists of the injection of a liquid carrier containing the suspended solid powders into the plasma jet. Therefore, particles must be properly dispersed to provide a stable suspension without excessive agglomeration or settlement, or both. This is achieved with the help of appropriate dispersant and using milling processes before and mixing during the injection process to prevent overly enlarged agglomerates and to break them up if formed. A novel technology, called suspension plasma spray (SPS), was developed for the production of ceramic powders. This technique reduces the time and energy [19]. (Suspension plasma spraying: SPS). The nanometer-sized particles are dispersed into the liquid phase by means of dispersants: the suspension is then injected either as a liquid stream or as drops after nebulization. Depending upon the injection and plasma jet conditions, the liquid stream or droplets are fragmented due to flow shear forces and vaporized. Plasma spray coatings from liquid feedstock have generated numerous new scientific articles and conference contributions, particularly during the last 6-7 years. All these works are based on results that emerged in the late-1990s making it possible to manufacture nanostructured thick (from about ten to hundred micrometers) coatings exhibiting numerous unique properties, such as good thermal insulation and resistance to thermal shock, excellent wear resistance and improved catalytic behavior. The two processes used are:

- 1) Suspension thermal spraying with feedstock made of nanometer- or sub-micrometer sized particles in suspension;
- 2) Liquid precursor thermal spraying with feedstock made of a solution.

### **1.3.2 Solution Precursor Plasma Spray (SPPS)**

Karthikeyan was the first to publish on using a solution precursor [20-22]. This early work served as a proof-of-concept for the solution precursor, but well-adhered coatings were still not able to be formed. Research continued, and in 2001 a refined process was published that could produce thermal barrier coatings [23], YAG films [24], and silicon ceramic coatings [25]. Research on the technology has continued and grown, with the University of Connecticut and Inframat Corporation leading much of it. The resulting SPPS is a thermal spray process where a feedstock solution is heated before being deposited. Basic properties of the process are fundamentally similar to other plasma spraying processes. However, instead of injecting a powder into the plasma plume, a liquid precursor is used. The benefits of utilizing the SPPS process include the ability to create unique nanometer-sized microstructures without the injection feed problems normally associated with powder systems, as well as flexible, rapid exploration of novel precursor compositions. Solution precursor plasma spray is a coating deposition process that uses conventional plasma spray equipment and solution precursors rather than ceramic or metal powders as starting materials.

### **1.2.3 Photovoltaic device**

Following the decision of oil crisis to stop the flow of oil to the West during the 1973 oil embargo, there was unrest in the West as the price of oil increased and a shocking picture of the Prime Minister of Belgium riding a bicycle to his office appeared in many newspapers around the world. This instigated the search for an alternative source of energy. Western scientists therefore concluded that the best alternative is renewable energy [26].

Conventional energy sources based on oil, coal, and natural gas have proven to be highly effective deliverers of economic progress, but at the same time damaging to the environment and to human health. Furthermore, they tend to be cyclical in nature, due to the effects of oligopolies in production and distribution. These traditional fossil fuel-based energy sources are facing increasing pressure along a host of environmental fronts. Perhaps the most serious challenge is to supply modern energy services to more than 2 billion people who lack access to electricity and still use traditional solid fuels [27]. This challenge may even be one of the most pressing problems facing humanity today [28]. Therefore, power generation systems using renewable energy such as concentrating solar power, hydropower, geothermal, wind power, solar cells, and so on have been studied at length.

Thin film coatings are used to protect photovoltaic devices such as solar cells, which are a key renewable energy source and part of a quickly-growing renewable energy industry. Although silicon has been mainly used in solar cells there are two types of silicon photovoltaic cells: bulk types with required film thickness of 200  $\mu\text{m}$ , and amorphous silicon photovoltaic cells with required film thickness of 0.001  $\mu\text{m}$ . Amorphous silicon is produced by depositing silicon thin film onto substrate. While the cost is lower compared to crystalline types because less silicon is used, even in this process the fabrication cost is still high [29,31].

Another type of photovoltaic device is the dye-sensitized solar cell (DSSC). Dye-sensitized solar cell (DSSC) is the third generation of solar cell which was developed by O` Regan and Gratzel in 1991 [32]. Dye-sensitized solar cell without using silicon has been spotlighted recently. The dye-sensitized solar cell consists of transparent electrodes, a photovoltaic device, electrolytes, and catalytic electroconductive electrodes like platinum and/or carbon [29]. The advantages of DSSC are that it can be engineered into flexible sheets, low cost of sensitization material

production, ease of fabrication and low process temperature. Due to the low cost of the overall production of DSSC, it has been expected that the DSSC type of solar cell will give a higher return of investment (ROI) when compared to Siliconbased solar cell (Si-SC) [31].

In DSSC, titanium oxide anatase is the primary type used as a photovoltaic device. The importance of  $\text{TiO}_2$  as a photocatalytic material was discovered by Fujishima and Honda in 1972 [32].

In the photocatalytic process  $\text{TiO}_2$  is activated by illumination with (UV) light having an energy higher than the band gap. Given a band gap of  $E_g = 3.2$  eV for anatase and 3.0 eV for rutile.

$\text{TiO}_2$  has several naturally occurring modifications, the most common ones being rutile, anatase and brookite [33]. Titanium oxide also has been widely used in various industries. As for the utility,  $\text{TiO}_2$  has been used for not only insulator and paints but also antibacterial coat [9].  $\text{TiO}_2$  is almost the only material suitable of industrial use at present ,and also probably in the future. This is because  $\text{TiO}_2$  has the most efficient photoactivity, the highest stability and the lowest cost.  $\text{TiO}_2$  used as a photo-catalyst was only anatase type with large band gap.

One of the important goals of current solar cell research and manufacturing is to simplify processing steps (this reduces fabrication costs and increases the yield) and reduce equipment costs [30]. On DSSC, the electric power conversion efficiency can be raised to 30% [29].

#### **1.2.4 Atmospheric plasma spray**

The torch for plasma spraying is based on the Gerdien-type plasma generator (Gerdien and Lotz, 1922). The process of spraying with the use of a plasma has been patented by Gage et al. (1962), as well as by Giannini and Ducati (1960). [34] The plasma generator, depicted in Fig. 1.1, consists of a circular anode, [34] usually of copper, and a cathode of thoriated tungsten [35]. The

cathode is made of graphite in a water-stabilized torch. The electric arc discharge, supported by a generator through the connectors [36, 37] heats up the working gases [38], which expand in the atmosphere, forming a jet. The powder suspended in a carrier gas, is injected into the jet. The particles of the powder after being melted and accelerated in the jet impact the substrate and form the coating. Fig. 1.2 shows a commercial plasma torch installed onto a robot arm. Atmospheric plasma spray is the most versatile of all thermal spray processes. Using an electric arc to ionize flowing process gases, the hot gas stream can be controlled to melt a very wide range of powder feedstock materials to apply high-quality coatings of metals, metallic alloys, carbides, cermets, and oxide ceramics. Atmospheric plasma spray coatings are used for many different applications, just a few of which include bond coats, corrosion coatings for many different service environments and temperatures, wear coatings, restoration coatings, and thermal barrier materials.

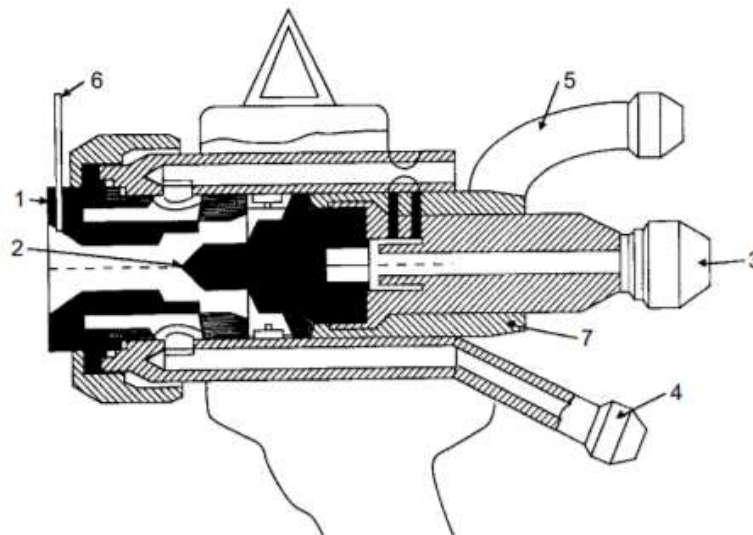


**Figure 1.1** Schematic of a section of a plasma torch: (1) anode; (2) cathode; (3) water outlet and cathode connector; (4) water inlet and anode connector; (5) inlet for working gases; (6) powder injector; (7) electrical insulator<sup>1</sup>.

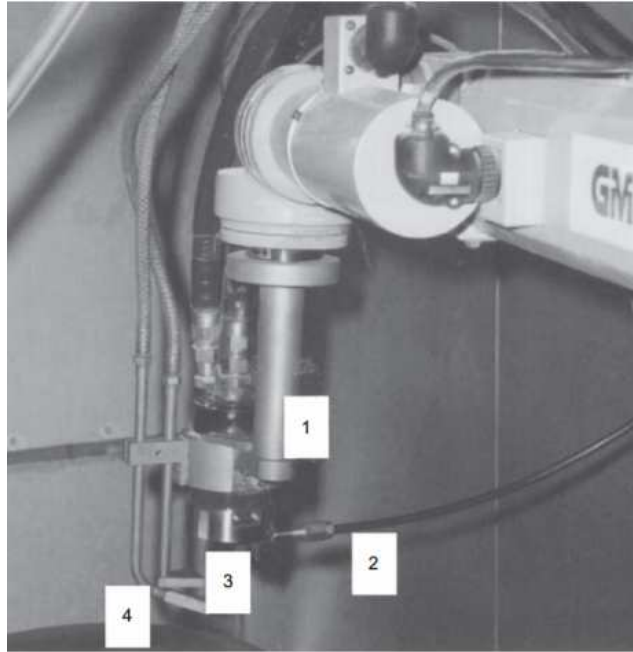


**Figure 1.2** A modern plasma torch installed on a robot: (1) torch; (2) compressedair barrier; (3) compressed-air cooling; (4) powder injector (Pawlowski et al., 1991). Plasma torch installed in The Monash University, Melbourne, Australia.

# **CHAPTER 2:**

## **Design of Suspension and Solution Plasma Spray feedstock feeder parameters**

### **2.1 SPS Design Parameters**

#### **2.1.1 Introduction**

Thermal spray feedstock is discussed with attention to the quality of the coatings and components. The technological aspects, phases identified, and parameter optimization for each thermal spray process differ with various alloys. Suspensions consist of solid particles dispersed in a liquid medium. In coating applications, these are particles of the coating material to be deposited. The liquid medium's function is to carry the particles from a feed hopper to the torch. Suspensions for coating applications must have a high degree of consistency to ensure stable and repeatable deposition rates, efficiencies, and physical properties. Suspension consistency is difficult to establish because suspensions are inherently unstable unless certain measures are taken. Particles have a natural tendency to settle and stick together forming larger clusters or agglomerates (Fig 2.1). This behavior is detrimental to the operation of the liquid feed equipment and hinders the achievement of stable and repeatable material flow. For flow to be useful, the particles in the suspension must be well-dispersed and homogeneous throughout the coating operation. Although the stirring agitator in the liquid feed hopper assists in mixing, the suspension itself must be designed to resist settling and agglomeration. Particles as liquid suspensions used for coatings mostly range in size from a few microns down to 0.01 microns, or 10 nanometers. The suspended particles settle over time, which is called sedimentation. While smaller particles do not

settle as expeditiously as larger particles, they tend to stick together more readily due to electrostatic attraction, thence forming agglomerates. These clustered particles sediment in the same way that large single particles do. Sedimented particles are problematic for spray processes because they can clog the narrow orifices in the suspension feeder. Suspension and liquid feed systems must work together in an overall design to produce coatings with repeatable characteristics. This study develops suspensions that are optimized in performance for the prototype liquid feed equipment and achieve the desired properties for the micro- and nanoscale structures of the functional layers produced. In an ideal suspension, the particles are fully separated, or dispersed, in the liquid. If the particles are small and separated, the sedimentation process is much slower. The problems are dealt with in previous research where agglomeration is counteracted by a combination of chemical and mechanical processes:

- The agglomerates are pulled apart in the liquid through various types of high-energy mixing.
- The particles are treated in order to prevent them from sticking together.

This is commonly achieved using a class of chemical compounds called dispersants. Solid particles attract each other. For this reason, energy is needed to separate the particles from each other in the second step of the dispersion process. Also, solid particles must be stabilized after they have been separated from each other. The particles will move to each other and glue together again when particle-particle repulsion is insufficient. The spontaneous process of gluing together of solid particles in a liquid is called flocculation. The function of a dispersant is to prevent flocculation. Dispersants do their job because the molecules adsorb on the solid-liquid interface and assure repulsion between the particles. One example is the use of a dispersant that imparts either a positive or a negative surface charge to the particles to keep them separated through electrostatic repulsion. Well-dispersed suspensions also benefit from reduced viscosity, which allows them to flow more

easily in a pressurized feed system.

In this study, in order to avoid sedimentation of the hydroxide particles in the suspension, mechanical milling of the suspension was conducted to create an ideal suspension before using it as feedstock. A new ultrasonic wave container was designed to keep the suspension particles fully separated, or dispersed, in the liquid while the spray process occurs. One of the challenges of this research was the problem of TiO<sub>2</sub> particles settling to the bottom of the spray hopper during spraying. The settling particles had a strong tendency to clog inside of the external sprayer nozzle and reduce the quality of the coating achieved or even stop the spray entirely. In order to eliminate clogging, a new ultrasonic container feeder was developed to thoroughly suspend TiO<sub>2</sub> particles, which could be used while spraying (Fig 2.6). The new feeder is designed to ensure high efficiency and performance during spraying where the design works by low-energy input power (30 W) and a simple fabrication process and design. This new system of using ultrasonic waves to spray the suspension particles to the plasma jet proved successful in creating high-quality photocatalytic film coatings.

### **2.1.2 The Mechanism of The SPS Feeder**

The mechanism of the feeder works when an ultrasonic wave travels through a fluid, the phenomenon of attenuation results from several mechanisms of absorption. At the beginning of the propagation, the absorption is mainly due to the viscosity of the liquid since the thermal agitation did not have enough time to exert its influence. Each layer of the fluid tends to slow down the displacement of the adjacent layers causing thus the damping of the wave as it penetrates into the fluid. Besides viscosity, there is appearance of the conduction thermal phenomenon which results from the heat transfer between the regions of dilatation and compression. The wave

propagation causes a thermal agitation within the fluid characterized by the collisions of the atoms. and raise the thermal energy of the liquid at the same time less viscosity due to increased temperature of the liquid of 70°C shown in Fig 2.4. It is the Brownian motion which causes the coupling or energy exchange between the wave motion and the internal motion (translation, vibration, rotation). These waves motion keep the particles of the suspension vibrate and rotation while the ultrasonic works causing the particles fully separated, or dispersed, in the liquid. The Brownian motion is a random motion of microscopic particles with different velocities resulting from the increase in temperature and caused by the molecular shocks. The local periodic variation of the pressure due to the wave propagation involves a molecular displacement (rotation + translation). This displacement is caused by the increase in the internal energy of the fluid. The change of the potential energy causes a change of the structure of the fluid because of the modifications of the distances between the different atoms. To pass from one energy level to another, each atom acquires a certain energy, leaving a disorder explained by the presence of holes in the energy levels. These displacements are the same as those, which leads to the relaxation mechanism, i.e. the return to equilibrium after the modification of the positions and the structure of the fluid molecules. The return to the equilibrium is achieved after a certain time named relaxation time. The entropy of the fluid increased and any increases in entropy means the establishment of an irreversible equilibrium state accompanied by energy dissipation and dispersion in the frequency domain.

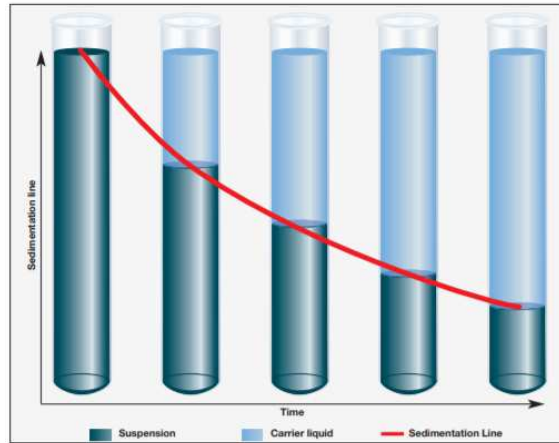


**Figure 2.1** The sedimentation rate is measured by resting the suspension in a glass container and observing the clear liquid phase over time. There is a sharp interface between the growing clear liquid layer at the top and the settling suspension containing the particles at the bottom.

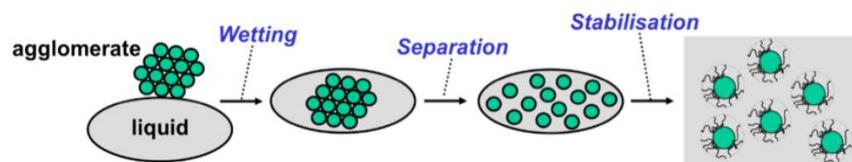


**Figure 2.2** Three steps in the dispersion process.

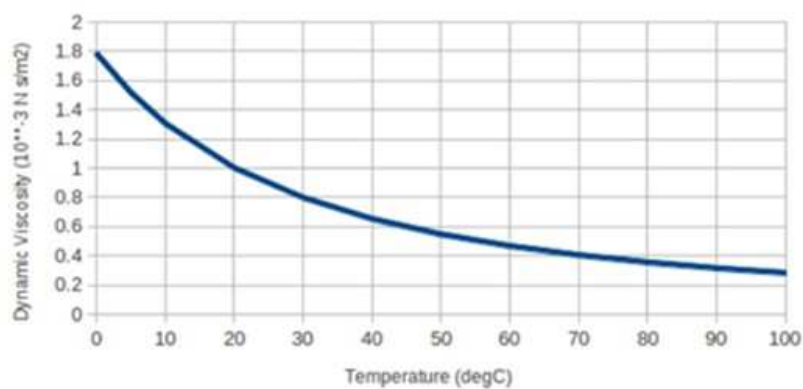


**Figure 2.3** Dynamic viscosity of water function of temperature

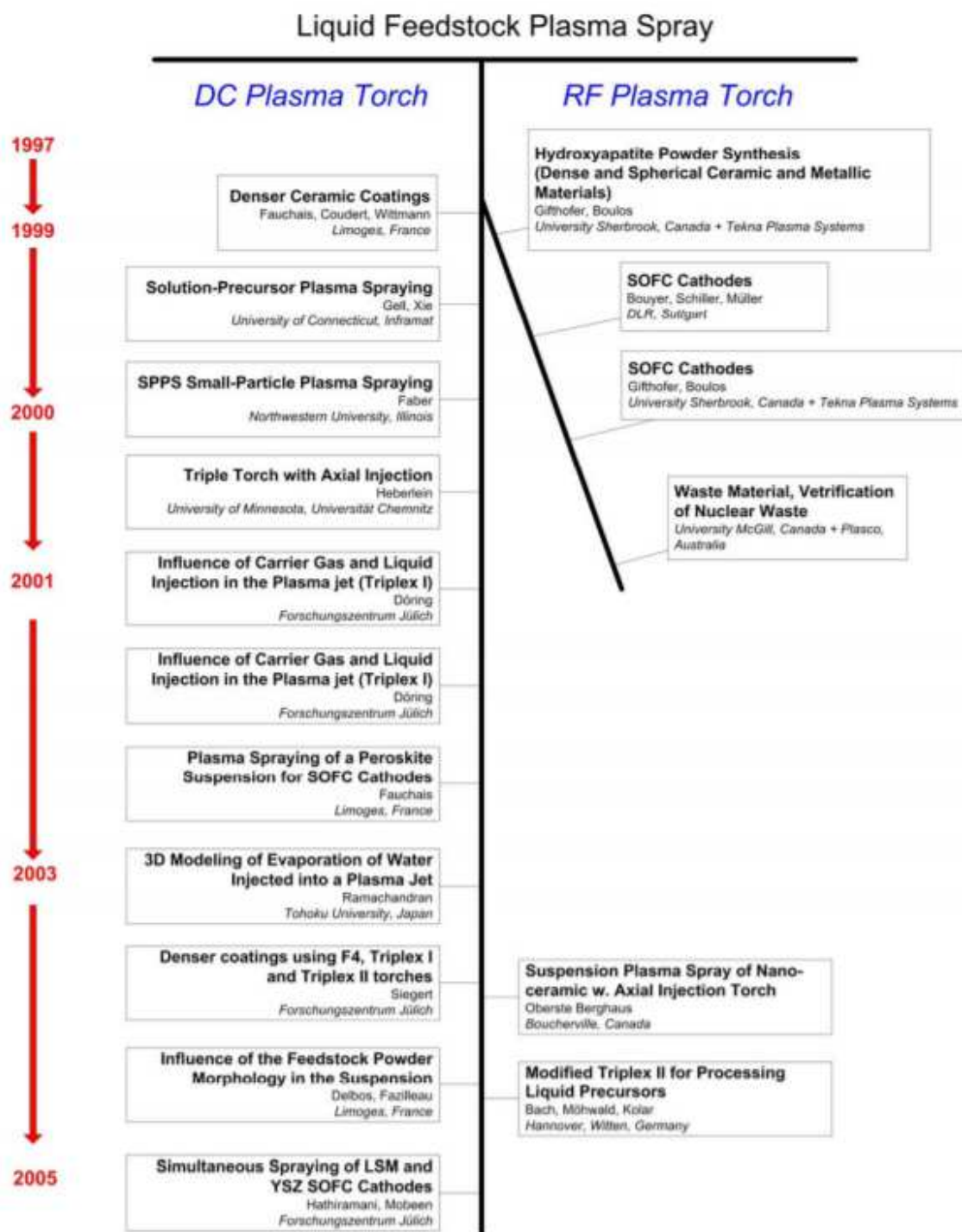
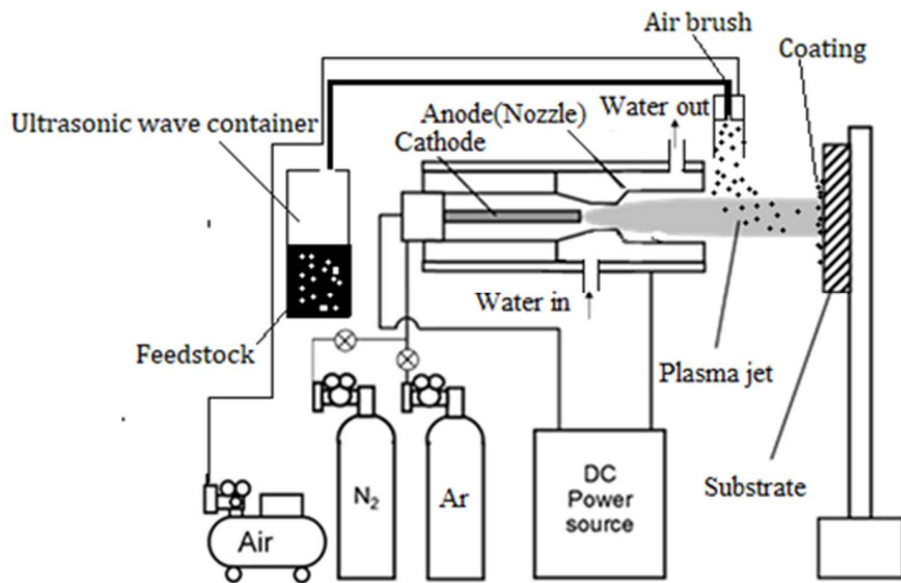


Figure 2.4 Some relevant research conducted in the optimization of the liquid feedstock plasma spray process

### 2.1.3 SPS Feeder Design Concept and Sketch

This method of the new ultrasonic feedstock mixer feeding system design covers the procedure for SPS is based to avoid the sedimentation process occur in the liquid and reduced viscosity of the liquid, which allows the TiO<sub>2</sub> particles to flow more easily in a pressurized feed system. An ultrasonic container uses a ceramic diaphragm vibrating at an ultrasonic frequency (0.5 - 1.7 MHz) to agitate the suspended particles and raise the temperature of suspension until 70 °C while spray to the plasma jet (Fig. 2.5). The spray method was external spray using an airbrush atomization feeding system where the suspension is first atomized and sprayed into the plasma jet.



**Figure 2.5** Schematic diagram of the suspension plasma spray (SPS) equipment.

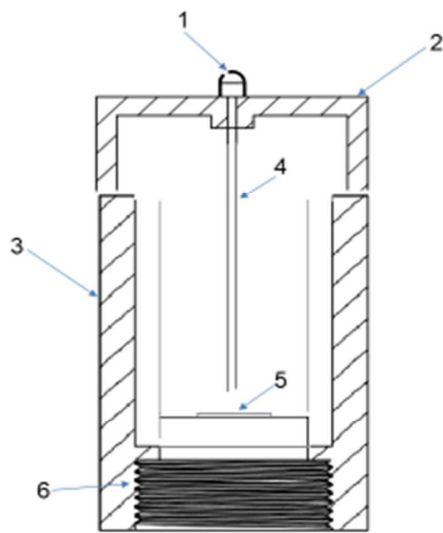


**Figure 2.6** Side view of the SPS feeder

**Table 2.1:** Feeder description in figure 1.1

<b>#</b>	<b>Feature</b>	<b>Description</b>
1	Materiel Outlet	Materiel outlet to the plasma jet
2	Top cover	Control Open close cover
3	Container	Contains liquid feedstock
4	Standpipe	Flexible Plastic Pipe
5	Ceramic diaphragm	Piezoelectric ceramic disk
6	Bottom cover	Control Open close cover



**Figure 2.7** Photo of the SPS feeder container.

## 2.1.4 Mechanical Components Drawing and Dimensions

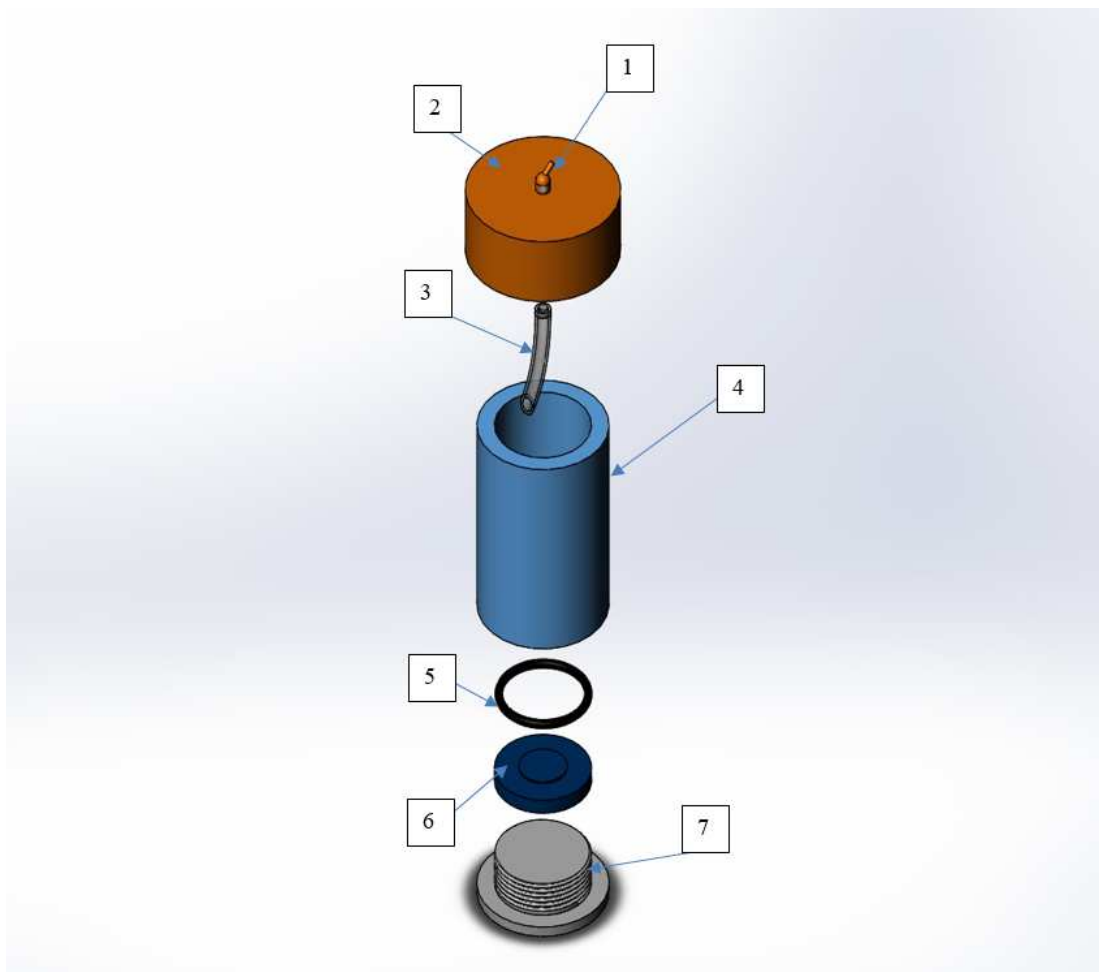


**Figure 2.8** Exploded view drawing of SPS feeder

**Table 2.2:** Feeder components in figure 2.9

#	components
1	Material Outlet
2	Top cover
3	Standpipe
4	Container
5	Gasket
6	Ceramic diaphragm
7	Bottom cover

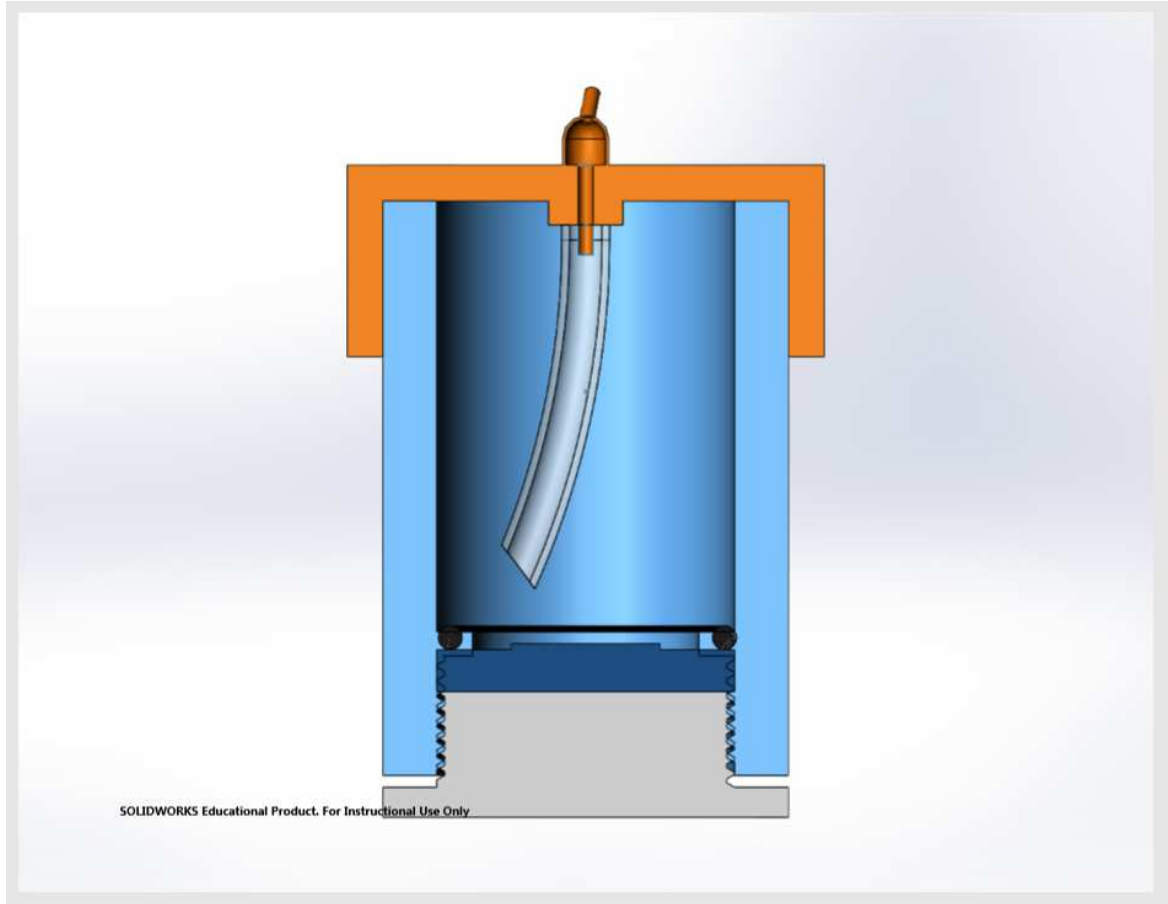


**Figure 2.9** SPS feeder section view

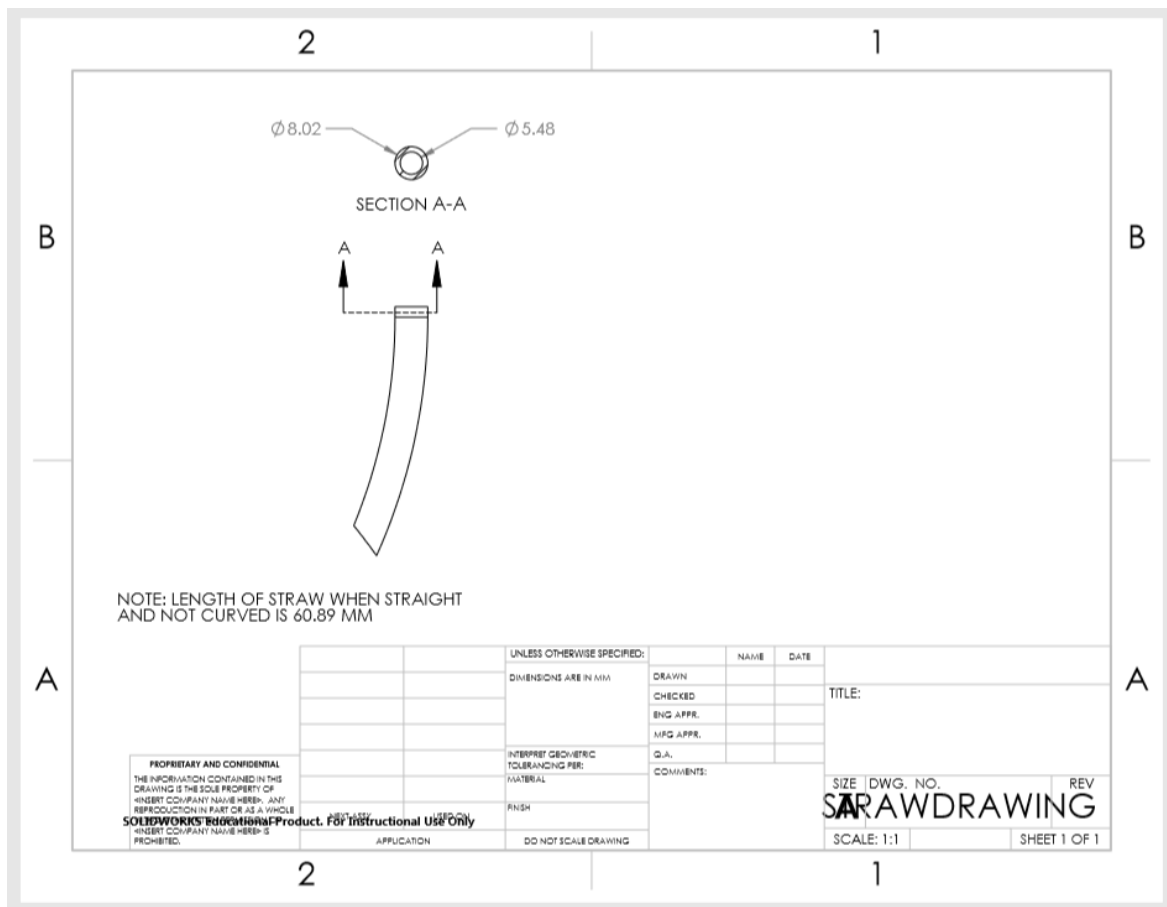


Figure 2.11 Mechanical drawing and dimensions of SPS feeder standpipe

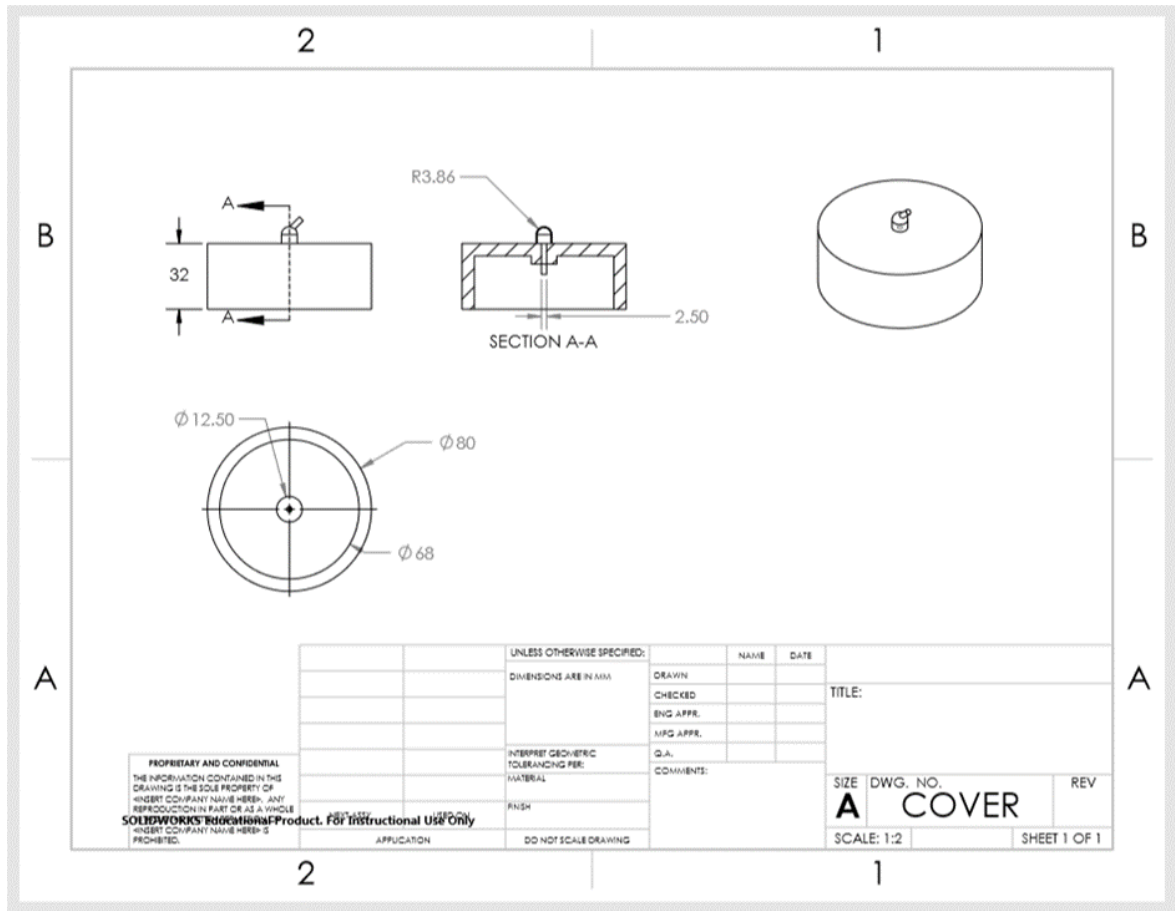


Figure 2.12 Mechanical drawing and dimensions of SPS feeder container

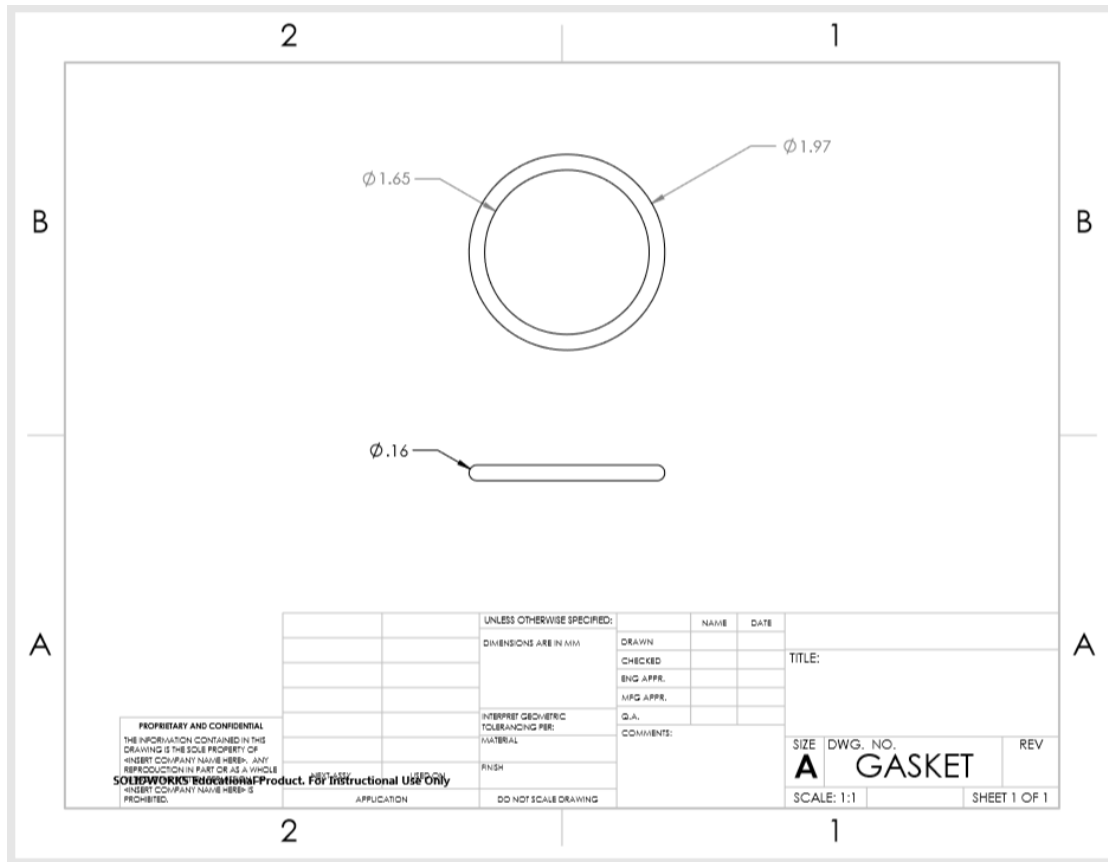
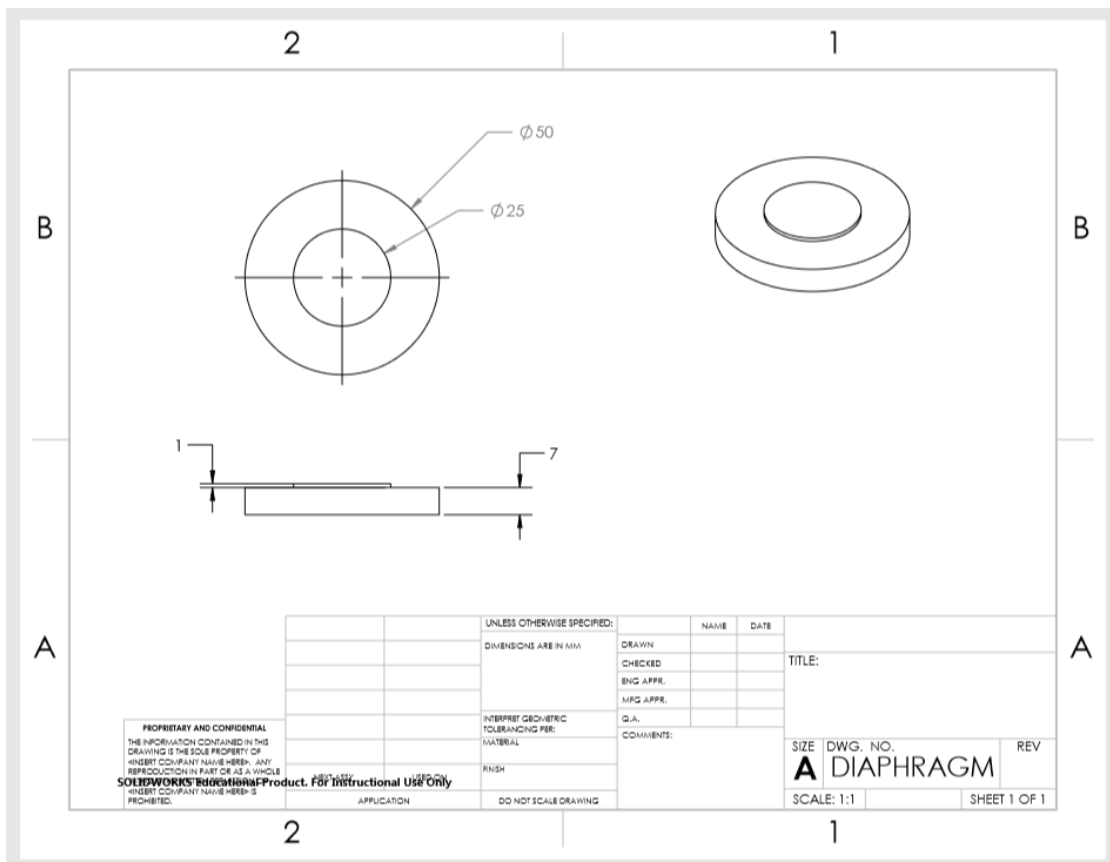
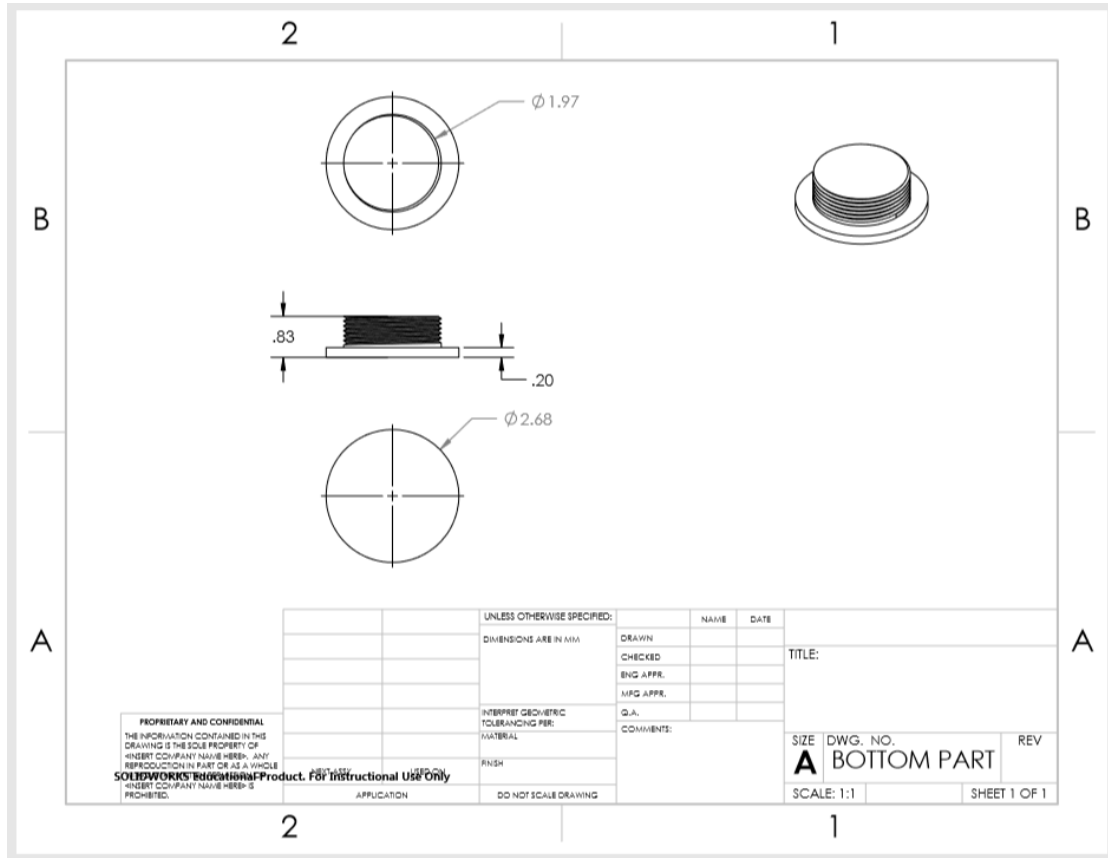


Figure 2.13 Mechanical drawing and dimensions of SPS feeder gasket



**Figure 2.14** Mechanical drawing and dimensions of SPS feeder ceramic diaphragm part



**Figure 2.15** Mechanical drawing and dimensions of SPS feeder bottom cover part

## **2.2 Ultrasonic Atomization Plasma Spray System UAPSS Design Parameters**

### **2.2.1 Introduction**

Photovoltaic and dye-sensitized solar technology both need the application of liquids and coatings during the manufacturing process. As most of these substances are very expensive, any losses due to over-spray or quality control are minimized with the use of the newly-designed ultrasonic feeding system. In efforts to reduce the manufacturing costs of solar cells, control was reduced to only a few millimeters of expensive catalyst material (flow rate range). The mist resulting from the ultrasonic atomizer is most commonly used in fuel cell coating application, highly porous and homogeneous coating, efficient combustion and particles heating, control of drop size, control of particle velocities, and has the possibility of using several gases instead of air. However, the air atomizing spray method has disadvantages such as getting agglomerates of catalyst in air spray droplets (Fig. 2.15), the nanoparticles remaining agglomerated, resulting in difficulty controlling the expensive catalyst material.

The morphology, crystalline structure, structural properties, optical properties, electronic properties, and stoichiometry of TiO<sub>2</sub> NPs and TFs have very sensitive deposition conditions. This is an inherent disadvantage for many physical vapor deposition methods [1, 2] such as laser ablation, where there are large variations in the optical and structural properties of the synthesized NPs and TFs [3]. These variations in NPs properties arise from small changes in the deposition conditions which are a key challenge in the development of techniques for the production of TiO<sub>2</sub> NPs and TFs at a large industrial scale. It is necessary to keep the deposition system as simple as possible and keep costs at a minimum while at the same time maximizing throughput. The new designed ultrasonic plasma spray offers such an opportunity.

Liquids breaking up into droplets results from the surface waves generated at the free surface of a thin film that forms as the liquid spreads over the atomizing surface. This technique is characterized by a fine atomization, a low spray velocity and simple liquid feeding equipment. Ultrasonic atomizers are well suited for medical sprays, techniques such as humidification, combustion, drying, applications in agriculture, metallic powders production and surface coating. Some experimental investigations dealing with ultrasonic atomization are available in the literature. There are three major techniques of atomizers: air blast, electrostatic, and ultrasonic. The spray pyrolysis technique using the electrostatic atomizer is called Electrostatic Spray Deposition (ESD), the technique using the air blast atomizer is named Pressurized Spray Deposition (PSD), and the technique using Ultrasonic atomizer is generally recognized as the ultrasonic or normal Spray Pyrolysis (SP). In this study ultrasonic atomization plasma spray system (UAPSS) was designed to provide a systematic and cost-effective mechanism which is capable of depositing nanoparticles and  $\text{TiO}_2$  thin films with consistent crystalline structure and stoichiometry. The common atomization techniques for feedstock feeding, which use pressure in order to generate feedstock mist, generally produce drops over 100 times more than the atomization technique using ultrasonic. UAPSS seeks to fulfill the need for more precise control of structural, morphological, and optical properties of  $\text{TiO}_2$  thin films. In this study the design was based on data and analysis results using MATLAB Mathematical Analysis Program. The program was used to obtain and estimate an idea for building input data design. The prototype was designed using the SolidWorks program for the final shape of the UAPSS design.

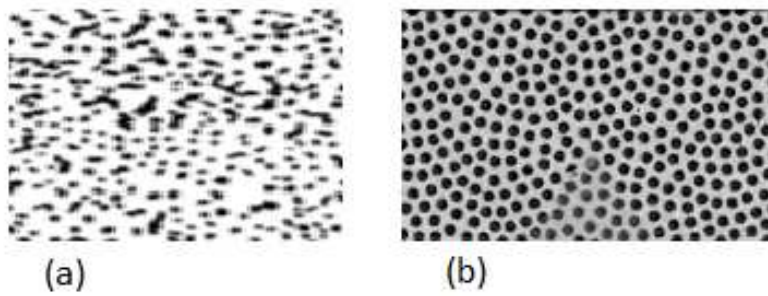


**Figure 2.16** Drop spray pattern. (a) Cross section of air spray droplet. (b) Cross section of the ultrasonically atomized droplet.

**Table 2.3.** Characteristics of atomizers commonly used in spray pyrolysis<sup>3</sup>

Atomizer	Droplet size ( $\mu\text{m}$ )	Atomization rate ( $\text{cm}^3/\text{min}$ )
Pressure	10-100	3-no limit
Nebulizer	0.1-2	0.5-5
Ultrasonic	1-100	<2
Electrostatic	0.1-10	

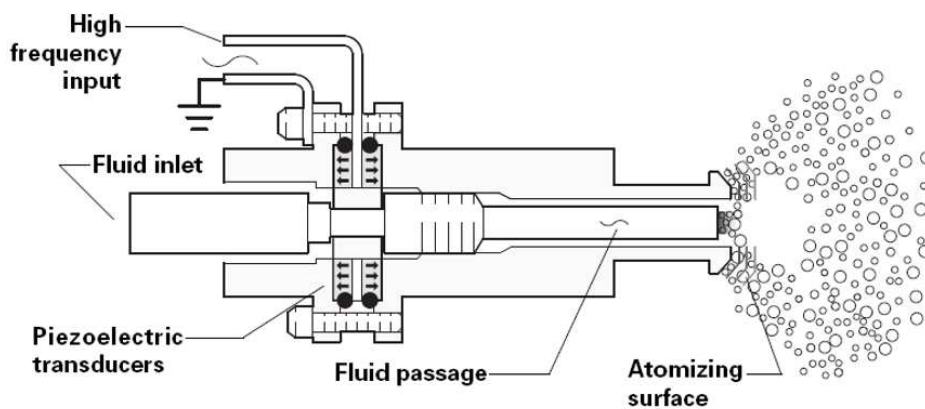


**Figure. 2.17** Schematic of commercial ultrasonic atomizer<sup>10</sup>.

### 2.2.3 Mechanism of The UAPSS Feeder

The mechanism of the ultrasonic atomization plasma spray system is shown in Fig. 2.12. The liquid flows through the micro pump unit, passing through the dispersion liquid delivery tube to the automation container unit. The liquid which drops as droplets onto the ceramic diaphragm by needle has 0.2 mm diameter to the piezoelectric ceramic disc that converts electrical energy to mechanical energy in the form of vibration. The disc oscillates in presence of electrical current at ultrasonic frequencies. As the frequency of oscillation of the plate increases, wave crests form and very minute droplets of liquid have enough energy to break the surface tension and disperse as mist. The mist is moved into the plasma jet by carrier gases pressure.

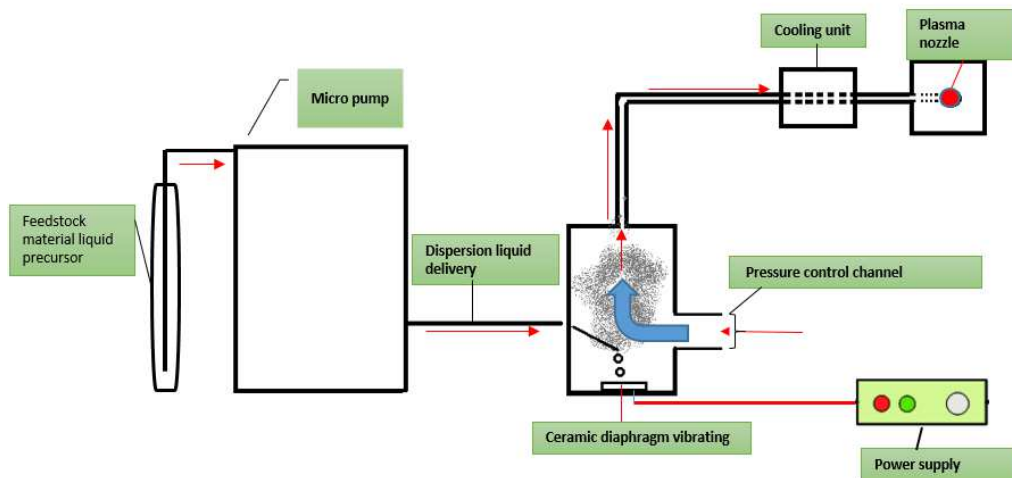


**Figure 2.18** Ultrasonic atomization plasma spray feeding system operation

## 2.3 Design analysis parameters

The design was based on several factors. These include:

- Nozzle type
- Liquid characteristics (e.g. viscosity, solids content)
- Flow rate
- Fluid mechanics

The final design uses the plasma jet nozzle type. The liquid characteristic was tested using different viscous precursors and the fluid viscosity was chosen for the automation process using the design. The precursor viscosity has been discussed in the experiments section.

### 2.3.1 Inlet carrier gas flow parameters

The inlet carrier gas flow parameters were calculated using MATLAB as seen in the following code, where  $N$  represents the number of holes,  $d$  is the diameter of the small holes in meters, and  $D$  stands for the diameter of the pipe in meters. Other variables and calculated values are explained using comments in the code. In this program, air flow at the inlet,  $Q_0$  ( $\text{m}^3/\text{s}$ ), is calculated by multiplying the pipe's cross-sectional area,  $A$ , by an assumed constant factor of 0.1 m/s.

The equations are conservation of mass for equations (1-3), and Bernoulli's equation for (4, 5). The variables are:  $N$  is the number of holes,  $Q_i$  for the volumetric flow rate between the  $i$ 'th control volume (shown as dotted lines in the figure),  $q_i$  are the volumetric flow rate leaving each hole  $i$ ,  $p_i$  is the pressure in the  $i$ 'th control volume,  $a$  is the area of a hole, and  $A$  is the cross-sectional area of the pipe.  $\rho$  is the air density at the operating temperature.

There are  $N$  mass conservation equations for the  $N$  holes,  $N$  equations for the flow rate  $q_i$  leaving each hole, and  $N - 1$  equations for the pressure drop between holes, giving  $3N - 1$  equations total.  $Q_0$  is the inlet flow rate and must be specified by the user. In the code, the equations (5) were simplified using equations (4) to eliminate the pressures.

$$0 = Q_0 - Q_1 - q_1 \quad \text{for } i = 1 \quad (1)$$

$$0 = Q_{i-1} - Q_i - q_i \quad \text{for } i = 2..N - 1 \quad (2)$$

$$0 = Q_{N-1} - q_N \quad \text{for } i = N \quad (3)$$

$$p_i = \frac{1}{2} \rho \left( \frac{q_i}{a} \right)^2 \quad i = 1..N \quad (4)$$

$$p_{i+1} - p_i = \frac{1}{2} \rho \left( \frac{Q_i}{A} \right)^2 \quad i = 1..N - 1 \quad (5)$$

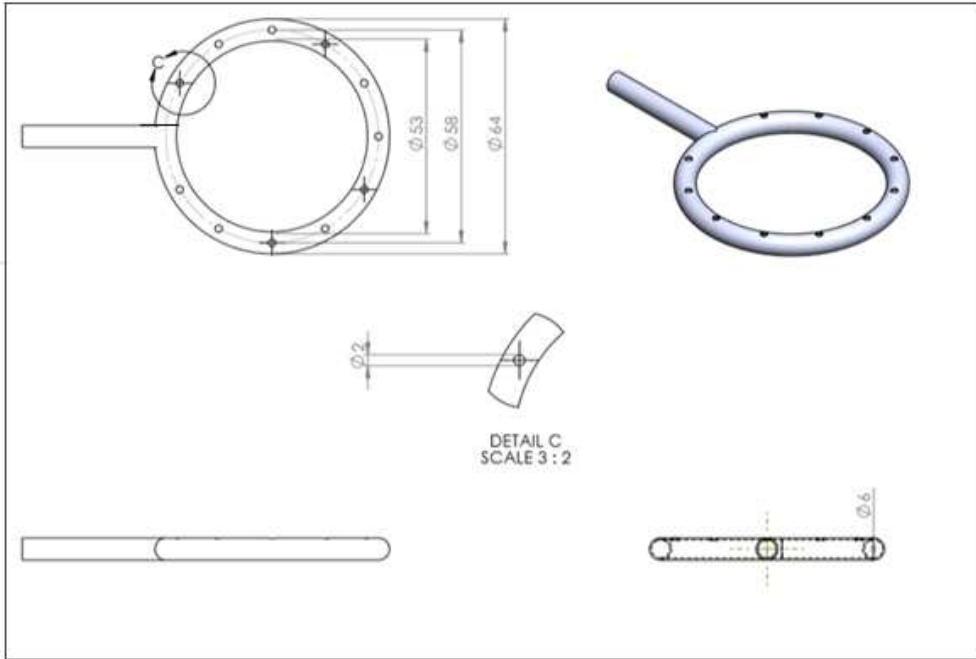


**Figure. 2.19** Inlet gas flow rate pipe with holes.

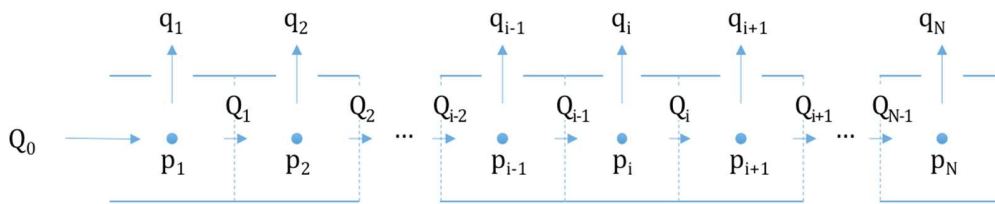


**Figure 2.20** Inlet gas flow rate pipe with holes.

```

%%%%%%%%%%%%%%%%%%%%%%%%%%%%%%%%%%%%%%%%%%%%%%%%%%%%%%%%%%%%%%%%%%%%%%%%%%
% Inlet gas flow rate pipe with holes simulation
%%%%%%%%%%%%%%%%%%%%%%%%%%%%%%%%%%%%%%%%%%%%%%%%%%%%%%%%%%%%%%%%%%%%%%%%%%
N = 11; %number of holes
d = 0.005; %m diameter of small holes
D = 0.03; %m diameter of pipe

rho = 1.2; %kg/m^3 density of air at sea level

a = pi*d^2/4; %area of small holes
A = pi*D^2/4; %area of pipe cross-section

Q_0 = 0.1*A; %m^3/s flow rate

Q = linspace(Q_0,0, N-1); %Q_0*ones(1,N-1); %flow rates in
pipe between holes
q = zeros(1,N); %flow rate out of the holes
p = ones(1,N); %pressure below each hole

x0 = [Q,q,p];
options =
optimoptions('fsolve','MaxFunctionEvaluations',500*(3*N)^2,
...
'MaxIterations', 500*(3*N), 'Algorithm','trust-region-
dogleg')
x = fsolve(@governingEquations(x, Q_0, a, A, rho,
N),x0,options);

Q = x(1:N-1);
q = x(N:(2*N-1));
p = x(2*N:(3*N-1));

figure(1)

```

```

subplot(3,1,1);
plot(1:N, q/a, 'o');
xlabel('hole number');
ylabel('velocity (m/s)');
ax = gca;
ax.FontSize = 16;

subplot(3,1,2);
plot(1:N, p, 'o');
xlabel('hole number');
ylabel('pressure (Pa)');
ax = gca;
ax.FontSize = 16;

subplot(3,1,3);
plot(1:(N-1), Q, 'o');
xlabel('hole number');
ylabel('flow between holes (m^3/s)');
ax = gca;
ax.FontSize = 16;

function F = governingEquations(x, Q_0, a, A, rho, N)
Q = x(1:N-1);
q = x(N:(2*N-1));
p = x(2*N:(3*N-1));

%mass balances
k = 1;
F(k) = Q_0 - Q(1) - q(1); %equation (1)
for i=2:(N-1)
    k = k+1;
    F(k) = Q(i-1) - Q(i) - q(i); %equations (2)
end %for i
k=N;
F(k) = Q(N-1)-q(N); %equation (3)

%hole pressure equations
for i = 1:N
    k=k+1;
    F(k) = p(i) - 0.5*rho*(q(i)/a)^2; %equations (4)
end %for i

%between-hole pressure jump equations
for i = 1:(N-1)
    k = k+1;
    F(k) = q(i+1)^2 - q(i)^2 - (a/A)^2*Q(i)^2; %equations
(5)
end %for i
end %function governingEquations

```

**Listing 2.1** Inlet gas flow rate pipe with holes simulation

### 2.3.2 The output of inlet carrier gas

The following figures show the inlet carrier gas pressure, velocity, and the flow rate between the holes inside the ultrasonic atomization plasma spray as a function of the number of holes. The pressure increases gradually from hole number 1 to hole number 11. Likewise, the air velocity is increased gradually from hole number 1 to hole number 11, whereas the flow rate between the holes is decreased gradually from hole number 1 to hole number 11.

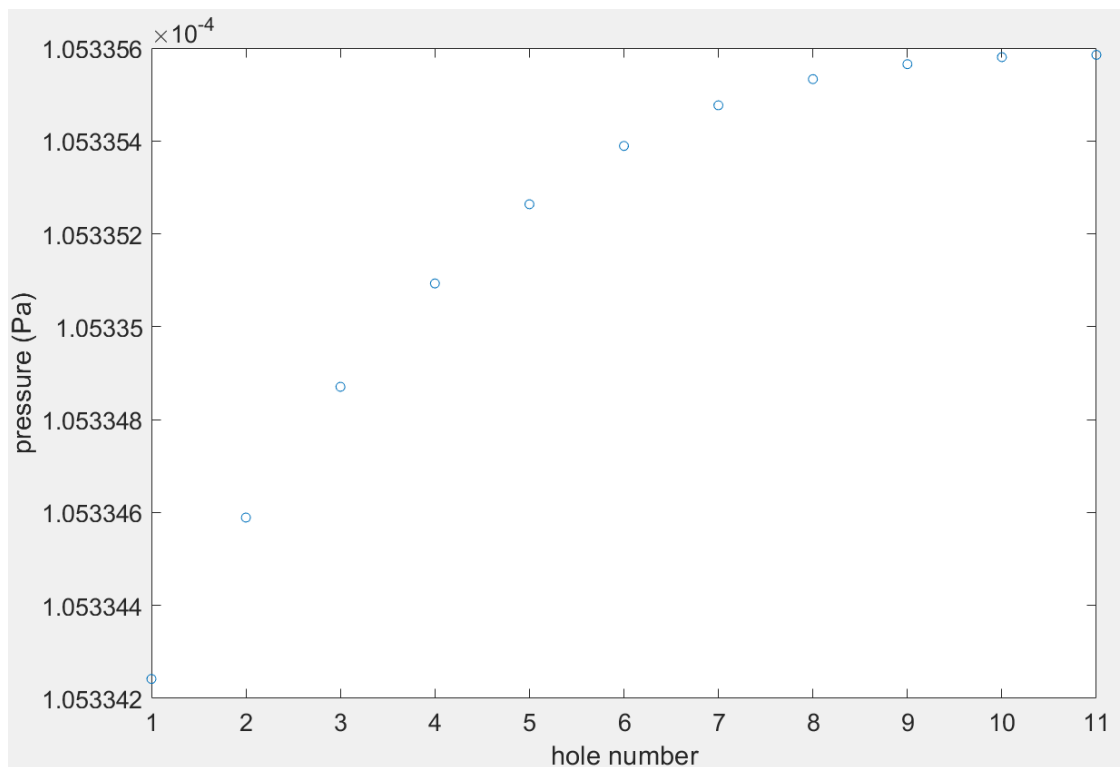


**Figure 2.21** The calculated hole air pressure as a function of hole number.

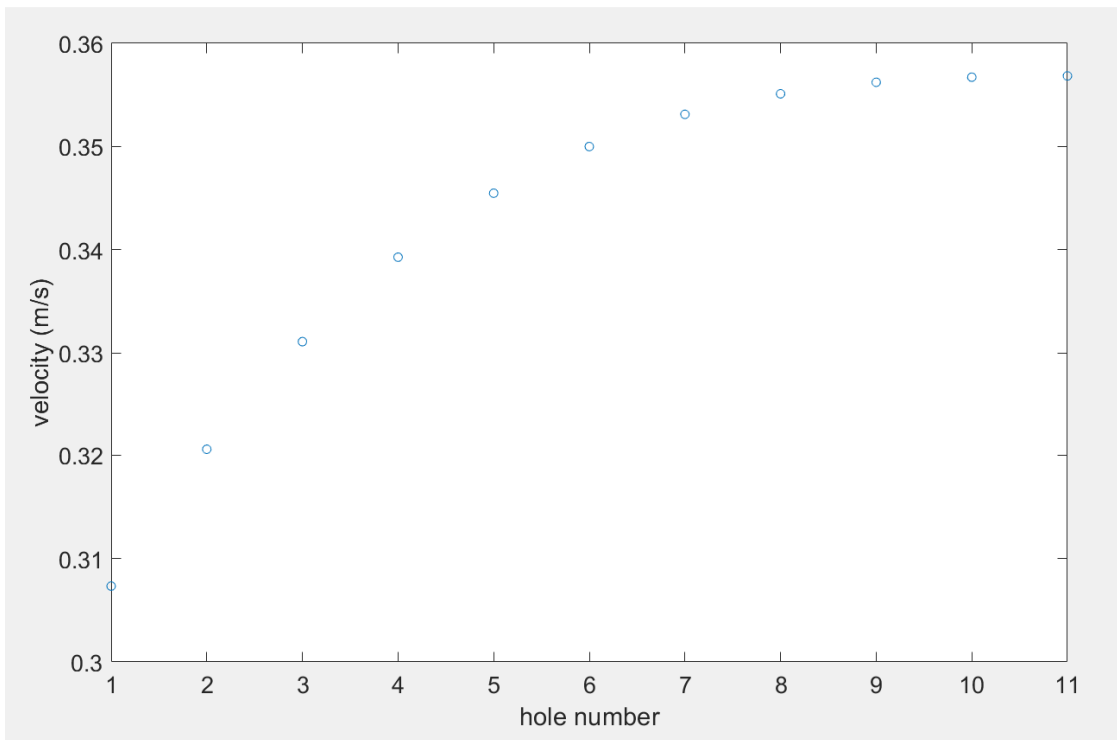


**Figure 2.22** The calculated hole air velocity as a function of hole number.

### 2.3.3 The flow between station A and station B for design

The calculation analysis using MATLAB for the design is based on conservation of mass for equations (6-8), and Bernoulli's equation for equations (9-13). The  $Q_{ij}$  are the volumetric flow rates between points i and j.  $p_i$  is the pressure at point i, and  $A_i$  is the cross-section area at point i. where i and j are any of the points A..F in the apparatus.  $\rho$  is the air density at the operating temperature.

$$Q_{AE} = Q_{EF} \quad (6)$$

$$Q_{EF} = Q_{FD} \quad (7)$$

$$Q_{FD} + Q_{CD} = Q_{DB} \quad (8)$$

$$P_A + \frac{1}{2}\rho\left(\frac{Q_{AE}}{A_A}\right)^2 = P_E + \frac{1}{2}\rho\left(\frac{Q_{AE}}{A_E}\right)^2 \quad (9)$$

$$P_E + \frac{1}{2}\rho\left(\frac{Q_{EF}}{A_E}\right)^2 = P_F + \frac{1}{2}\rho\left(\frac{Q_{EF}}{A_E}\right)^2 \quad (10)$$

$$P_F + \frac{1}{2}\rho\left(\frac{Q_{EF}}{A_F}\right)^2 = P_P + \frac{1}{2}\rho\left(\frac{Q_{DB}}{A_D}\right)^2 \quad (11)$$

$$P_D + \frac{1}{2}\rho\left(\frac{Q_{DB}}{A_D}\right)^2 = P_B + \frac{1}{2}\rho\left(\frac{Q_{DB}}{A_B}\right)^2 \quad (12)$$

$$P_C + \frac{1}{2}\rho\left(\frac{Q_{CD}}{A_C}\right)^2 = P_D + \frac{1}{2}\rho\left(\frac{Q_{DB}}{A_D}\right)^2 \quad (13)$$

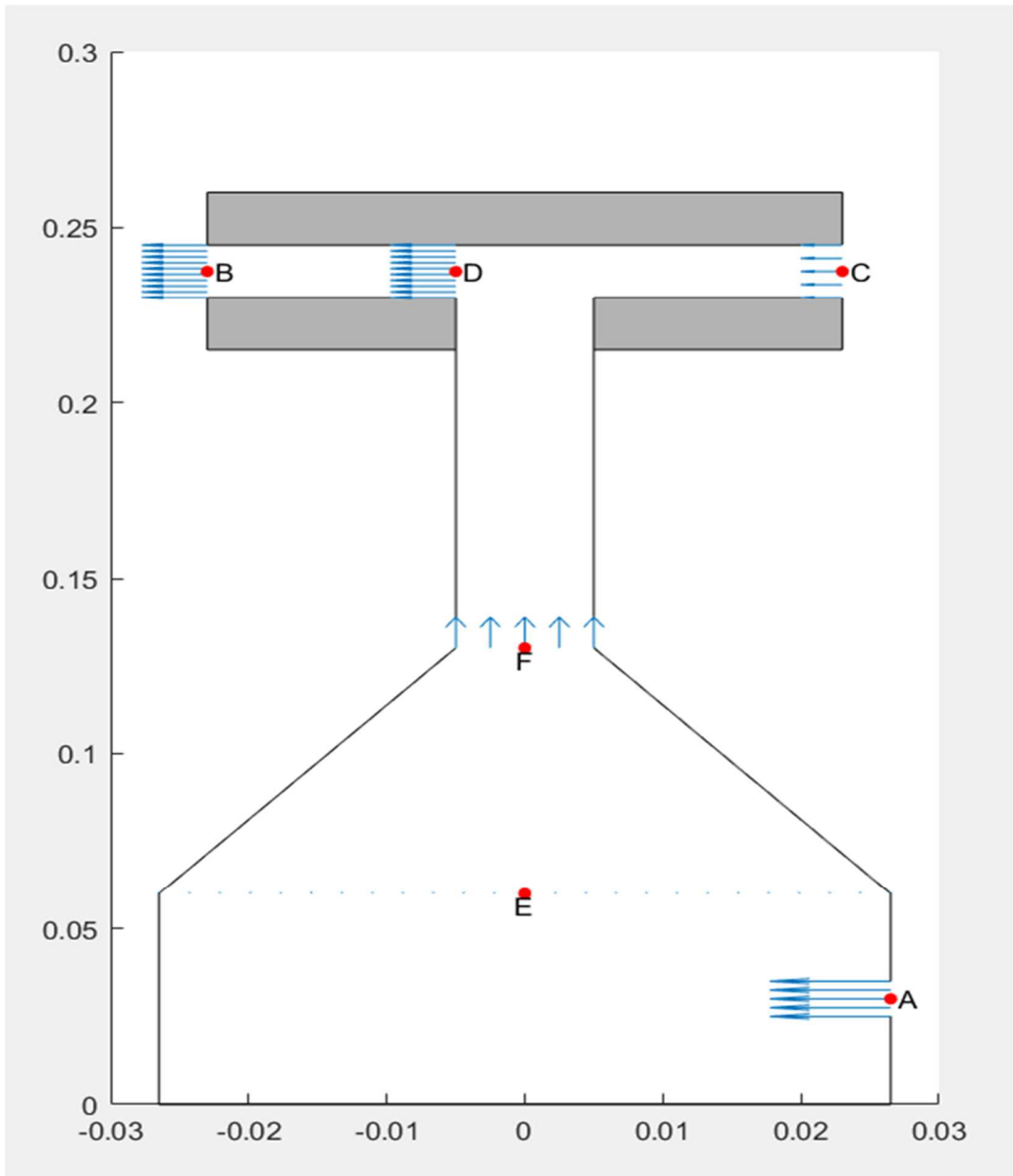


**Figure 2.23 Shows a flow system. For steady flow between station A and station B. Velocity arrows were calculated with the Plasma torch flow rate script in Listing 2.**

```

%%%%%%%%%%%%%%%%%%%%%%%%%%%%%%%%%%%%%%%%%%%%%%%%%%%%%%%%%%%%%%%%%%%%%%%%
% Plasma torch TiO2 script 3/27/18
%%%%%%%%%%%%%%%%%%%%%%%%%%%%%%%%%%%%%%%%%%%%%%%%%%%%%%%%%%%%%%%%%%%%%%%%
clear all

%define constants
g = 9.81; %m/s^2 - acceleration of gravity
M = 0.039948; %kg/mol molecular weight of Argon
Ru = 8.3144598; %J/(K-mol) universal gas constant
R = Ru/M; %gas constant for Argon

%define parameters
p_room = 101300; %Pa - pressure of air in room
T_room = 20+273.15; %K - temperature of air in room
gamma = 1.67; %specific heat ratio
par.rho = p_room/(R*T_room); %kg/m^3 - density of air (assumed
constant)
par.mu = 0.02*1e-3; %Pa-s viscosity
par.a = sqrt(gamma*R*T_room); %m/s speed of sound
par.D_A = 25e-3; %m
par.D_B = 7e-3; %m
par.D_C = 7e-3; %m
par.D_D = 7e-3; %m
par.D_E = 53e-3; %m
par.D_F = 6e-3; %m
par.A_A = 0.25*pi*par.D_A^2;
par.A_B = 0.25*pi*par.D_B^2;
par.A_C = 0.25*pi*par.D_C^2;
par.A_D = 0.25*pi*par.D_D^2;
par.A_E = 0.25*pi*par.D_E^2;
par.A_F = 0.25*pi*par.D_F^2;
par.L1 = 60e-3; %m
par.L2 = 70e-3; %m
par.L3 = 100e-3; %m
par.L4 = 50e-3; %m
par.L5 = par.L1/2; %m

%define input pressures
par.p_B = -0.06; %Pa
par.p_C = -0.01; %Pa
par.p_E = -0.005; %Pa

%solve the equations
x0 = zeros(1,8);

```

```

options = optimset('Display','iter'); % show iterations
x = fsolve(@(x)equations(x,par),x0, options);
par.p_A = x(1);
par.p_D = x(2);
par.p_F = x(3);
par.Q_AE = x(4);
par.Q_EF = x(5);
par.Q_FD = x(6);
par.Q_CD = x(7);
par.Q_DB = x(8);
par.V_A = par.Q_AE/par.A_A;
par.V_B = par.Q_DB/par.A_B;
par.V_C = par.Q_CD/par.A_C;
par.V_D = par.Q_DB/par.A_D;
par.V_E = par.Q_FD/par.A_E;
par.V_F = par.Q_FD/par.A_F;

par
V = abs([par.V_A, par.V_B, par.V_C, par.V_D, par.V_E,
par.V_F]);
D = [par.D_A, par.D_B, par.D_C, par.D_D, par.D_E, par.D_F];
Re = par.rho*V.*D/par.mu;
minRe = min(Re)
maxRe = max(Re)
maxMach = max(abs(V)/par.a)

%%%%%%%%%%%%%%%%%%%%%%%%%%%%%%%%%%%%%%%%%%%%%%%%%%%%%%%%%%%%%%%%%%%%%%%%
% This function has the equations in it, in the form g(x) = 0
% where x = [p_A p_D p_F Q_AE Q_EF Q_FD Q_CD Q_DB] and the
% par are par.p_B,p_C,p_E, rho, A_A, A_B, A_C, A_D, A_E, A_F,
L1, L2, L3]
%%%%%%%%%%%%%%%%%%%%%%%%%%%%%%%%%%%%%%%%%%%%%%%%%%%%%%%%%%%%%%%%%%%%%%%%
function deviation = equations(x, par)
    p_A = x(1);
    p_B = par.p_B;
    p_C = par.p_C;
    p_E = par.p_E;
    p_D = x(2);
    p_F = x(3);
    Q_AE = x(4);
    Q_EF = x(5);
    Q_FD = x(6);
    Q_CD = x(7);
    Q_DB = x(8);
    rho = par.rho;
    A_A = par.A_A;
    A_B = par.A_B;
    A_C = par.A_C;
    A_D = par.A_D;
    A_E = par.A_E;
    A_F = par.A_F;

```

```

    deviation(1) = Q_AE - Q_EF; %equation (6)
    deviation(2) = Q_EF - Q_FD; %equation (7)
    deviation(3) = Q_FD + Q_CD - Q_DB; %equation (8)
    deviation(4) = p_A + (0.5*rho/A_A)^2*Q_AE*abs(Q_AE) - p_E -
(0.5*rho/A_E)^2*Q_AE*abs(Q_AE); %equation (9)
    deviation(5) = p_E + (0.5*rho/A_E)^2*Q_EF*abs(Q_EF) - p_F -
(0.5*rho/A_F)^2*Q_EF*abs(Q_EF); %equation (10)
    deviation(6) = p_F + (0.5*rho/A_F)^2*Q_EF*abs(Q_EF) - p_D -
(0.5*rho/A_D)^2*Q_DB*abs(Q_DB); %equation (11)
    deviation(7) = p_D + (0.5*rho/A_D)^2*Q_DB*abs(Q_DB) - p_B -
(0.5*rho/A_B)^2*Q_DB*abs(Q_DB); %equation (12)
    deviation(8) = p_C + (0.5*rho/A_C)^2*Q_CD*abs(Q_CD) - p_D -
(0.5*rho/A_D)^2*Q_DB*abs(Q_DB); %equation (13)
end %function equations

%%%%%%%%%%%%%%%%%%%%%%%%%%%%%%%%%%%%%%%%%%%%%%%%%%%%%%%%%%%%%%%%%%%%%%%%
%%%%%%%%%%%%%%%%%%%%%%%%%%%%%%%%%%%%%%%%%%%%%%%%%%%%%%%%%%%%%%%%%%%%%%%%
% Draw the picture with labels
%%%%%%%%%%%%%%%%%%%%%%%%%%%%%%%%%%%%%%%%%%%%%%%%%%%%%%%%%%%%%%%%%%%%%%%%
%%%%%%%%%%%%%%%%%%%%%%%%%%%%%%%%%%%%%%%%%%%%%%%%%%%%%%%%%%%%%%%%%%%%%%%%
function drawApparatus(x, par)
p_A = x(1);
p_B = par.p_B;
p_C = par.p_C;
p_E = par.p_E;
p_D = x(2);
p_F = x(3);
Q_AE = x(4);
Q_EF = x(5);
Q_FD = x(6);
Q_CD = x(7);
Q_DB = x(8);
R_A = par.D_A/2;
R_B = par.D_B/2;
R_C = par.D_C/2;
R_D = par.D_D/2;
R_E = par.D_E/2;
R_F = par.D_F/2;
V_A = par.V_A;
V_B = par.V_B;
V_C = par.V_C;
V_D = par.V_D;
V_E = par.V_E;
V_F = par.V_F;
L1 = par.L1;
L2 = par.L2;
L3 = par.L3;
L4 = par.L4;
L5 = par.L5;

figure('Position', [1000 1000 600 900]);
hold on;

```

```

%axis square

%Plot the device outline

%Put the coordinate system at the centerline
X = [0,0;
     R_E, 0;
     R_E, L5-R_A]; %bottom right corner
plot(X(:,1),X(:,2), 'k');

X = [R_E, L5+R_A;
     R_E, L1;
     R_F, L1+L2;
     R_F, L1+L2+L3;
     L4/2,L1+L2+L3]; %right side
plot(X(:,1),X(:,2), 'k');

X = [0,0;
     -R_E, 0;
     -R_E, L1;
     -R_F, L1+L2;
     -R_F, L1+L2+L3;
     -L4/2,L1+L2+L3]; %left side
plot(X(:,1),X(:,2), 'k');

rectangle('Position',[-L4/2, L1+L2+L3+2*R_B, L4, 2*R_B],...
          'FaceColor',[.7 .7 .7]);

rectangle('Position',[-L4/2, L1+L2+L3-2*R_B, L4/2-R_F,
2*R_B],...
          'FaceColor',[.7 .7 .7]);

rectangle('Position',[R_F, L1+L2+L3-2*R_B, L4/2-R_F, 2*R_B],...
          'FaceColor',[.7 .7 .7]);

%Draw the velocity vectors
N_F = 5; %number of velocity vectors to draw across the section
F

%section A:
N_A = N_F*round(R_A/R_F); %number of velocity vectors to draw
across the section A
y_A = linspace(L5-R_A,L5+R_A, N_A);
x_A = R_E*ones(size(y_A));
u_A = -V_A*ones(size(y_A));
v_A = zeros(size(y_A));

%section B:
N_B = N_F*round(R_B/R_F); %number of velocity vectors to draw
across the section B
y_B = linspace(L1+L2+L3, L1+L2+L3+2*R_B, N_B);
x_B = -0.5*L4*ones(size(y_B));
u_B = -V_B*ones(size(y_B));

```

```

v_B = zeros(size(y_B));

%section C:
N_C = N_F*round(R_C/R_F); %number of velocity vectors to draw
across the section C
y_C = linspace(L1+L2+L3, L1+L2+L3+2*R_B, N_C);
x_C = 0.5*L4*ones(size(y_C));
u_C = -V_C*ones(size(y_C));
v_C = zeros(size(y_C));

%section D:
N_D = N_F*round(R_D/R_F); %number of velocity vectors to draw
across the section D
y_D = linspace(L1+L2+L3, L1+L2+L3+2*R_B, N_D);
x_D = -R_F*ones(size(y_D));
u_D = -V_D*ones(size(y_D));
v_D = zeros(size(y_D));

%section E:
N_E = N_F*round(R_E/R_F); %number of velocity vectors to draw
across the section E
x_E = linspace(-R_E, R_E, N_E);
y_E = L1*ones(size(x_E));
u_E = zeros(size(x_E));
v_E = V_E*ones(size(x_E));

%section F:
x_F = linspace(-R_F, R_F, N_F);
y_F = (L1+L2)*ones(size(x_F));
u_F = zeros(size(x_F));
v_F = V_F*ones(size(x_F));

x = [x_A, x_B, x_C, x_D, x_E, x_F];
y = [y_A, y_B, y_C, y_D, y_E, y_F];
u = [u_A, u_B, u_C, u_D, u_E, u_F];
v = [v_A, v_B, v_C, v_D, v_E, v_F];
quiver(x,y,u,v, 'AutoScale', 'on', 'AutoScaleFactor', 0.3);

%Draw the text to label points
X= [R_E,L5;
    -L4/2,L1+L2+L3+R_B;
    L4/2,L1+L2+L3+R_B;
    -R_F,L1+L2+L3+R_B;
    0,L1;
    0,L1+L2];
plot(X(:,1),X(:,2), '.r', 'MarkerSize', 16);
X(:,1) = X(:,1) + R_E*0.02;
text(X(1,1),X(1,2), 'A', 'HorizontalAlignment', 'left');
text(X(2,1),X(2,2), 'B', 'HorizontalAlignment', 'left');
text(X(3,1),X(3,2), 'C', 'HorizontalAlignment', 'left');
text(X(4,1),X(4,2), 'D', 'HorizontalAlignment', 'left');
text(X(5,1)- R_E*0.02,X(5,2)-

```

```

L2*0.05, 'E', 'HorizontalAlignment', 'center');
text(X(6,1)- R_E*0.02,X(6,2)-
L2*0.05, 'F', 'HorizontalAlignment', 'center');

end %function drawApparatus

```

**Listing 2.3** Program to calculate the flow rates and velocities at different points in the apparatus.

```

par =

struct with fields:

    rho: 1.6603
    mu: 2.0000e-05
    a: 319.2072
    D_A: 0.0100
    D_B: 0.0150
    D_C: 0.0080
    D_D: 0.0150
    D_E: 0.0530
    D_F: 0.0100
    A_A: 7.8540e-05
    A_B: 1.7671e-04
    A_C: 5.0265e-05
    A_D: 1.7671e-04
    A_E: 0.0022
    A_F: 7.8540e-05
    L1: 0.0600
    L2: 0.0700
    L3: 0.1000
    L4: 0.0460
    L5: 0.0300
    p_B: 2
    p_C: 2.3000
    p_E: 2.5000
    p_A: 0.7948
    p_D: 2
    p_F: 0.7948
    Q_AE: 1.2362e-04
    Q_EF: 1.2362e-04
    Q_FD: 1.2362e-04
    Q_CD: 2.7225e-05
    Q_DB: 1.5085e-04
    V_A: 1.5740
    V_B: 0.8536

```

```
V_C: 0.5416  
V_D: 0.8536  
V_E: 0.0560  
V_F: 1.5740
```

```
minRe = 246.5412
```

```
maxRe = 1.3067e+03
```

```
maxMach = 0.0049
```

**Listing 2.4** Output of the plasma torch flow rate script.

### **2.3.4 Characteristics of flow in the UAPSS and gases mixing point**

Table 2.1 shows the characteristics of flow in different locations in the UAPS feeder. The air flow rate inlet as a carrier gas and Ar flow rate was calculated to figure out the efficient mixing points based on knowing the type of flow. Turbulent mixing occurs in jets and in other flows, so it may be regarded as a universal phenomenon of turbulence. However, the higher turbulence flow point found at location B suggests the efficient mixing point is at location B in the plasma nozzle.

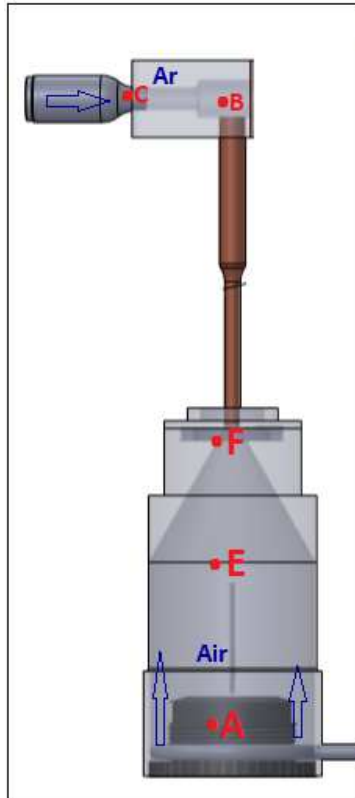


**Figure 2.24** Air carrier gas and Ar gas flow inside the UAPSS Feeder

**Table 2.4** Characteristics of flow in different location in said the UAPSS feeder. The cutoff for turbulence was taken to be  $Re_{crit} = 4000$ .

Location	$\rho$ $kg/m^3$	$\mu$ $kg/m \cdot s$	$v$ $m/s$	$D$ $m$	$Re$	Types of Flow
A	1.2	$1.8 \times 10^{-5}$	0.125	0.065	541	Laminar
E	1.2	$1.8 \times 10^{-5}$	0.125	0.065	541	Laminar
F	1.2	$1.8 \times 10^{-5}$	14.8	0.006	5920	Turbulent
C	1.6	$1.8 \times 10^{-5}$	5.2	0.009	1970	Laminar
B	1.6	$1.8 \times 10^{-5}$	4.9	0.15	6533	Turbulent

# 2.4 UAPSS Feeder Mechanical Components Drawing and Dimensions

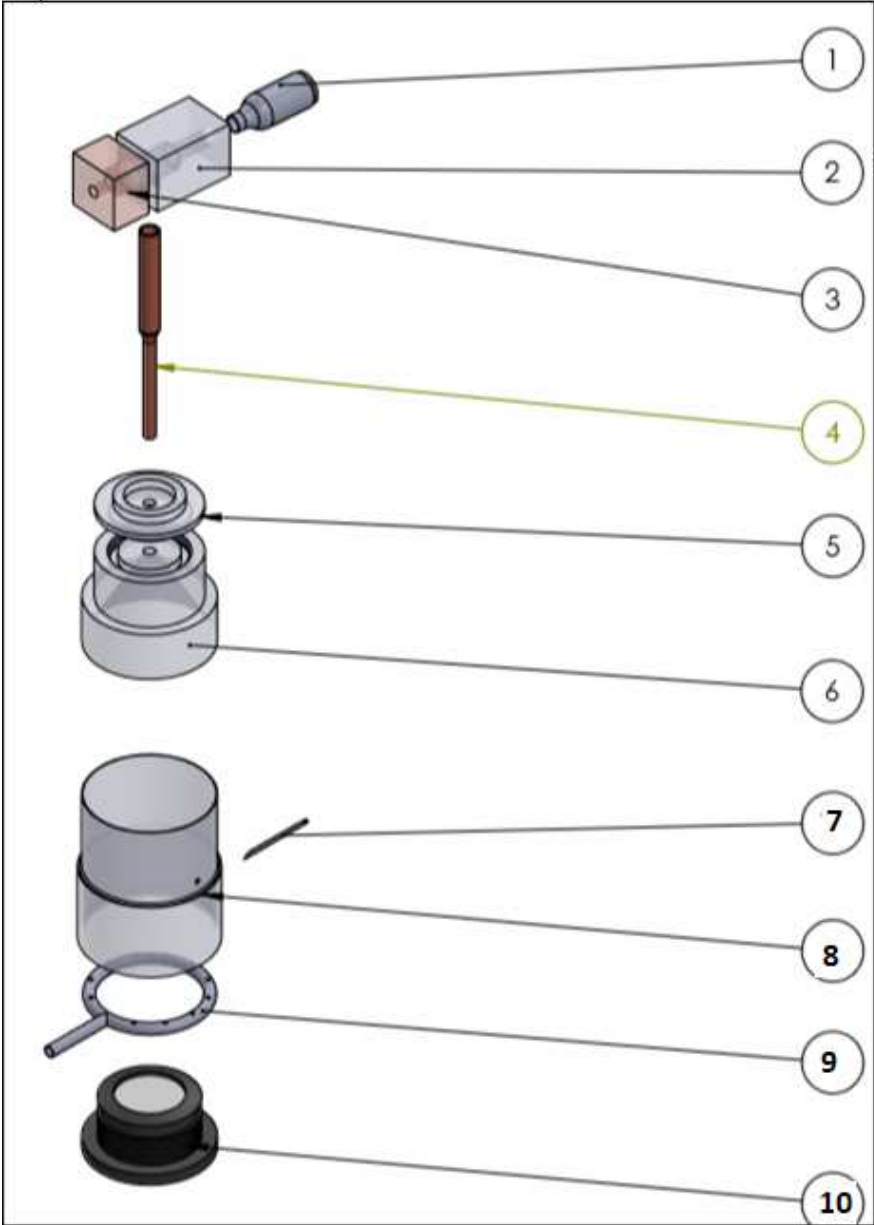
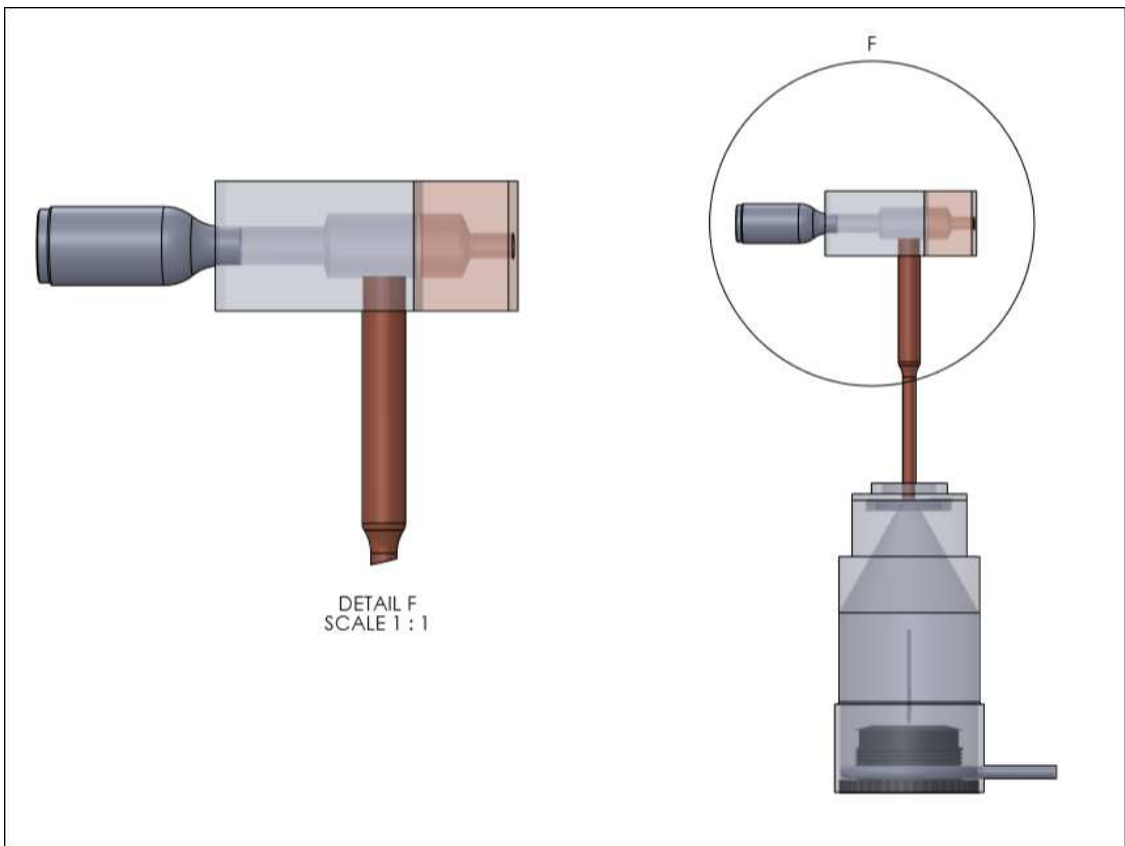


Figure 2.25 Exploded view drawing of UAPSS feeder.

**Table 2.4** Feeder components in figure 1.1

#	components
1	Argon Nozzle
2	Nozzle part 1
3	Nozzle part 2
4	Copper Pipe
5	Cover
6	Top conical shape
7	Droplet pipe
8	container
9	Inlet gas flow rate pipe with holes
10	Ceramic diaphragm with bottom cover



**Figure 2.26** Detail view of UA ultrasonic atomization plasma spray system.



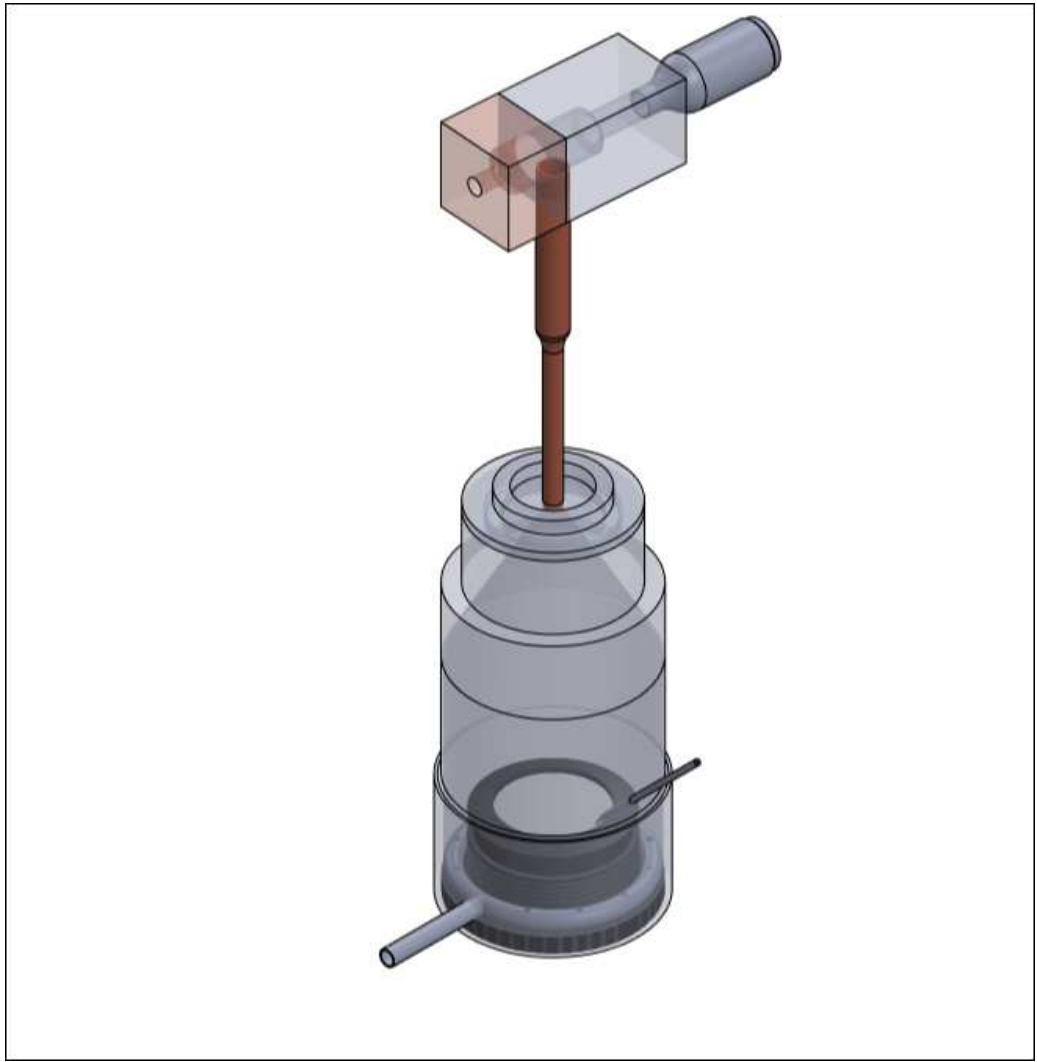


**Figure 2.27** 3D view of UAPSS

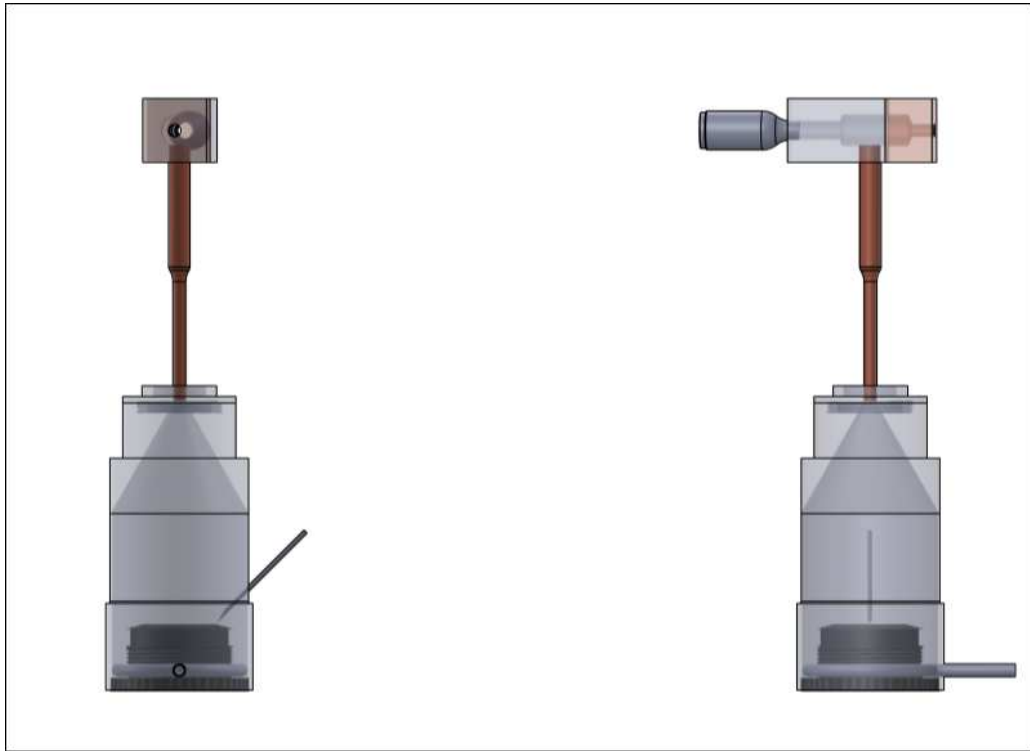


**Figure 2.28** Different side view of UAPSS

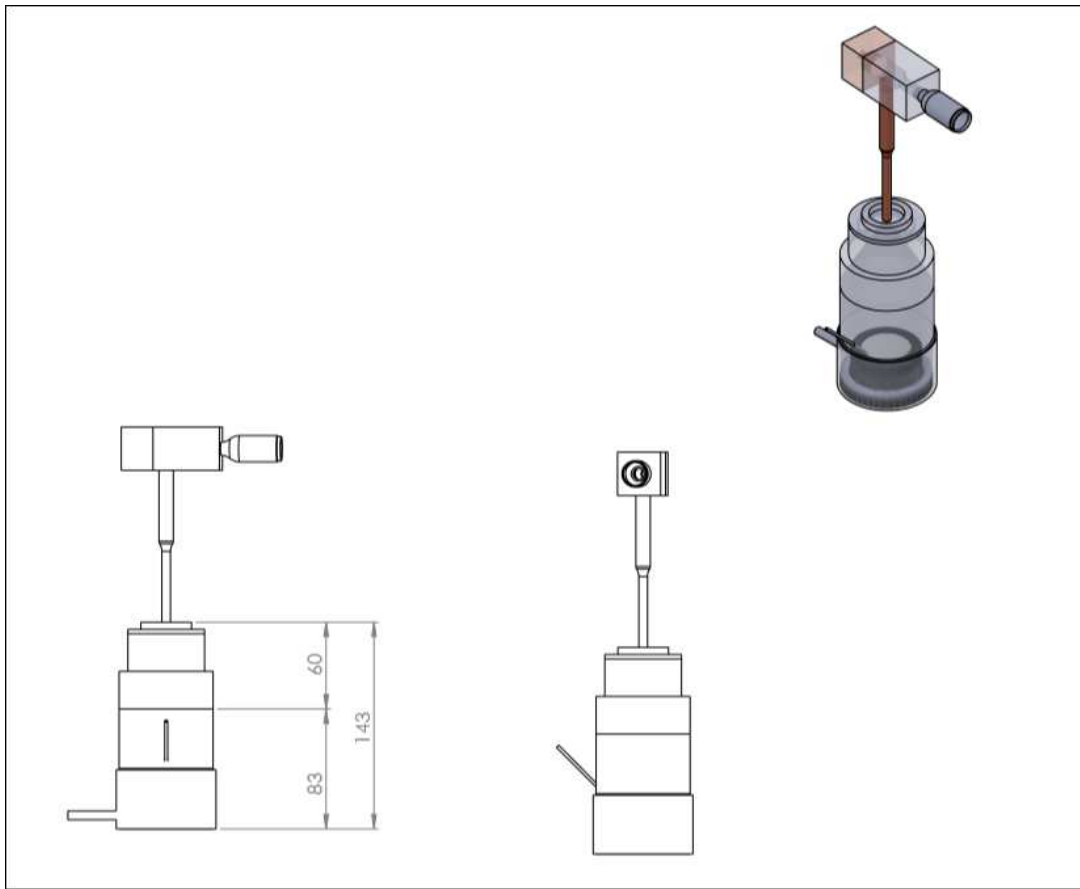


**Figure 2.29** Sketch of UAPSS container in millimeter scale

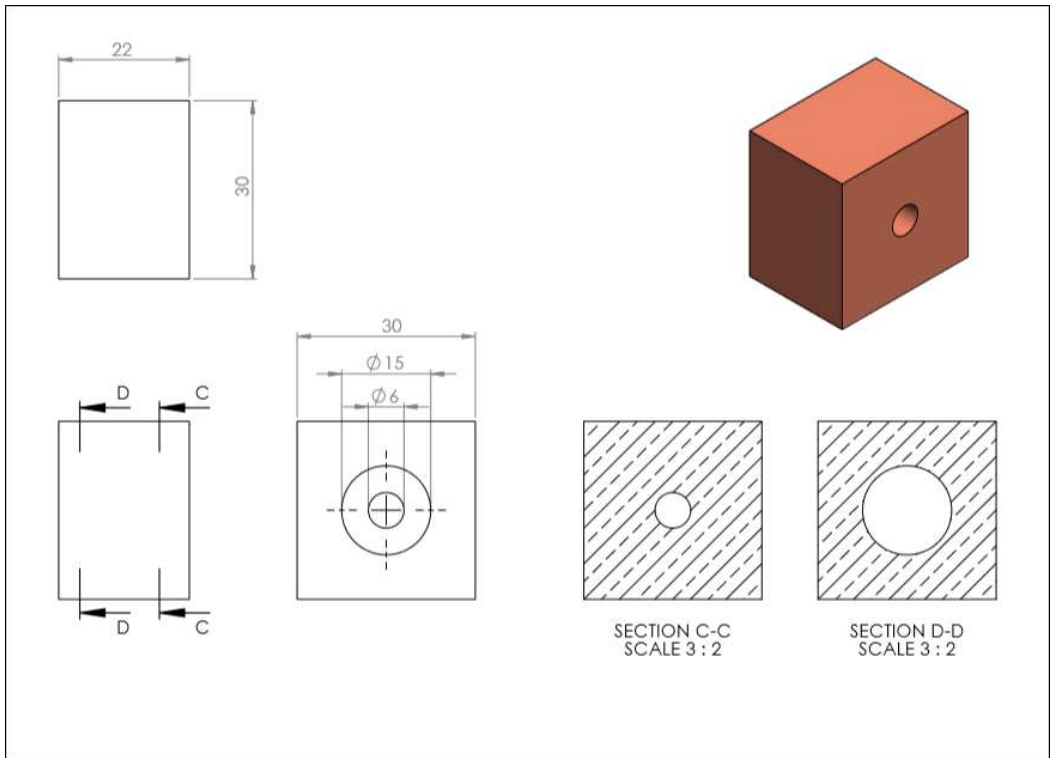


**Figure 2.30** Section view of nozzle No.2

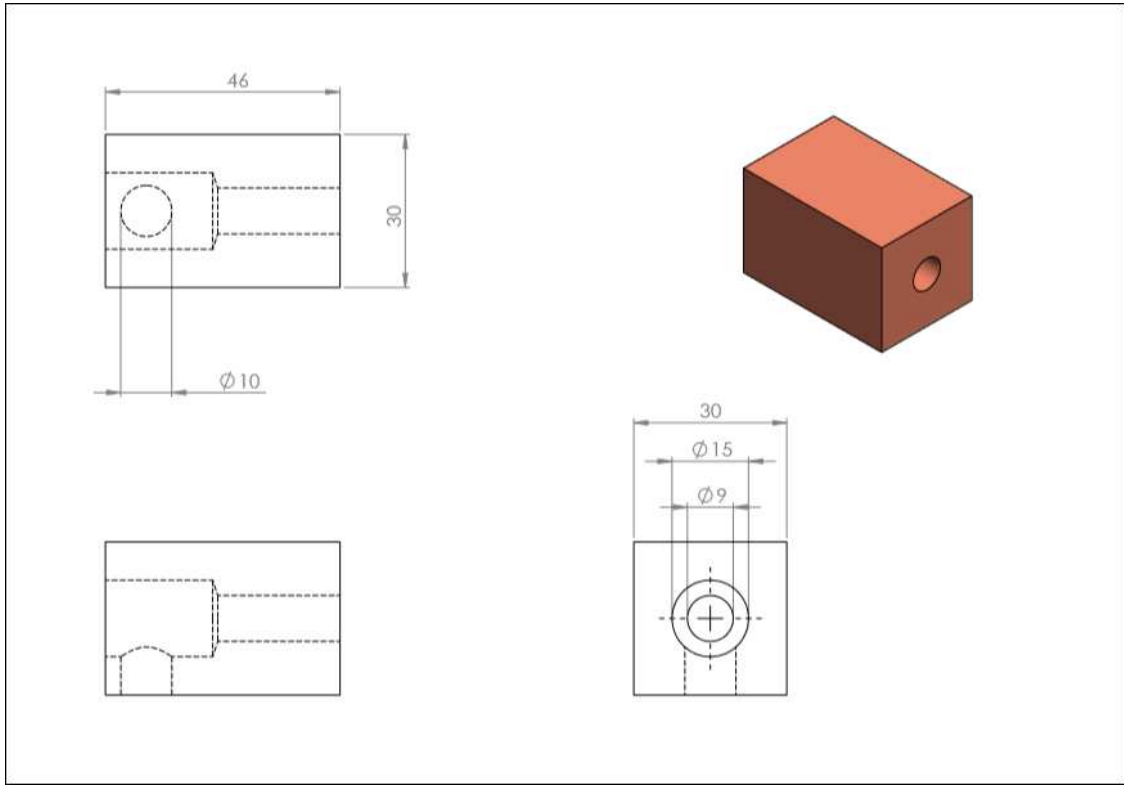


**Figure 2.31** Section view of nozzle No.1

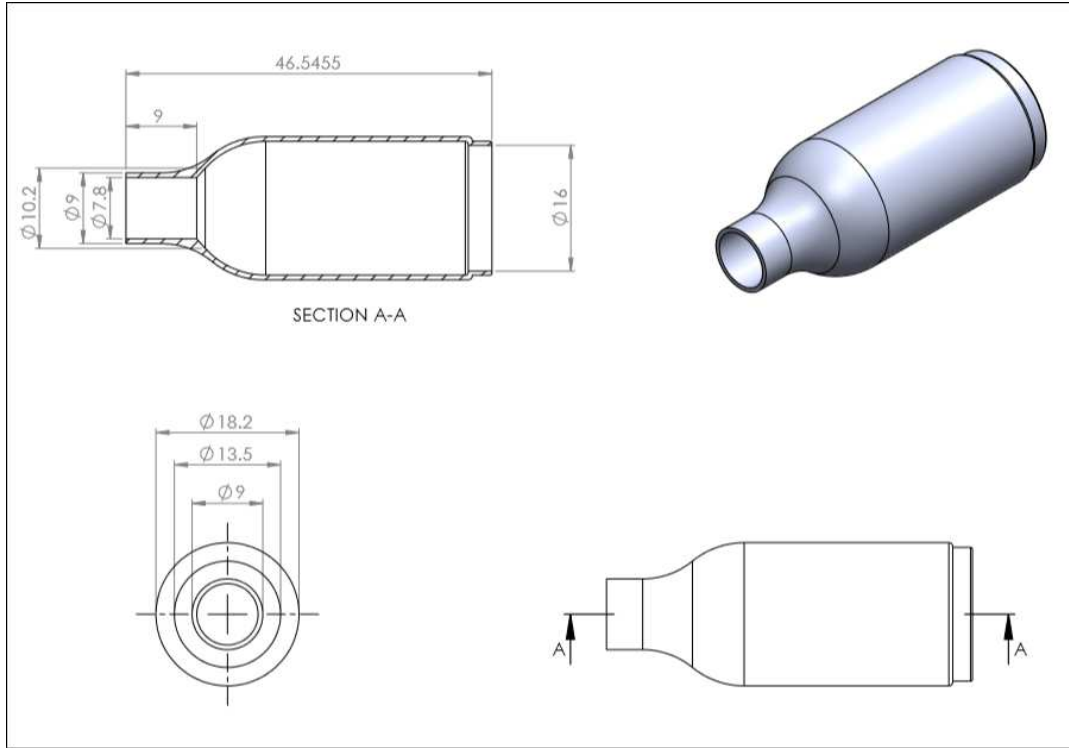


**Figure 2.32** Section view of Ar inlet nuzzle

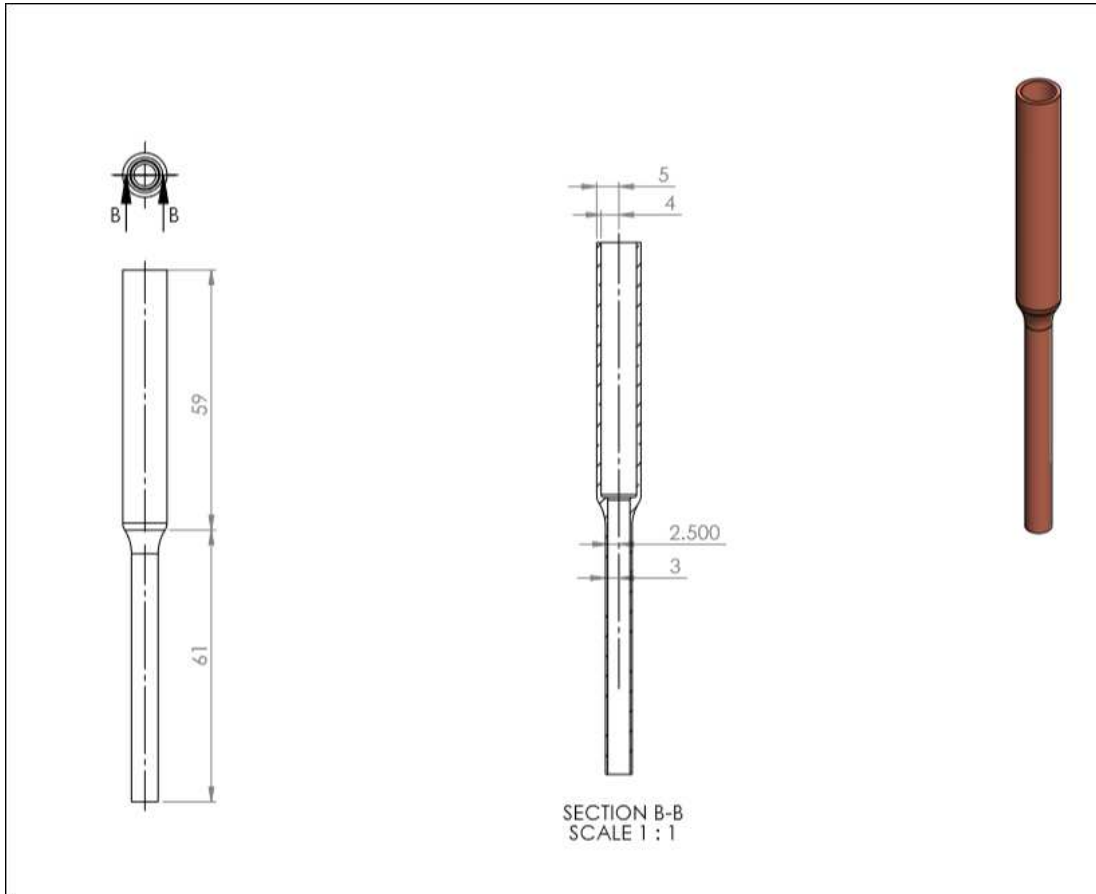


**Figure 2.33** Section view of copper pipe (Gas transmission line)

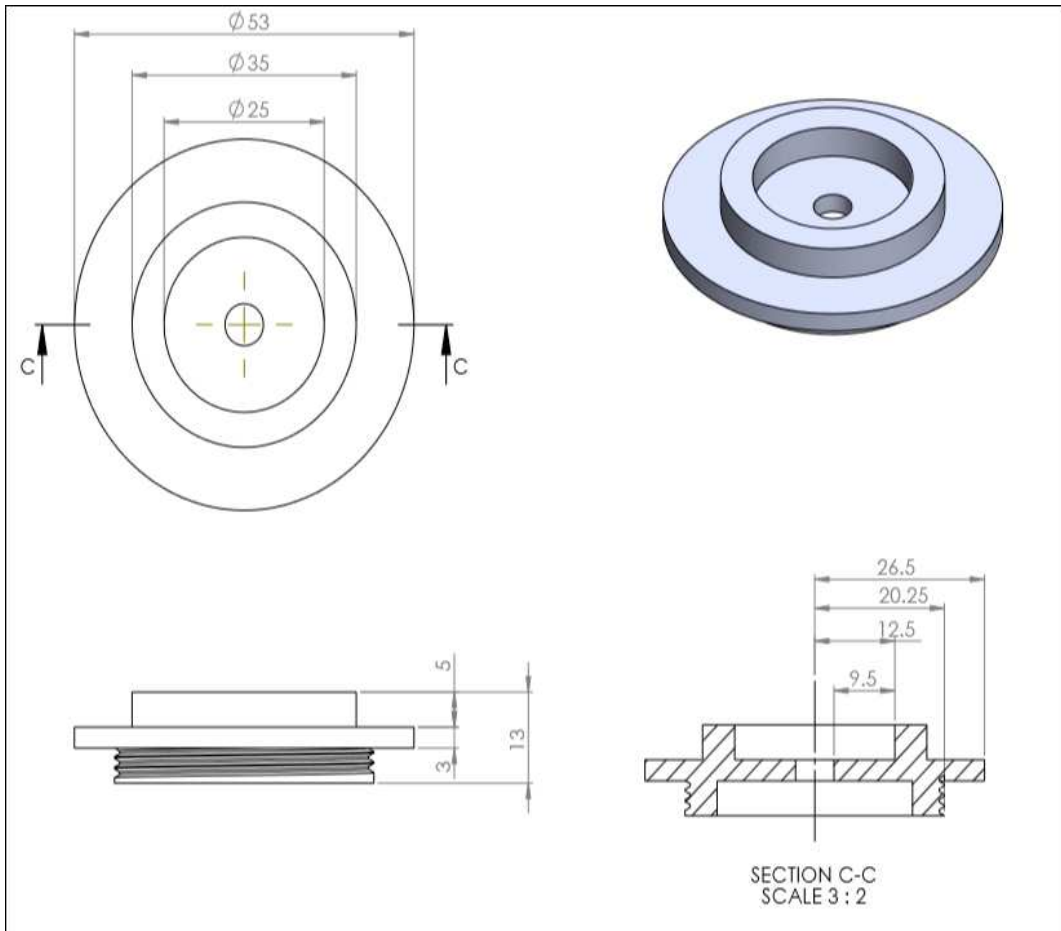


**Figure 2.34** Section view of top cover

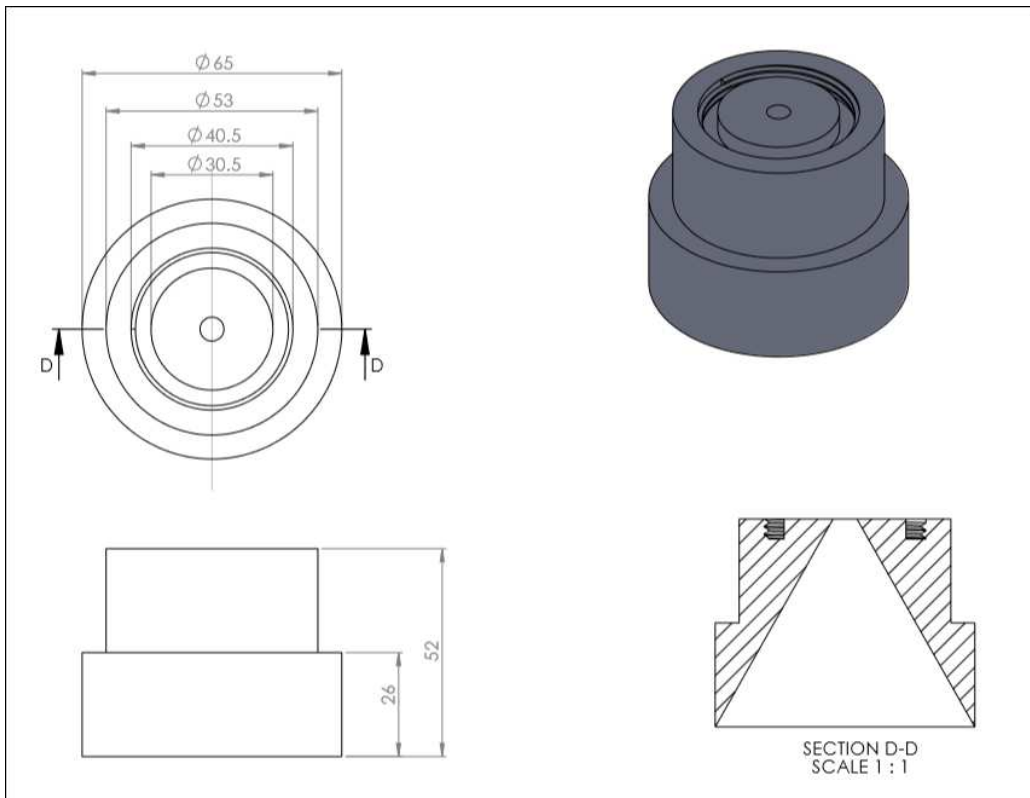


**Figure 2.35** Section view of top conical shape (Gas transmission line)

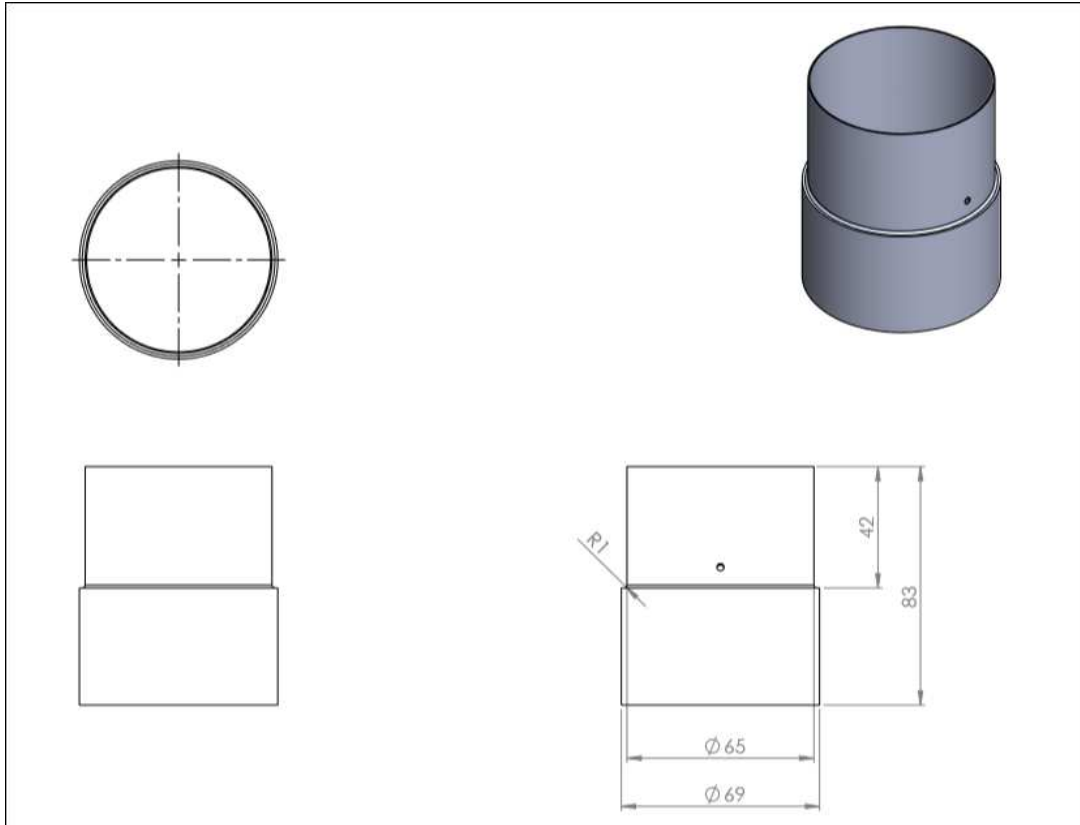


**Figure 2.36** Section view of the container

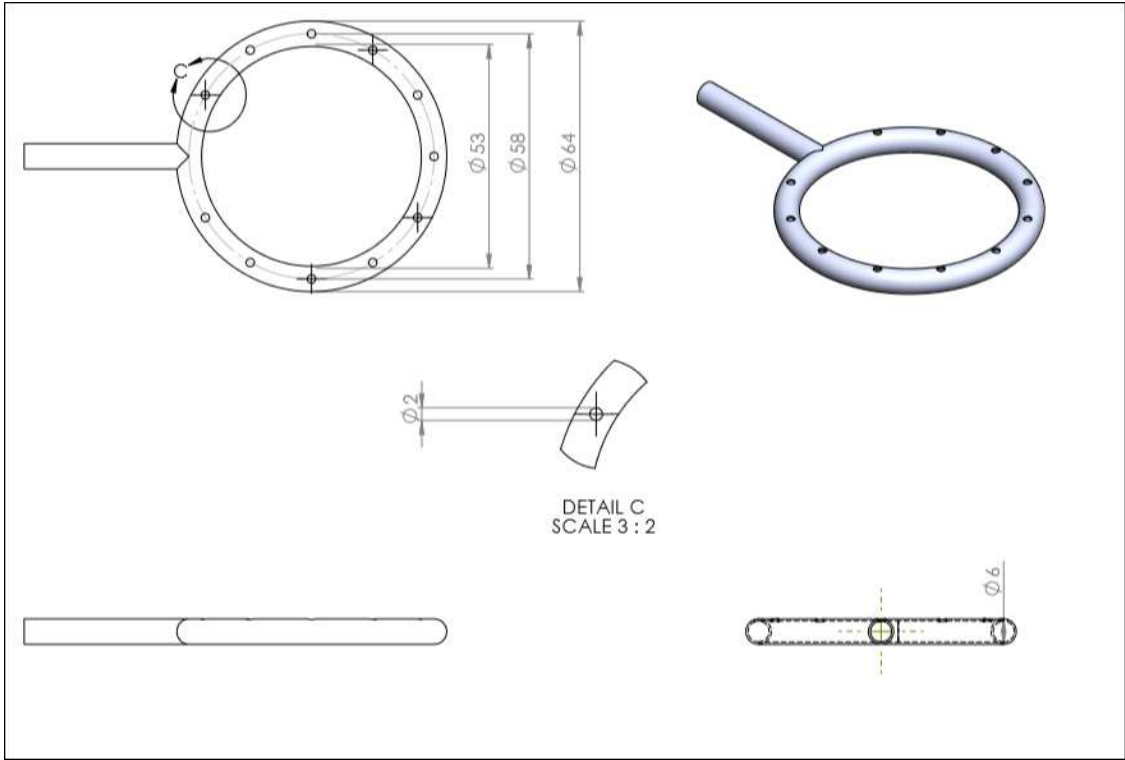


**Figure 2.37** Mechanical drawing and dimensions of UAPSS feeder bottom cover with ceramic diaphragm measurements are in millimeters



**Figure 2.38** 3D view of droplet line pipe

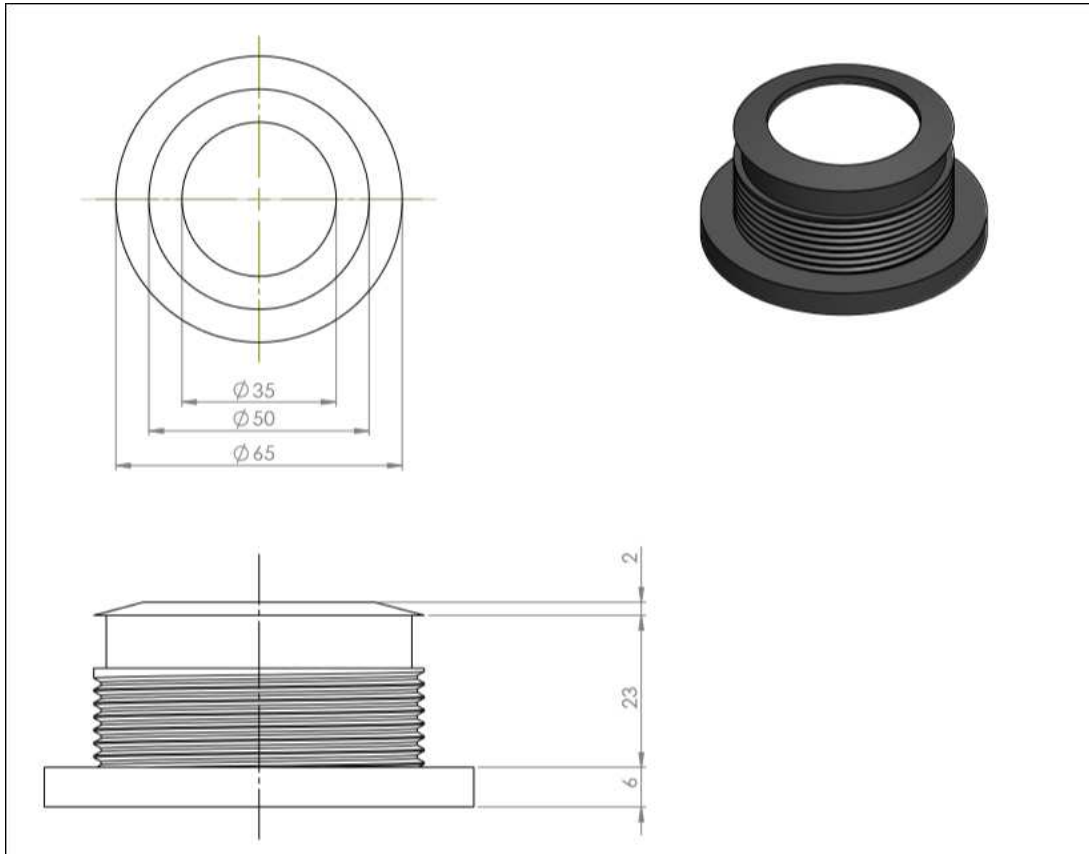


**Figure 2.39** Mechanical drawing and dimensions of SPS feeder bottom cover with ceramic diaphragm measurements are in millimeters



# **CHAPTER 3:**

## **Development of a Fabrication Process Using Suspension Plasma Spray for Titanium Oxide Photovoltaic Device**

**Abstract:** In order to reduce the feedstock production cost of suspension, titanium hydroxide particle dispersed suspension creation method by hydrolysis of titanium tetra iso butoxide (TTIB) was developed. To avoid sedimentation of the hydroxide particles in the suspension, mechanical milling of the suspension was conducted in order to create colloidal suspension. Consequently, through the creation of colloidal suspension, coating deposition could be conducted without sedimentation of the hydroxide particles in the suspension during the deposition process. Though the as-deposited amorphous coating was deposited, the coating became anatase rich. In addition, it was confirmed that the post heat treated anatase rich coating which had enough photo-catalytic activity to decolor methylene-blue droplets by post heat treatment on the condition of 630 °C for 60 min. From these results, this technique was found to have high potential in the low-cost photo-catalytic titanium coating production process.

### **3.1 Introduction**

Thin titanium oxide films for photo-catalytic application (anatase TiO<sub>2</sub>, etc.) can be deposited by various deposition techniques such as sputtering [39], metal-organic chemical vapour deposition (MOCVD) [40], spray pyrolysis [41], the sol-gel process [42], thermal spray [43,46], or by various other methods. However, there are several engineering problems associated with these deposition processes, such as the necessity of vacuum equipment, low deposition rates, deposition time, the requirement of special and costly equipment, as well as feedstock powder [47]. Recently,

some atmospheric thermal plasma processes for titanium deposition have been successfully developed [48]. It is still difficult to develop the atmospheric thermal plasma process, especially in cases where low power DC arc discharge equipment is being used. In our previous study, in order to reduce equipment costs, a thermal spray process for photo-catalytic titanium oxide coating was fabricated using 1 kW class Atmospheric Solution Precursor Plasma Spray (ASPPS) equipment. Titanium oxide film deposition was then carried out [47, 49]. Although photo-catalytic anatase rich titanium oxide films were successfully deposited, the feedstock cost could not be decreased because of the necessity of expensive anhydrous ethanol which is required to create the low viscosity titanium iso butoxide solution (TTIB,  $\text{Ti}(\text{OC}_4\text{H}_9)_4$ ) without hydration of TTIB due to residual water in the ethanol. Although the anhydrous ethanol-titanium-oxide-suspension method is a possible solution to the above problems, it is difficult to use this method in practice. This method creates large secondary particles as a result of hydrolysis due to the presence of TTIB as well as the fact that titanium dioxide is insoluble in water. It has large particles, which solidify when in contact with water (hydrolysis). These properties prevent the suspension from being stable and mixing with nanoparticles in water. It is also difficult to inject or spray such a mixture. Titanium tetra-butoxide was developed in the form of a titanium hydroxide suspension by using nothing but stable water to prepare the titanium hydroxide suspension and then by milling and filtering the suspension. The suspension plasma spray (SPS) that developed new feedstock material seems to be highly promising as a low cost starting material and in the rapid formation of functional thin films.

## **3.2 Experimental Procedure**

### **3.2.1 Method**

The tools used for mixing titanium oxide with water are shown in Fig. 3.1. They consist of a micro filter, a mixer, and a special container (mortar and pestle) for mixing as well as for crushing

and grinding. An amount of 2 mL of TTIB is diluted with stable water, and 20 mL of water is gradually added to the TTIB. It is then mixed from one to 4 minutes before performing suspension filtration, in which we force large particles to pass through the holes of the filter and take the shape and size of the filter holes in the form of submicron particles. In order to reduce the particles to a smaller size than the holes of the filter, milled particles are used. Mixing of the suspension is continued after this grinding/milling process, until the suspension is ready to use and is then injected into the plasma jet. Titanium oxide deposited by the suspension plasma spray is shown in Fig. 3.2. Heat treatment is then performed on all samples using an electric furnace. The heat treatment is performed by gradually increasing the heat of the samples from 30 to 630 °C for approximately 60 min.

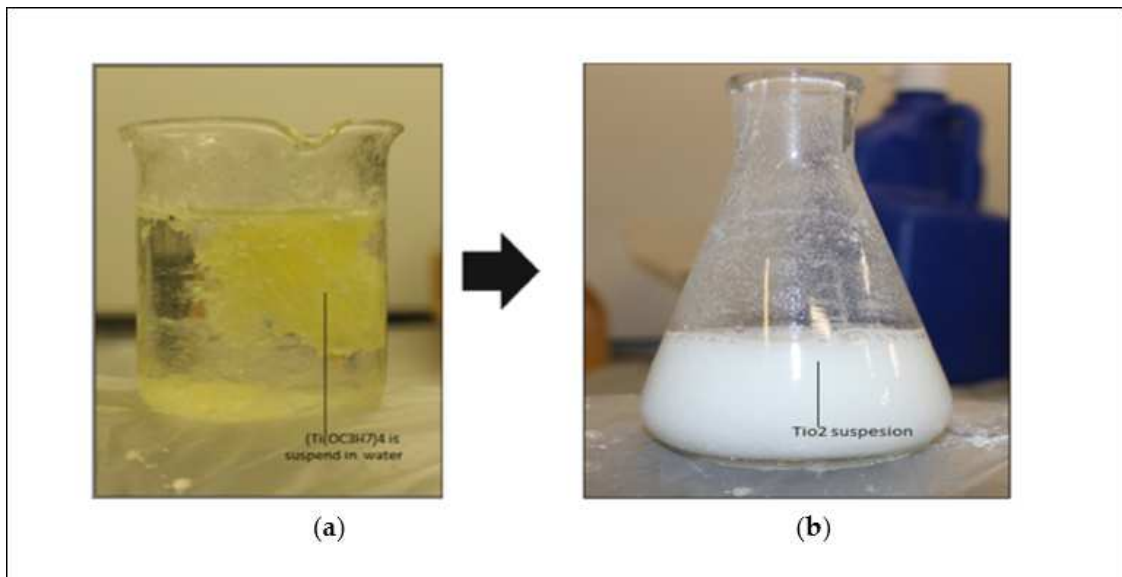


**Figure 3.1** Creation of the titanium hydroxide suspension.  
(a) Before hydrolysis; (b) After hydrolysis.

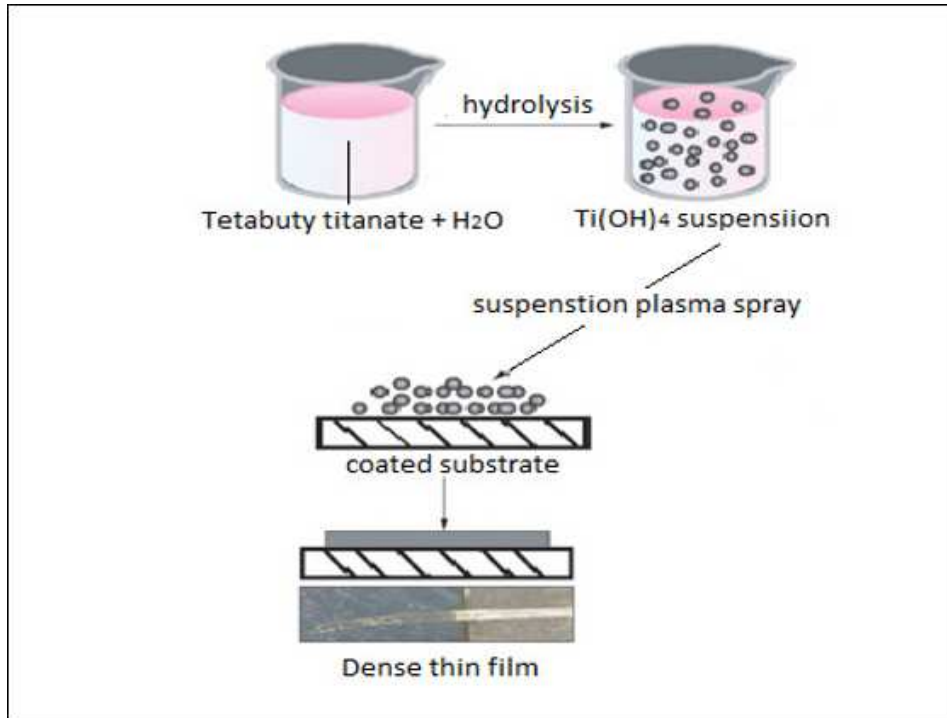


**Figure 3.2** Illustration of the estimated film deposition mechanism in this suspension plasma spray (SPS) process

The equipment used consists of a plasma torch, a DC power feeding system, an air-pressure spray (starter material feed), and a working Ar gas feeding system. The plasma torch is cooled by a water flow around the nozzle. The anode, which has a suspension feeding port at its head, has a constrictor that is 6 mm in diameter. The nozzle shown in Figs. 3.3 and 3.4 explain how this equipment was made for the experiment in this study. In order to promote the vaporization of the starting material and to raise the temperature of titanium particles, Ar was used as the working gas. Mass flow rate of the gas was fixed at 5–10 SLM, and the discharge current was fixed at 50–60 A. The titanium hydroxide (Ti(OH)<sub>4</sub>) suspension submicron particles were suspended in water.

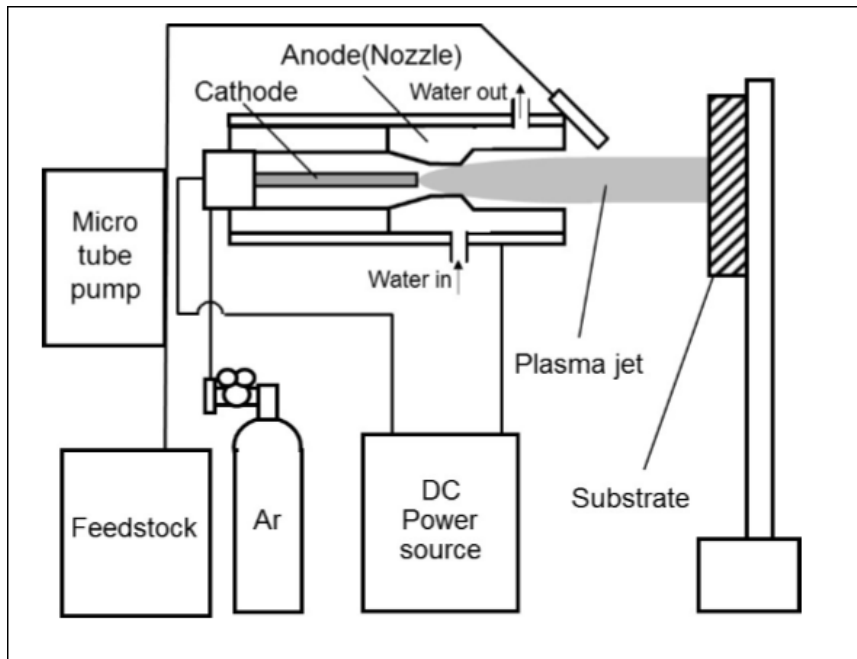


**Figure 3.3** Schematic diagram of the SPS equipment



**Figure 3.4** Plasma jet generated by our thermal spray equipment

### 3.2.2 Plasma spray parameter

Plasma Spray Parameters Titanium oxide deposited by suspension plasma spraying is shown in Table 3.1. The anode, which has a suspension feeding port at its head, has a constrictor that is 6 mm in diameter. The nozzle shown in Fig 3.4 demonstrates how this equipment was configured for the experiment in this study. The anode is 450 mm in length and 20 mm in width.

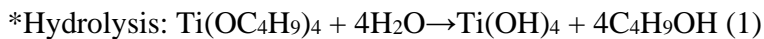
**Table 3. 1:** Suspension plasma spray parameters used to deposit the TiO<sub>2</sub> coatings in the present study.

Process parameter	Initial spray parameters: experimental 1-5
Sandblasting realized	Always
Working gas	Ar
Working gas flow rate, L/min	5-15
Spray distance, mm Out side	100-150
Discharge condition, A	60 - 50
Suspension liquid	water
Feedstock ml	Ti(OC <sub>4</sub> H <sub>9</sub> ) <sub>4</sub> diluted in water 22ml (suspension)*
Suspension composition	Ti(OH) <sub>4</sub> + O <sub>2</sub> → TiO <sub>2</sub> + H <sub>2</sub> O
Suspension feed rate, ml/min	11
Feedstock nozzle injector diameter, mm	0.4
Deposition distance, mm	60-80
Static pressure in suspension container, Mpa	0.25
Substrate, mm	SUS304 (20×20×3)
Deposition time, min	2-3

\*Created by hydrolysis of titanium tetra iso butoxide (TTIB, Ti(OC<sub>4</sub>H<sub>9</sub>)<sub>4</sub>) (Volume ratio of TTIB/H<sub>2</sub>O=2/20)

### 3.2.3 Suspension Preparation

Ethanol has solvent properties and is a versatile solvent, miscible with water and titanium tetra-butoxide among many other materials. However, it is expensive. One way to solve the problem of cost is to use a starting material that does not require ethanol and which uses only distilled water. In this process, the reaction between the alkoxide precursor and the desired amount of water occurred in an anhydrous alcohol medium. The hydrolysis and condensation reactions can be summarized as follows:;



\*Polymerization and crystallization (in the plasma jet and on the substrate):



It is difficult to inject or spray the suspension before the filtration process because of the size of the particles. Therefore, it is necessary to use equipment to facilitate mixing titanium oxide with water. The equipment consists of a filter funnel, a mixer, and a special container (mortar and pestle), which is used for crushing, grinding, and mixing, as shown in Fig. 3.5. Then begins the process of mixing for one to four minutes before the commencement of suspension filtration in which we force large particles to pass through the holes of the filter and take the shape and size of the holes to form of submicron particles. In order to obtain a smaller particle size than the holes of the filter, we use the milled particles, and mix the suspension after this process until the suspension is ready for use. At this point, it is injected into the plasma jet.

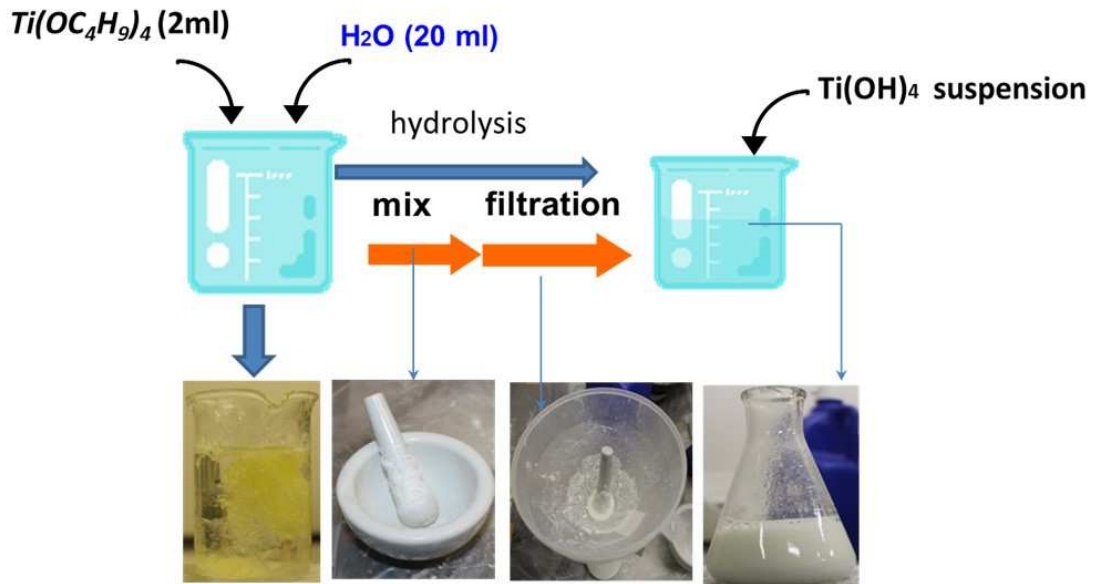


**Figure 3.5** Procedure of fine particles dispersed suspension.

### 3.2.4 Injection Method

A radial injection of the suspension feedstock was made by using two different modes: (i) an internal injection mode (Fig. 3.6 a) using an airbrush atomization feeding system, which was 0.4 mm in diameter in Table 1, and an internal port 6 mm in diameter; an external injection mode (Fig. 3.6 b) using the same system, where the suspension is first atomized and then injected into the plasma jet.

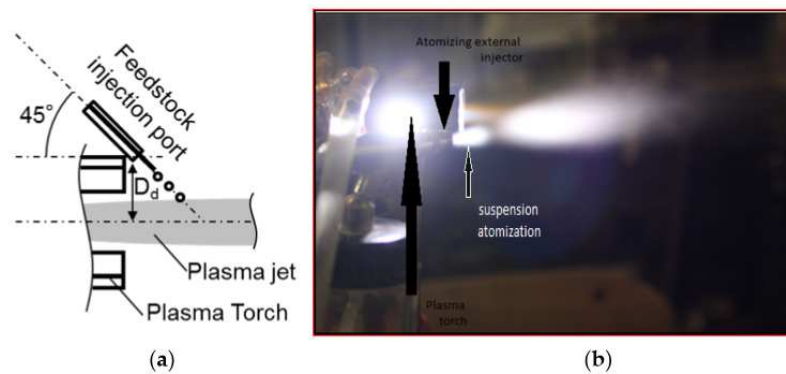


**Figure 3.6** Configuration of the suspension plasma spray torch.

(a) Illustration of the feedstock injection port; (b) Appearance of the plasma jet.

### 3.3 Results and Discussion

#### 3.3.1 SPS Titanium Oxide Film

The coated samples before heat treatment seemed to be in an amorphous phase (Fig. 3.7). When the deposition was performed with a low substrate temperature, the starting material did not have enough mobility to form a crystalline structure. Following that, heat treatment was conducted on all of the titanium oxide films that were deposited on the substrate. The films were heated gradually from 30 to 630 °C with a temperature increase of 10 °C·min<sup>-1</sup> for approximately 60 min. In respect to the XRD patterns of the heat treated films, anatase crystalline peaks appeared for all samples and became sharper by increasing distances from  $d = 60$  mm to 80 mm. Fig. 3.8 shows the XRD pattern of the samples deposited at 80 mm, 60 mm deposition distance. At 80 mm in deposition distance, the starting material heating time was longer than that of the 60 mm sample. Therefore, the quantity of deposited particles at 80 mm was thought to be higher than the quantity of the 60 mm sample. From these results, it was proven that crystallization of the titanium films occurred during heat treatment.

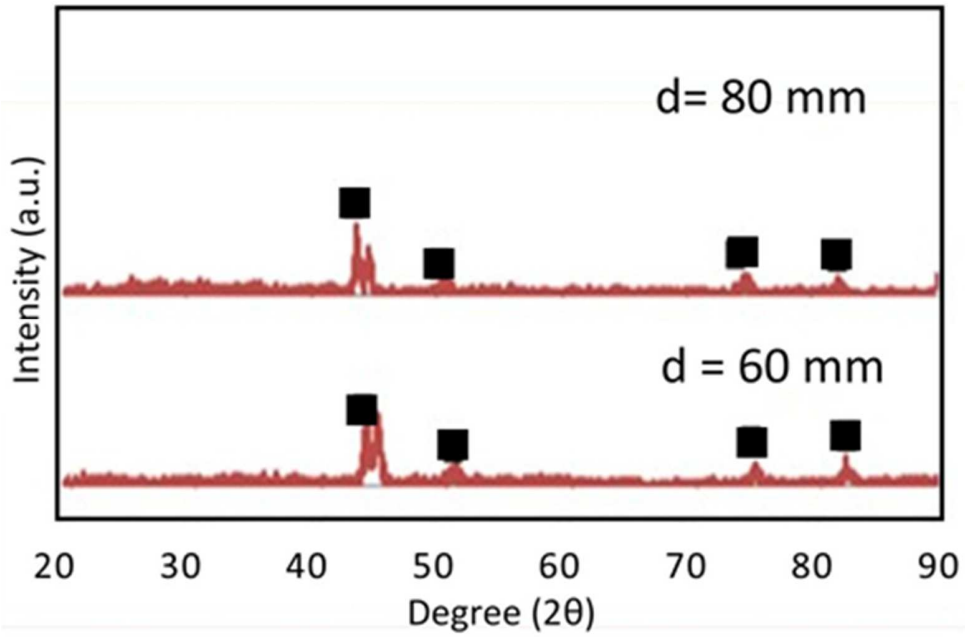


**Figure 3.7** XRD patterns of SPS films before heat treatment. ( $d$  = deposition distance,  $\blacksquare$ : Fe (substrate)).

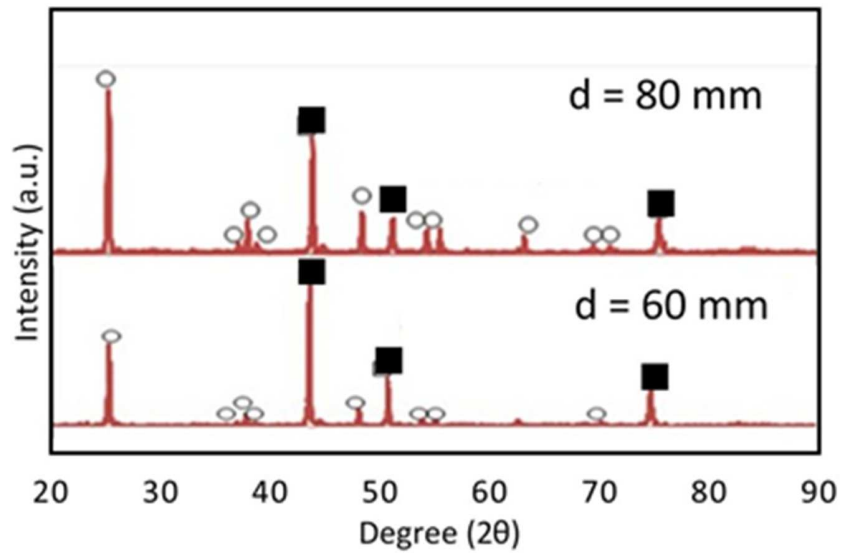
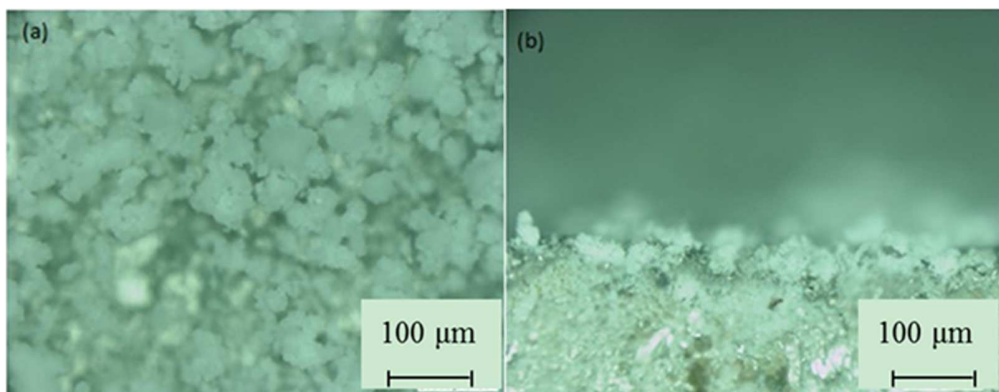


**Figure 3.8** XRD patterns of SPS films after heat treatment ( $d$  = deposition distance,  $\circ$ : Anatase,  $\blacksquare$ : Fe (substrate)).

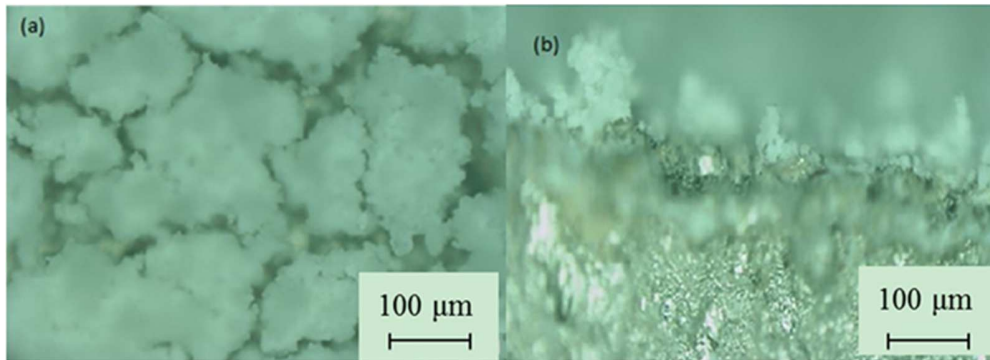
The top-surface and cross-section micrographs of suspension sprayed coating using differing distances are shown in Figs 3.9 and 3.10. The microstructural investigations revealed that the suspension plasma coating presented a morphology, which was caused by the way that the suspension was injected into the plasma jet. The coating, in the case of 60 mm in spray distance ( $d = 60$  mm), is homogeneous and has a grainy structure. The top-surface microscope analyses revealed the presence of agglomerates of grains that are porous, loosely bound, and have a thick film. On the other hand, in the case of  $d = 80$  mm, the film had a grainy and porous structure. The difference in the coatings' microstructure and surface shape can be related to the type of suspension and evolution of the suspension droplets in the plasma jet. According to the particle sizes shown, the film deposition rate dramatically increased with increasing deposition distance.



(a) Top-surface

(b) Cross-section.

**Figure 3.9** Micrographs of suspension sprayed coating deposited at  $d = 60$  mm.



(a) Top-surface

(b) Cross-section.

**Figure 3.10** Micrographs of suspension sprayed coating deposited at  $d = 80$  mm.

### 3.3.2 Photocatalytic Activity of TiO<sub>2</sub> Coating

In order to confirm the photo-catalytic property of the coatings, photo-catalytic activity of the sprayed TiO<sub>2</sub> suspension coating was evaluated by using UV irradiation equipment and measurements of the degradation of an aqueous solution of methylene-blue were conducted (decoloration test) (Fig.3.11) [9]. Fig 3.12 shows the results of the methylene-blue decoloration test in the case of the coating deposition at a distance of  $d = 80$  mm. In both cases of the coatings at the distances of  $d = 60$  mm and 80 mm, decoloration could be confirmed after 1 week of UV irradiation. From these results, it was confirmed that this technique has enough potential to deposit photo-catalytic titanium oxide films.

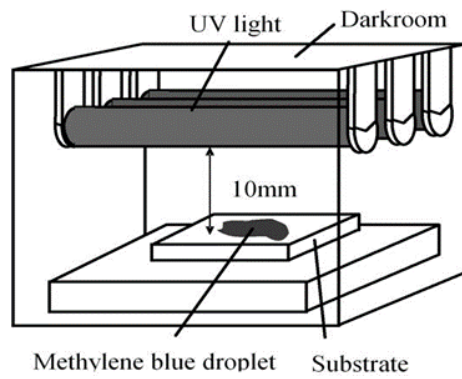


**Figure 3.11** Schematic diagram of the equipment used in methylene-blue decoloration test.

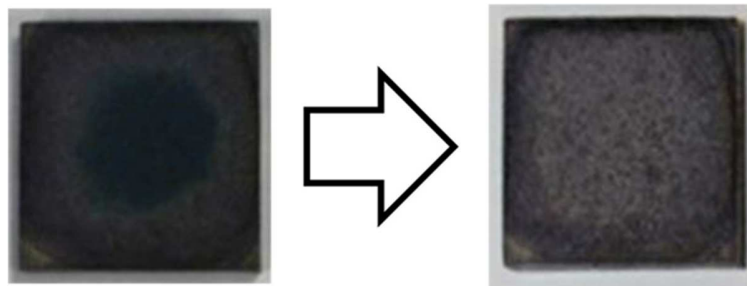


**Figure 3.12** Results of methylene blue decoloration test when the coating was deposited at  $d = 80$  mm ( $d$  = deposition distance).

(a) Before UV irradiation; (b) After 7-day UV irradiation.

### **3.4 Conclusions**

In order to develop low cost materials that can be used for the titanium dioxide film deposition process, deposition of high-rate film using low cost materials was carried out. Thick photo-catalyst film was obtained using an atmospheric suspension plasma spray with spray injectors as a fabrication process. Consequently, anatase film was obtained, and it was confirmed that the anatase films had photo-catalytic properties by using a methylene-blue droplet test and its discoloration test. These results show that this low-cost starting material with atmospheric SPS has the potential for a high rate and low cost, functional, oxide film deposition.

## CHAPTER 4

### Deposition of photo-catalytic TiO<sub>2</sub> film by low power atmospheric suspension plasma spray using Ar/N<sub>2</sub> working gas

**Abstract:** As a photo-catalytic titanium oxide film deposition process, thermal spray is hoped to be utilized practically on the condition that it is relatively easy to deposit anatase rich films. However, because of its high equipment and feedstock powder costs, it is very difficult to introduce thermal spray equipment into small companies. In this study, to develop a low cost thermal spray system, low power atmospheric suspension plasma spray equipment is used with a titanium hydroxide suspension created by hydrolysis of titanium tetra iso butoxide using Ar and N<sub>2</sub> as working gases. For avoiding sedimentation of the hydroxide particles in the suspension, mechanical milling of the suspension was conducted to create colloidal suspension before using it as feedstock. Moreover, an Ultrasonic wave container was used to keep the suspension particles moving while the spray process was conducted. After the film deposition, as for the coating, anatase rich TiO<sub>2</sub> film could be obtained. For characterization of the film, microstructure observation by optical microscope and X-ray diffraction was carried out. Consequently, by creation of colloidal suspension, deposition could be conducted without sedimentation of the hydroxide particles in the suspension during operation. Thus it was proved that the film had enough photo-catalytic property to discolour methylene-blue droplet.

#### 4.1 Introduction

TiO<sub>2</sub> is almost the only material suitable for industrial use at present, and probably in the foreseeable future as well. This is because TiO<sub>2</sub> has the most efficient photo activity, the highest stability, and the lowest cost [50]. Various deposition techniques can deposit thin titanium oxide

films for photo-catalytic applications (anatase–TiO<sub>2</sub>, etc.). For example, sputtering [51], metalorganic chemical vapor deposition (MOCVD) [52], spray pyrolysis [53], the sol-gel process [54], thermal spray [55], and various other methods. However, there are several engineering problems associated with these deposition processes, such as the necessity of vacuum equipment, low deposition rates, deposition time, the requirement of special and costly equipment, as well as feedstock powder [56]. In this study, the purpose is to develop a low cost thermal spray system and low power atmospheric suspension plasma spray equipment. A thermal spray process for photo-catalytic titanium oxide coating was fabricated using 1 kW class Atmospheric Suspension Plasma Spray (ASPS) equipment. Ar and N<sub>2</sub> are mostly used for their mass [57]. Since Ar is a costly gas, a low running cost deposition condition such as using a low cost N<sub>2</sub> dominant working gas was required. Feedstock material was created by hydrolysis of titanium tetra iso butoxide using Ar and N<sub>2</sub> as working gases. In order to avoid sedimentation of the hydroxide particles in the suspension, mechanical milling of the suspension was conducted to create a colloidal suspension before using it as feedstock. A new ultrasonic wave container was used to keep the suspension particles from moving and separated while the spray process was conducted. In this study, in order to develop 1-kw-class ASPS equipment, Ar/N<sub>2</sub> were used as the working gases as well as the photocatalytic titanium oxide film deposition made by using the ASPS equipment which we developed.

## 4.2 Materials and Methods

Fig. 4.1 shows the schematic diagram of the thermal spray equipment used in this study. This equipment consists of a plasma torch, DC power source, feed-stock using ultrasonic supplying system and a working gas supply system. Table 4.1 shows the deposition conditions. The tools used for mixing titanium oxide with water are the same as the one shown in Fig. 3.5. It consists of a micro filter, a mixer, and a special container (mortar and pestle) for mixing as well as for crushing

and grinding. An amount of 2 mL of TTIB is diluted with stable water, and 20 mL of water is added to the TTIB and mixed to form submicron particles. The hydrolysis and condensation reactions can be summarized as follows: \*Hydrolysis:  $\text{Ti}(\text{OC}_4\text{H}_9)_4 + 4\text{H}_2\text{O} \rightarrow \text{Ti}(\text{OH})_4 + 4\text{C}_4\text{H}_9\text{OH}$  (1) \*Polymerization and crystallization (in the plasma jet and on the substrate):  $\text{Ti}(\text{OH})_4 \rightarrow \text{TiO}_2 + 2\text{H}_2\text{O}$  (2). An ultrasonic container uses a ceramic diaphragm vibrating at an ultrasonic frequency (0.5 - 1.7 MHz) to agitate the suspended particles (Fig. 4.2) and raise the temperature of suspension until 70 °C (Fig.4.3) while spray to the plasma jet (Fig.4.4). The spray method was external spray using an airbrush atomization feeding system where the suspension is first atomized and sprayed into the plasma jet (Figs.4.4, 4.5). Three hundred and four 15 × 15 × 1 mm stainless steel plates with polished surfaces were used as the substrate. The substrate was horizontally set on the substrate holder, and the central area of the sample was placed perpendicular to the axial center of the plasma jet. The spray distance (the distance between the nozzle outlet of the plasma torch and the surface of the substrate) was varied from 40 to 120 mm. The deposition time was 15 min. The input power for discharge was fixed at 50 A. Deposition temperature (the substrate temperature during the film deposition) was measured by a thermometer (IGA-CST2, LEC Co. Ltd.). After the titanium oxide film deposition, the microstructures of the films were investigated by X-ray diffraction (CuK $\alpha$ , 40 kV, 100 mA). In order to confirm photocatalytic property of the film, methylene-blue wettability and decoloration test using UV irradiation equipment (Fig. 4.6) were carried out.

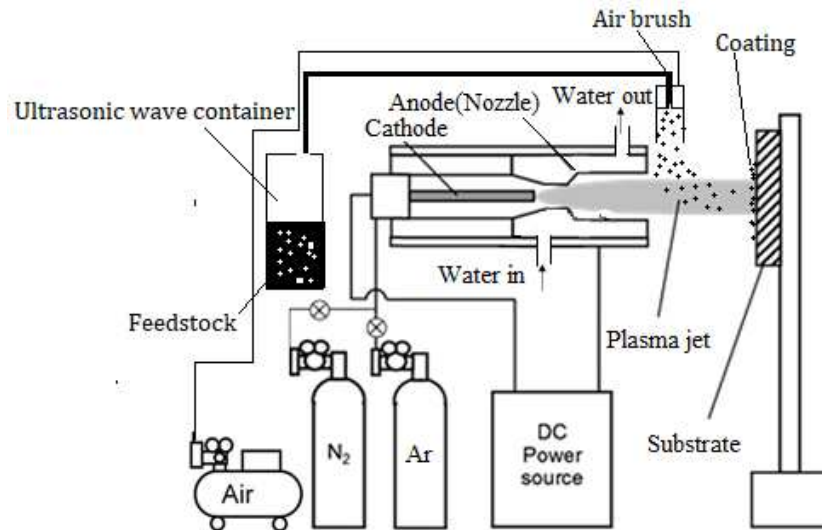


**Figure 4.1** Schematic diagram of the suspension plasma spray (SPS) equipment.

**Table 4.1.** Suspension plasma spray parameters used to deposit the TiO<sub>2</sub> coatings in this study.

Process Parameter	Value
Sandblasting realized	Always
Working gas composition	Ar/N <sub>2</sub>
Working gas flow rate, L/min	Ar 5 /N <sub>2</sub> 0.136
Spray distance, mm	40–120
Discharge current, A	50
Constrictor diameter of plasma torch nozzle, mm	8
Feedstock	Ti(OH) <sub>4</sub> suspension *
Feedstock spray port, diameter, mm	7
Deposition distance, mm	40-80-120

\* Created by hydrolysis of titanium tetra-isobutoxide (TTIB, Ti(OC<sub>4</sub>H<sub>9</sub>)<sub>4</sub>) (volume ratio of TTIB/H<sub>2</sub>O = 8/70).

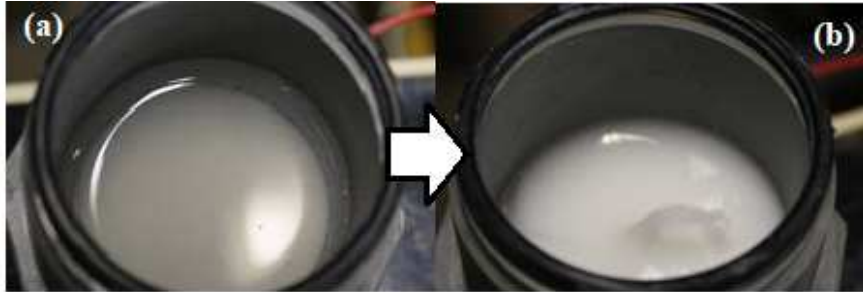


**Figure 4.2** Appearance of the suspension particles located at the bottom of the container

(a) Before agitate the suspended particles

(b) After agitate suspended particles using ultrasonic waves.

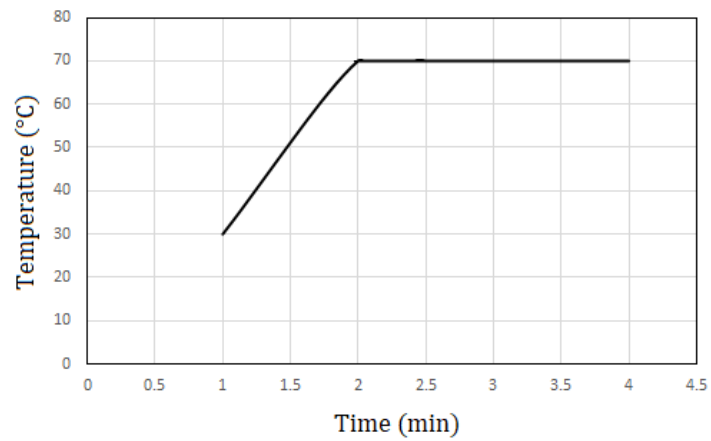


**Figure 4.3** Temperature of liquid (suspension) as a function of time on the frequency of 2.4MHz.

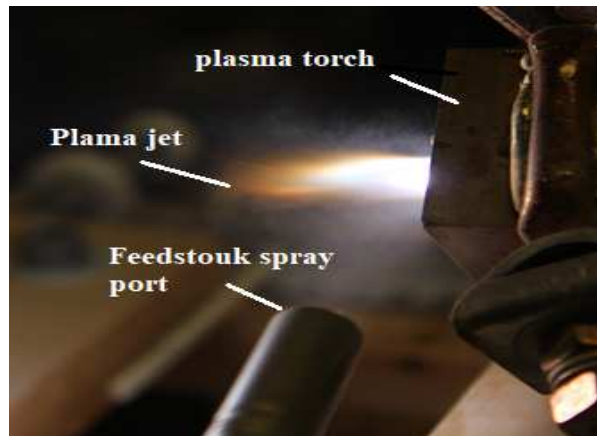


**Figure 4.4** Appearance of the external feedstock sprat to the plasma jet.

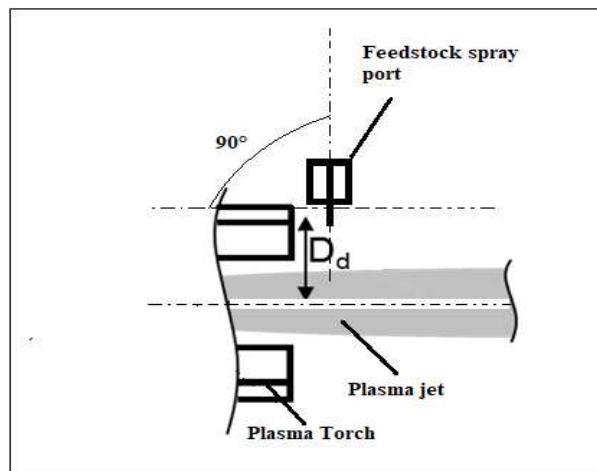


**Figure 4.5** Configuration of the suspension plasma spray torch with Illustration of the feedstock spray port.

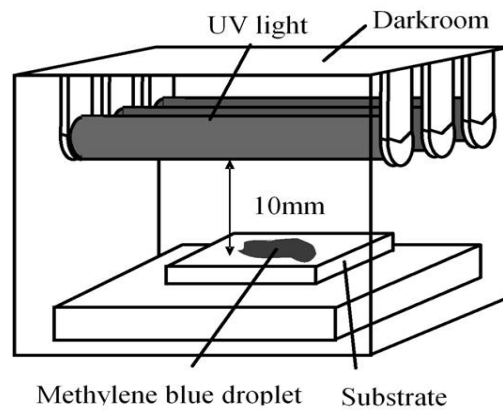


**Figure 4.6** Schematic diagram of the equipment used in methylene-blue decoloration test.

### 4.3 Results

One of the challenges of our research was the problem of  $\text{TiO}_2$  particles settling to the bottom of the spray hopper while spraying. The settling particles had a strong tendency to clog inside of the external sprayer nozzle and reduce the quality of the coating achieved or stop the spray entirely. In order to eliminate clogging, we had to develop a new kind of ultrasonic container to thoroughly suspend  $\text{TiO}_2$  particles, which could be used while spraying Fig. 4.7.

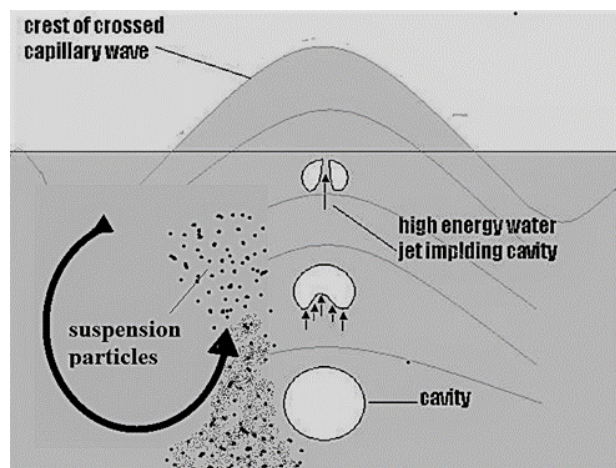


**Figure 4.7** Mechanism of movement for the suspension particles during exposure to the ultrasonic wave.

This container uses ultrasonic vibrations at 0.5 MHz to 2.4 MHz to vibrate the TiO<sub>2</sub> particles in the suspension. Vibration is started at 0.5 MHz and the frequency is increased gradually to 2.4 MHz to prevent excessive splashing. Vibrating at 2.4 MHz ensures uniform suspension of particles. As a side effect of the vibration, the suspension temperature is raised by either friction or cavitation from 40 °C to 70 °C shown in Fig.4.3. Spraying is commenced once the suspension reaches 70 °C.

Substrate temperature: In our experiments, we found that the substrate temperature was quite low, the surface temperature increases with decreasing the spraying distance shown in Fig. 4.8.

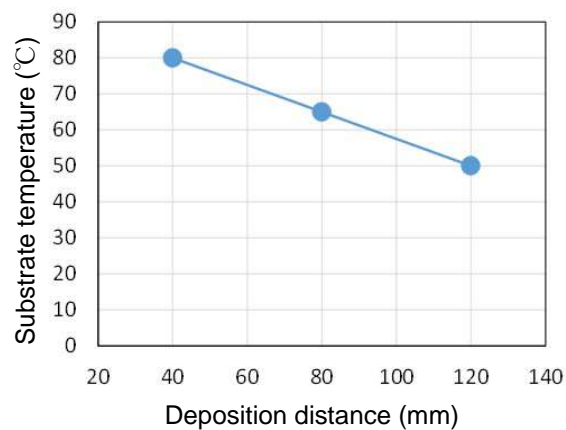


**Figure 4.8** Substrate temperature as a function of distance.

In the case of d=40 mm the substrate temperature was 80°C and d=80 mm was 65°C d=120 was 50°C which enables this coating to be sprayed on materials sensitive to heat damage. Spraying this coating on glass, for example, should present no risk of damage. Despite the high temperature of the plasma jet, due to the effect of heat transfer when the suspension is aerosolized, the temperature at the surface of the substrate is significantly reduced. In our previous study, it was discovered that the addition of N<sub>2</sub> increased the thermal energy of the Ar plasma jet. However, in the previous study, N<sub>2</sub> was used at a rate of 2.5L per minute, whereas in this study N<sub>2</sub> was used at a rate of 0.1L per minute.

In general, when working with Ar plasma jets, the thermal energy increases with increased Ar working gas flow rate. However, in this case, the thermal energy of the jet increases as a result of the working gas being a mixture of Ar and N<sub>2</sub>. This is critical as high temperature is needed in order to phase change the TiO<sub>2</sub> particles from the amorphous phase to the anatase phase without damage the substrate. By using this Ar/ N<sub>2</sub> mixture, a high temperature plasma jet was able to be achieved. In general, when working with Ar plasma jets, the thermal energy increases with increased Ar working gas flow rate. This is critical as high temperature is needed in order to change the TiO<sub>2</sub> particles from the amorphous to the anatase phase, but not so hot as to damage the substrate. By using this Ar / N<sub>2</sub> mixture, it was possible to achieve high thermal energy at the front of the plasma jet, but lower the energy near the substrate, allowing for low substrate temperature.

Although low substrate temperature usually impedes photo-catalytic film, excellent photo-catalytic film was still obtained when spraying at 40mm shown in Fig. 4.9.

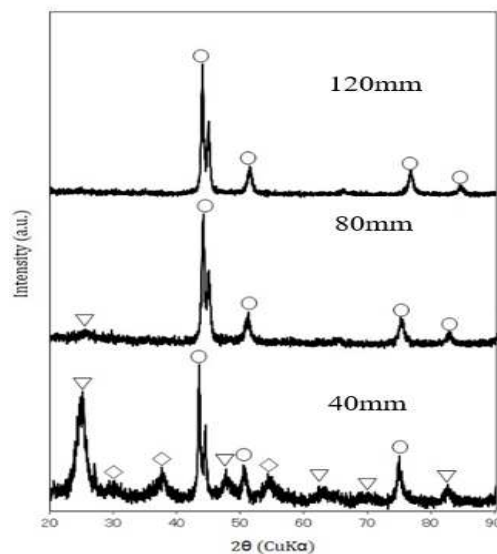


**Figure 4.9** XRD patterns of the samples. (Δ: anatase, ◇: rutile, ○: Fe(substrate)).

XRD patterns of the films deposited at the different deposition distance using. A white color film with smooth surface was obtained with deposition distance of 40 mm. And also, a white color film with coarse surface was deposited with deposition distance of 80 mm. According to the XRD results, though well crystallized anatase and rutile were included in the film deposited with deposition distance of 40 mm, the degree of crystallinity of the film decreased with increasing deposition distance. Finally, amorphous TiO<sub>2</sub> film was deposited with deposition distance of 120 mm. Good photo-catalytic results were obtained at 40mm. At 120mm however, the coating was amorphous and the plasma jet lacked sufficient thermal energy to effectively provide the substrate with a photocatalytic coating.

Fig. 4.10 shows the optical micro graphs of the surface and fracture cross-section of the titanium oxide film deposited sample on the condition of 40 mm. As shown in this figure, a porous structure film was deposited. On the conditions of 40 and 80 mm, films with almost the same microstructure were deposited. The film with almost uniform thickness distribution could be obtained on any conditions. Furthermore, this film had enough photo-catalytic property to decolor the methylene blue perfectly by 20 h ultraviolet irradiation Fig. 4.11.

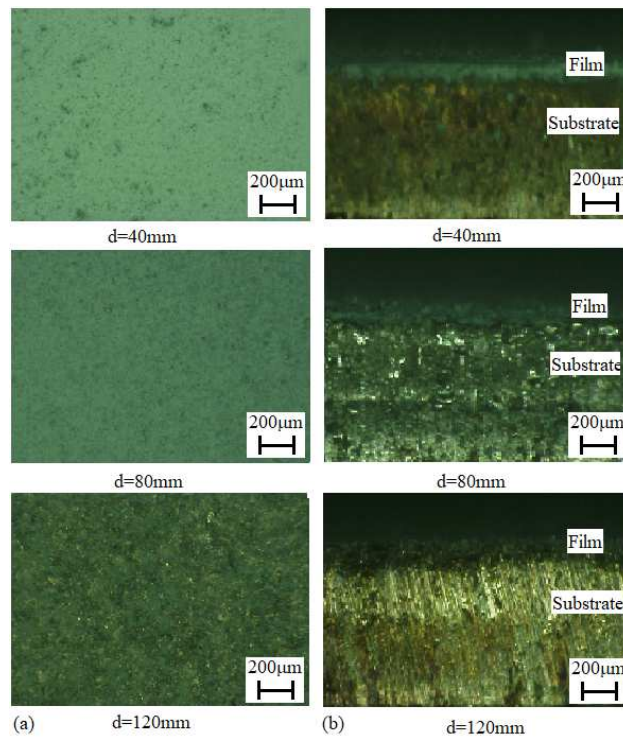


**Figure 4.10** Optical micrographs of the cross sections and surface morphologies of the titanium oxide films deposited on all distance. (a) Surface morphology (b). Cross-section.

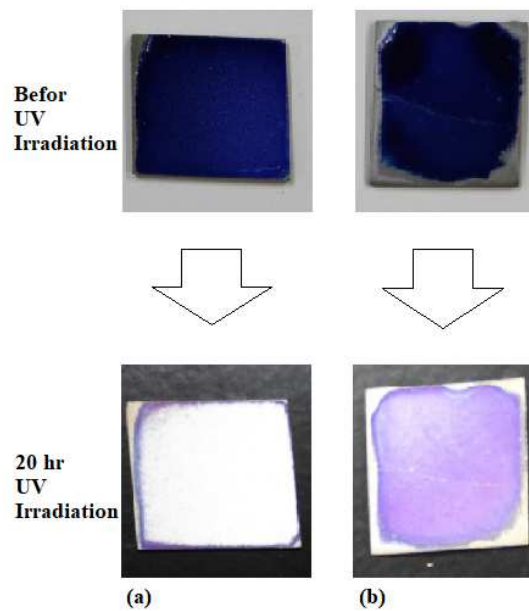


**Figure 4.11** Results of methylene blue decoloration test. (a)  $d = 40\text{ mm}$ . (b)  $d = 80\text{ mm}$ .

In order to measure photocatalytic properties, UV radiation testing and a decoloration test using methylene blue were conducted. By observing the decoloration of the coating, the photocatalytic activity of the film could be conclusively determined in both cases of 40mm and 80mm in spray distance. Although the coated samples were stained with methylene blue, the decoloration of the methylene blue was complete after 20 hours of UV irradiation (Fig. 4.11). From these results, it was proven that highly crystallized film could be deposited in distance of 40mm by perfect vaporization of suspension particles starting material spray to the plasma jet using the newly developed system.

## **4.4 Conclusions**

In order to develop low cost materials that can be used for the titanium dioxide film deposition process, deposition of high-rate film using low cost materials was carried out. Thick photo-catalytic film was obtained using an atmospheric suspension plasma spray with external spray as a fabrication process. Consequently, excellent photo-catalytic film was obtained, and it was confirmed that the anatase films had photo-catalytic properties by using a methylene-blue droplet test and its decoloration test. This new system using ultrasonic waves to spray the suspension particles to the plasma jet proved successful in coating high-quality photo-catalytic film. From these results, this low cost starting material with new atmospheric SPS has the potential for a high rate and low cost, functional, oxide film deposition.

## CHAPTER 5:

### Design and Optimization of Ultrasonic Atomization Plasma Spray System for Coating Photo-Catalytic TiO<sub>2</sub> Thin Films

**Abstract:** The designed ultrasonic atomization plasma spray system (UAPSS) provided a systematic and cost-consistent crystalline structure and stoichiometry. UAPSS seeks to fulfill the need for more precise control of structural, morphological, and optical properties of TiO<sub>2</sub> thin films. In the experiment, an ultrasonic atomizer set to a frequency of 1.7MHz was used to atomize the starting material, ethanol titanium tetra butoxide. The carrier gas was Ar and its flow rate was 1.6 L/min. The working gas was Argon, and its flow rate was 3.4 L/min. Deposition distance was varied from 20 to 100 mm and spray time was 15 minutes. TiO<sub>2</sub> thin film including rutile and anatase was deposited. Methylene blue decolorization testing suggests that the deposited TiO<sub>2</sub> film has effective photo-catalytic properties. The deposited films featured a porous structural morphology and uniform thickness. From these results, the newly designed ultrasonic atomization plasma spray system seems to be highly promising for the rapid fabrication of functional thin films.

#### 5.1 Introduction

Titanium dioxide (TiO<sub>2</sub>) is one of the most researched semiconductor oxides that has revolutionized technologies in the field of environmental purification and energy generation. It has found extensive applications in heterogenous photocatalysis for removing organic pollutants from air and water, and also in hydrogen production from photocatalytic water-splitting [58]. TiO<sub>2</sub> semiconductor is the most popular variety of photocatalyst because of its excellent optical and electrical properties, low cost, non-toxicity, and chemical and thermal stability [59]. TiO<sub>2</sub> has been

used for antibacterial coatings, dye-sensitized solar cells and other applications because of its good photo-catalytic property [60]. In TiO<sub>2</sub> deposition, solution precursor plasma spray (SPPS) has many advantages over other processes, due to its high deposition rate and lack of requirement of a vacuum chamber unlike in other processes. However, in conventional SPPS, initial costs and running costs are high because of the customized SPPS equipment commercial feedstock powder required. On the other hand, photovoltaic and dye-sensitized solar technology both require the application of liquids and coatings during the manufacturing process. With most of these substances being very expensive, any losses due to over-spray or quality control problems are minimized with the use of new ultrasonic atomization plasma spray system (UAPSS). An effort to reduce the manufacturing costs of solar cells was made by precise control and wide range of flow rate (from 0.01l/min to 12l/min). The new UAPSS can be most commonly used in fuel cell coating applications. It provides highly porous and homogeneous coating, efficient combustion and particle heating, controllable drop size, controllable particle velocities and the possibility of using several different gases instead of air as a carrier gas.

On the other hand, the commercial ultrasonic spray nozzle systems can be used for only spray pyrolysis applications as a thermal deposition application while the new UAPSS design can be used for different thermal deposition processes such as plasma spray process. In this study, a low cost thermal spray system for photo-catalytic TiO<sub>2</sub> film deposition was created. Low power atmospheric solution precursor plasma spray (SPPS) equipment based on commercial welding equipment was also created for this study. TTIB, Ti(OC<sub>4</sub>H<sub>9</sub>)<sub>4</sub> was used as feedstock for titanium oxide film deposition. Using this new UAPSS and material, photo-catalytic film was successfully deposited.

## 5.2 Experimental

Figures 5.1 and 2,3 show the schematic diagram and 3D view of the UAPSS ,SPPS equipment used in this study. This equipment consists of a plasma torch, DC power source, and a feedstock supply system which utilizes an ultrasonic atomization plasma spray system. The ultrasonic atomization plasma spray system consists of a ceramic diaphragm vibrating at an ultrasonic frequency (1.7 MHz), micro pump, feedstock, Ar carrier gas control flow rate channel, plasma feed nozzle, cooling unit, and a material feed nozzle shown in Fig 5.2.

For the ultrasonic atomization plasma spray feeding system operation the liquid flows through the micro pump unit, then passes through the dispersion liquid delivery tube to the automation container unit. The liquid drops as droplets on the ceramic diaphragm, a piezoelectric ceramic disc that converts electrical energy to mechanical energy in the form of vibration. The disc oscillates in presence of electrical current at ultrasonic frequencies. As the frequency of oscillation of the plate increases, wave crests form and very minute droplets of liquid have enough energy to break the surface tension and disperse as mist. The mist is moved into the plasma jet by air compressor pressure shown in Fig 5.1.

The working gas was Argon, and its flow rate was 3.4 L/min. The carrier gas was Ar and its flow rate was 1.6 L/min. Film deposition was conducted using Ar working gas, 20V/ 70A input power and 20-100mm deposition distance shown in Table 5.1. The TTIB undergoes a nucleophilic substitution reaction with ethanol, in which the butoxide group substitutes for the hydroxyl on ethanol, forming Ethyl Butyl Ether and Titanium Hydroxide. In equation 1, ethanol is the nucleophile, in the reaction of TTIB and water, water is the nucleophile. The reaction of TTIB with water is referenced in Chapter 4. Water is a stronger nucleophile than ethanol, thus the reaction of TTIB with water proceeds more quickly than reaction TTIB with ethanol. This is the reason why

titanium hydroxide is evolved. The reaction of TTIB with ethanol can be summarized as shown in eq. (1).

Ether and Titanium Hydroxide, The reaction can be summarized as shown in eq. (1).

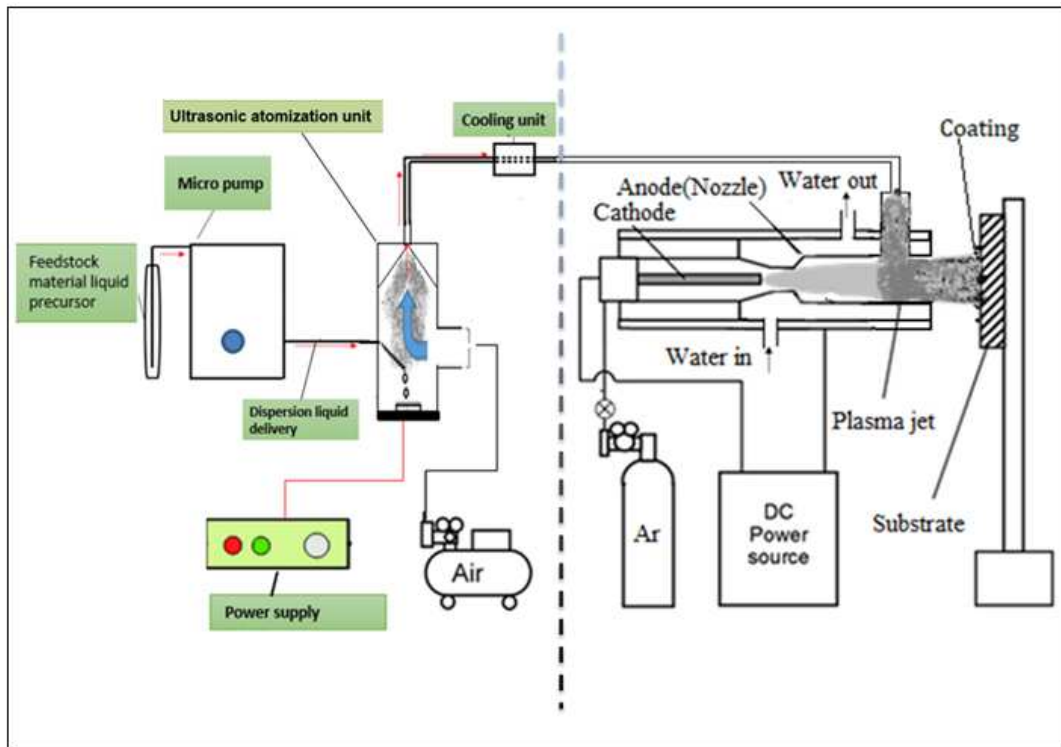


**Figure 5.1** Schematic diagram of SPPS,UAPSS equipment.

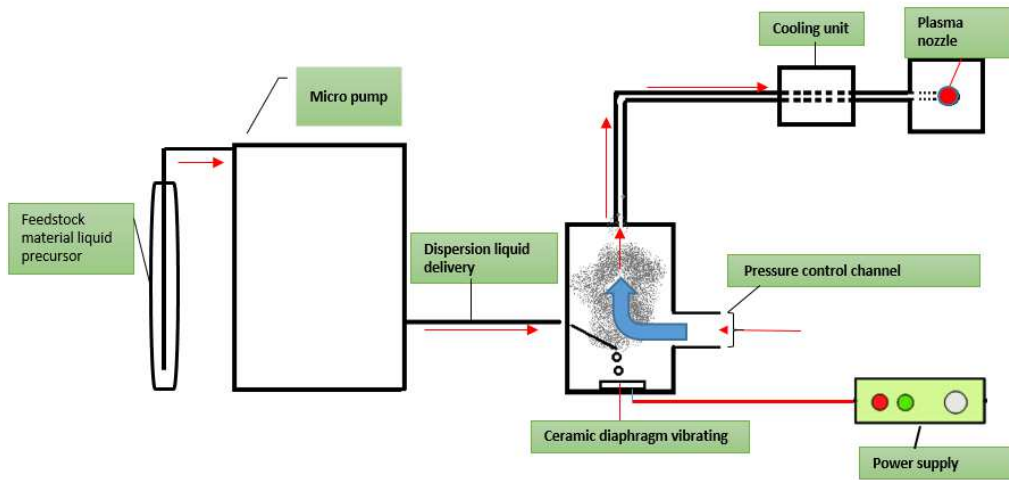


**Figure 5.2** Ultrasonic atomization plasma spray feeding system operation

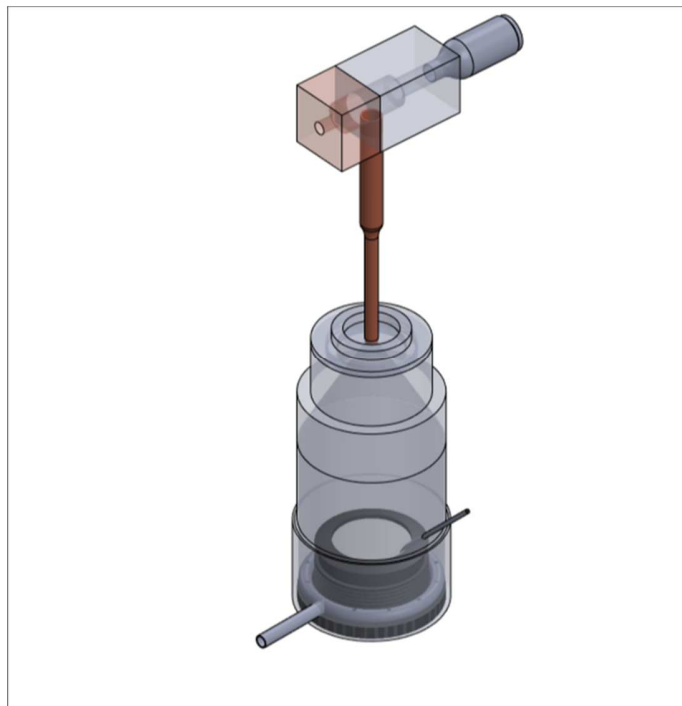


**Figure 5.3** 3D view of UAPSS design

**Table 5.1.** Solution plasma spray parameters used to deposit the TiO<sub>2</sub> coatings in this study.

\* Created by titanium tetraisobutoxide (TTIB, Ti(OC<sub>4</sub>H<sub>9</sub>)<sub>4</sub>) (volume ratio of TTIB/C<sub>2</sub>H<sub>5</sub>OH = 2/20).

Process Parameter	Value
Sandblasting realized	Always
Working gas	Ar
Working gas flow rate, L/min	5
Carrier gas	Air
Carrier gas flow rate, L/min	1.6
Ultrasonic atomizer set MHz	1.7
Deposition distance, mm	20,40,60
Discharge current, A	70
Constrictor diameter of plasma torch nozzle, mm	15
Feedstock	C <sub>2</sub> H <sub>5</sub> OH diluted TTIB* solution
Feedstock spray port, diameter, mm	7

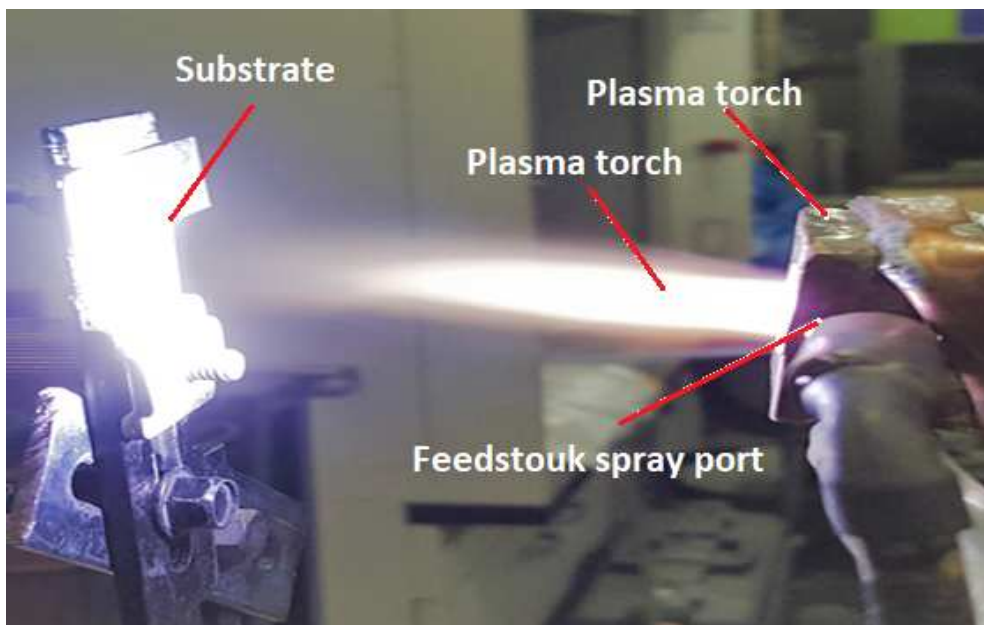


**Figure 5.4** Appearance of the internal feedstock spray to the plasma jet

## 5.3 Results

Photovoltaic and dye-sensitized solar technology both require the application of liquids and coatings during the manufacturing process. As most of these substances are very expensive, any losses due to overspray or quality control problems are minimized with the use of this newly-designed ultrasonic feeding system. By controlling as little as a few millimeters of expensive catalyst material, a thin film of TiO<sub>2</sub> with rutile and anatase was deposited using the new UAPSS. However, several factors affect the ability of a liquid to be atomized. These include viscosity, solids content, miscibility of components, and the specific dynamic behavior of the liquid. There are no hard-and-fast rules governing a liquid's atomizability using ultrasonics. Some liquids that seem easy to atomize at first can prove difficult, while others that seem impossible actually perform well. There are, however, guidelines that offer a good indication of the probability for success. Liquids can be categorized as follows: pure, single component liquids (water, alcohol, bromine, etc.), true solutions (salt water, polymer solutions, etc.), and mixtures with undissolved solids (coal slurries, polymer beads/water, silica/ alcohol, suspensions, etc.). For solutions, the only factor limiting atomizability is viscosity.

In general, the upper limit of viscosity in the tested mixture is 0.0358 Pa·s., per Table 5.2. According to the XRD results, the degree of crystallinity of the film decreased with increasing deposition distance (Fig. 5.6), despite the inclusion of well-crystallized anatase and rutile in the film. Crystallized rutile was included in the film deposited at a distance of 20 mm, and crystallized anatase was included in the film deposited at a distance of 40mm. For the deposition distance of 60 mm, both crystallized anatase and rutile were included in the film. Fig. 5.5 shows the optical micrographs of the surface and the fracture cross-sections of the titanium dioxide film deposited

sample for the distances of 20 mm, 40 mm, and 60 mm. The surfaces are porous and have uniform thickness and distribution at almost the same deposition distances due to the fine size of the ultrasonically atomized particles. A coated sample was stained with methylene blue, and after 24 hours of UV irradiation the decolorization was complete, with measurements confirming degradation at spray distances of 20mm, 40mm, and 60mm (Fig. 5.12). The methylene blue decolorization testing suggests that the deposited TiO<sub>2</sub> film has effective photo-catalytic properties.

**Table 5.2** Properties of tested viscosity of TTiB, Ethanol mixture in deferent volume ratio of TTiB/C<sub>2</sub>H<sub>5</sub>OH

	<b>TTiB, Eth Mixture</b>	<b>Viscosity, Pa.s</b>
<b>1</b>	5% TTiB	0.0325
<b>2</b>	10% TTiB	0.0358
<b>3</b>	15% TTiB	0.0374
<b>4</b>	20% TTiB	0.0375
<b>5</b>	25% TTiB	0.0388

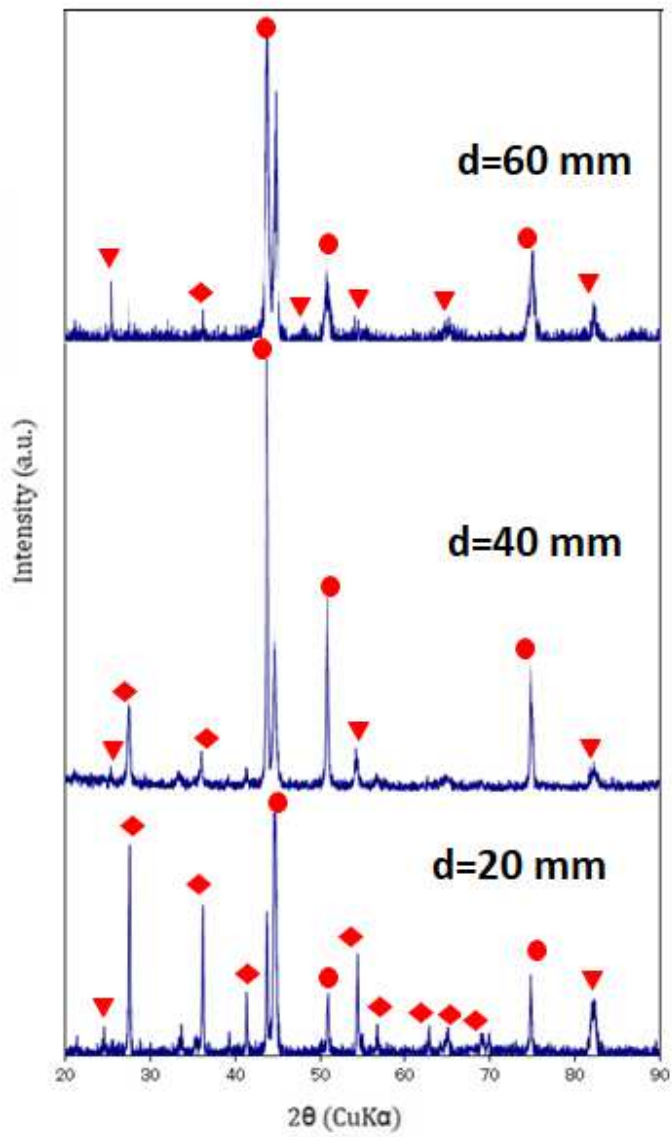


**Figure 5.5** XRD patterns of the samples. ( $\nabla$  : anatase,  $\diamond$  : rutile,  $\circ$  : Fe(substrate))

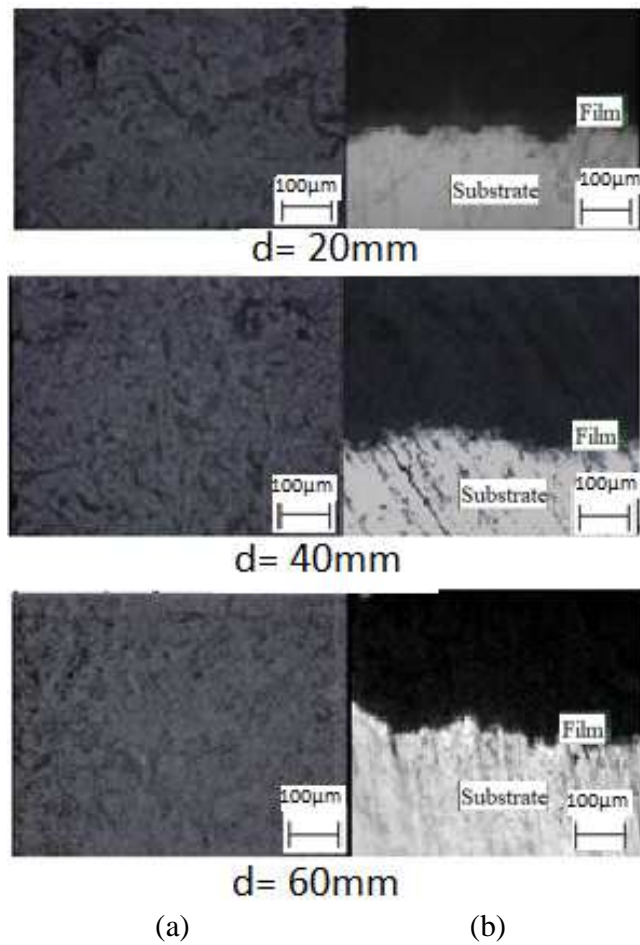


**Figure 5.6** Optical micrographs of the cross sections and surface morphologies of the titanium oxide films deposited at all distances. (a) Surface morphology, (b) Cross-section.

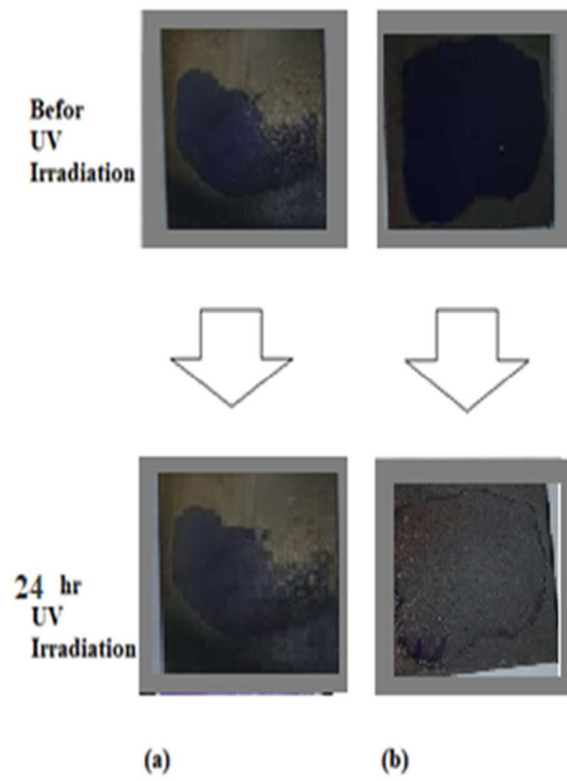


**Figure 5.7** Results of methylene blue decoloration test.  
(a)  $d = 20\text{mm}$  (b)  $d = 60\text{mm}$

## 5.4 Conclusion

In order to develop a low-cost titanium oxide film deposition process using thermal spray equipment, the new UAPSS was designed and oxide film deposition was carried out. Consequently, the following conclusions were obtained.

1. High-rate film using low cost materials was carried out.
2. Thin photo-catalyst film was obtained using an atmospheric SPPS with internal spray as a fabrication process.
3. Precise control of structural, morphological, and optical properties of methods for depositing titanium dioxide, and thin films can be obtained using new UAPSS.
4. Excellent photocatalytic film was obtained, and it was confirmed that the anatase films had photo-catalytic properties by using a methylene-blue droplet test and its discoloration test.
5. The new design system using UAPSS to spray the starting material solution particles to the plasma jet proved successful in coating high-quality photocatalytic film.

## **Chapter 6: Summary and Conclusion**

Development of fabrication processes using suspension and solution plasma spray for titanium oxide photovoltaic was completed for thermal plasma spray applications. The newly designed fabrication process for titanium deposition techniques were studied for different plasma output power, parameters, secondary and different carrier gasses, different flow rates. The new design for deposition of titanium oxide has important parameters for coating output efficiency.

Deposition of high rate films was carried out in order to develop low cost materials for the titanium oxide film deposition process. A fabrication process using an atmospheric suspension plasma spray produced thick photo-catalytic film. After obtaining anatase films, their photo-catalytic properties were obtained using a methylene-blue droplet test and its discoloration test. According to these results, there is potential for a high rate and low cost, functional, oxide film deposition using this low-cost starting material with atmospheric SPS.

This is achievable because of film quality control, film deposition efficiency and the new ultrasonic container which has been designed to utilize this low-cost starting material. Atmospheric suspension plasma spray with external spray produced thick photo-catalytic film. Using a methylene blue droplet test and discoloration test, the photo-catalytic properties of the anatase films were confirmed for the entire design plasma spray fabrication process. High-quality photo-catalytic films were successfully coated using ultrasonic waves to spray the suspension particles to the plasma jet. These results show the possibility for a high rate, low cost and functional oxide film deposition using the new atmospheric SPS.

The new UAPSS was designed and oxide film deposition was carried out in order to develop a low-cost titanium oxide film deposition process using thermal spray equipment. Thus the following conclusions were obtained: deposition of high rate film using low-cost materials. A

fabrication process utilizing atmospheric SPPS with internal spray produced thin photo-catalytic film. Using the new UAPSS, precise control of structural, morphological, and optical properties of methods for depositing titanium dioxide and thin films can be obtained. Excellent photo-catalytic film was obtained, and the photo-catalytic properties of the anatase films were confirmed using a methylene-blue droplet test and its discoloration test. The coating of high-quality photo-catalytic film was successful through the new design system which uses UAPSS to spray the starting material solution particles into the plasma jet. Hence, the present work focused on the preparation of starting material and designing new methods for fabrication of titanium oxide film. The new design was stable for all different deposition processes using different starting materials. These new designs and processes have great potential for the future development of thermal plasma spray technology.

## References

- [1] Lee, Sang Won, et al. "Self-heating characteristics of cobalt ferrite nanoparticles for hyperthermia application." *Journal of Magnetism and Magnetic Materials* 310.2 (2007): 2868-2870.
- [2] Zhang, Sam, et al. "Recent advances of superhard nanocomposite coatings: a review." *Surface and Coatings Technology* 167.2-3 (2003): 113-119.
- [3] Choy, K. L. "Chemical vapour deposition of coatings." *Progress in materials science* 48.2 (2003): 57-170.
- [4] Saparin, G. V., and S. K. Obyden. "Morphologic and cathodoluminescence studies of diamond films by scanning electron microscopy." *Scanning* 17.6 (1995): 337-347.
- [5] Heberlein, J., et al. "Thermal plasma deposition of nanophase hard coatings." *Surface and Coatings Technology* 142 (2001): 265-271.
- [6] Chen, Huang, and C. X. Ding. "Nanostructured zirconia coating prepared by atmospheric plasma spraying." *Surface and Coatings Technology* 150.1 (2002): 31-36.
- [7] Shaw, Leon L., et al. "The dependency of microstructure and properties of nanostructured coatings on plasma spray conditions." *Surface and coatings technology* 130.1 (2000): 1-8.
- [8] Schuegraf, Klaus K. *Handbook of thin-film deposition processes and techniques: principles, methods, equipment, and applications*. Noyes Data Corporation/Noyes Publications, 1988.
- [9] Maya, L., et al. "Gold nanocomposites." *Journal of Vacuum Science & Technology B: Microelectronics and Nanometer Structures Processing, Measurement, and Phenomena* 13.2 (1995): 361-365.
- [10] Onishi, Takashi, et al. "Influence of adding transition metal elements to an aluminum target on electrical resistivity and hillock resistance in sputter-deposited aluminum alloy thin films." *Journal of Vacuum Science & Technology A: Vacuum, Surfaces, and Films* 14.5

- (1996): 2728-2735.
- [11] Karthikeyan, J., et al. "Plasma spray synthesis of nanomaterial powders and deposits." *Materials Science and Engineering: A* 238.2 (1997): 275-286.
- [12] Xie, Liangde, et al. "Identification of coating deposition mechanisms in the solution-precursor plasma-spray process using model spray experiments." *Materials Science and Engineering: A* 362.1-2 (2003): 204-212.
- [13] Nolan, M. G., et al. "One step process for chemical vapour deposition of titanium dioxide thin films incorporating controlled structure nanoparticles." *Thin Solid Films* 515.4 (2006): 1956-1962.
- [14] Hwang, Heewon, et al. "Di (2-pyridyl) ketone stabilized titanium dioxide nanoparticles for the room temperature processed electron transporting layer in organic photovoltaics." *Organic Electronics* 28 (2016): 281-286.
- [15] Chaturvedi, Amita, et al. "Growth of anatase and rutile phase TiO<sub>2</sub> nanoparticles using pulsed laser ablation in liquid: influence of surfactant addition and ablation time variation." *Applied Surface Science* 396 (2017): 303-309.
- [16] Ando, Yasutaka, et al. "High Rate Zinc Oxide Film Deposition by Atmospheric TPCVD Using Ar/Air Plasma Jets." *Transactions of JWRI* 37.1 (2008): 33-37.
- [17] Heberlein, Joachim Viktor, Pierre Fauchais, and Maher I. Boulos. *Thermal spray fundamentals: From powder to part*. Springer, 2014.
- [18] Ando, Yasutaka, et al. "High Rate Zinc Oxide Film Deposition by Atmospheric TPCVD Using Ar/Air Plasma Jets." *Transactions of JWRI* 37.1 (2008): 33-37.
- [19] Kassner, Holger, et al. "Application of suspension plasma spraying (SPS) for manufacture of ceramic coatings." *Journal of thermal spray technology* 17.1 (2008): 115-123.
- [20] Karthikeyan, J., et al. "Preparation of nanophase materials by thermal spray processing of

- liquid precursors." *Nanostructured Materials* 9.1-8 (1997): 137-140.
- [21] Karthikeyan, J., et al. "Nanomaterial powders and deposits prepared by flame spray processing of liquid precursors." *Nanostructured Materials* 8.1 (1997): 61-74.
- [22] Karthikeyan, Jeganathan, et al. "Nanomaterial deposits formed by DC plasma spraying of liquid feedstocks." *Journal of the American Ceramic Society* 81.1 (1998): 121-128.
- [23] Padture, N. P., et al. "Towards durable thermal barrier coatings with novel microstructures deposited by solution-precursor plasma spray." *Acta materialia* 49.12 (2001): 2251-2257.
- [24] Parukuttyamma, Sujatha D., et al. "Yttrium aluminum garnet (YAG) films through a precursor plasma spraying technique." *Journal of the American Ceramic Society* 84.8 (2001): 1906-1908.
- [25] Bouyer, E., et al. "Thermal plasma chemical vapor deposition of Si-based ceramic coatings from liquid precursors." *Plasma Chemistry and Plasma Processing* 21.4 (2001): 523-546.
- [26] Wikipedia, "1973 oil crisis". [http://en.wikipedia.org/wiki/1973\\_oil\\_crisis](http://en.wikipedia.org/wiki/1973_oil_crisis). web 28 February 2013.
- [27] Herzog, Antonia V., Timothy E. Lipman, and Daniel M. Kammen. "Renewable energy sources." *Encyclopedia of Life Support Systems (EOLSS)*. Forerunner Volume- 'Perspectives and Overview of Life Support Systems and Sustainable Development (2001).
- [28] Landstr, Dudweiler, "The design and functionality of a solar chimney electric power plant." LAB LAMBER Academic Publishing Gmbh & Co. KG, ( 2011).
- [29] Ando, Yasutaka. "Titanium oxide film deposition on acrylic resin by atmospheric TPCVD." *IEEE Transactions on Plasma Science* 37.11 (2009): 2202-2206.
- [30] Luque, Antonio, and Steven Hegedus, eds. *Handbook of photovoltaic science and engineering*. John Wiley & Sons, 2011.
- [31] Ali, Riyaz Ahmad Mohamed, and Nafarizal Nayan. "Fabrication and analysis of dye-

- sensitized solar cell using natural dye extracted from dragon fruit." *International Journal of Integrated Engineering* 2.3 (2010).
- [32] Hashimoto, Kazuhito, Hiroshi Irie, and Akira Fujishima. "TiO<sub>2</sub> photocatalysis: a historical overview and future prospects." *Japanese journal of applied physics* 44.12R (2005): 8269.
- [33] Eufinger, K., et al. "TiO<sub>2</sub> thin films for photocatalytic applications in *Thin Solid Films: Process and Applications*." (2008): 189-227.
- [34] Pawlowski, Lech. *The science and engineering of thermal spray coatings*. John Wiley & Sons, 2008.
- [35] Gérard, Barbezat. "Application of thermal spraying in the automobile industry." *Surface and Coatings Technology* 201.5 (2006): 2028-2031.
- [36] Barbezat, G., and G. Wuest. "The advantages of the plasma spray process for the coating of cylinder bores on AlSi cast alloy in automotive industry." *Institute of Materials, Surface Modification Technologies XI(UK)*, (1998): 223-233.
- [37] Bartnik, Z., et al. "Improvements in Manufacturing Technology of Wear Resistant Plasma Sprayed Cr sub 2 O sub 3 Coatings." *Thermal Spray: International Advances in Coatings Technology* (1992): 983-993.
- [38] Batalov, M., Kosikowski, D. and Mohanty, P.S. (2005). *Design, fabrication and characterization of sprayed thermopiles* in *Proceedings of the International Thermal Spray Conference '05*, CD-Rom, ISBN 3-87155-793-5, DVS-Verlag, Düsseldorf, Germany.
- [39] Sima, C., et al. "Properties of TiO<sub>2</sub> thin films deposited by RF magnetron sputtering." *Journal of optoelectronics and advanced materials* 9.5 (2007): 1446-1449.
- [40] Cimpean, Anisoara, et al. "Effects of LP-MOCVD prepared TiO<sub>2</sub> thin films on the in vitro behavior of gingival fibroblasts." *Materials Chemistry and Physics* 125.3 (2011): 485-492.
- [41] Perednis, Dainius, and Ludwig J. Gauckler. "Thin film deposition using spray pyrolysis."

- Journal of electroceramics 14.2 (2005): 103-111.
- [42] Kajitvichyanukul, Puangrat, Jirapat Ananpattarachai, and Siriwan Pongpom. "Sol-gel preparation and properties study of TiO<sub>2</sub> thin film for photocatalytic reduction of chromium (VI) in photocatalysis process." *Science and Technology of Advanced Materials* 6.3-4 (2005): 352.
- [43] Zhao, Xiaobing, et al. "In vitro bioactivity of plasma-sprayed TiO<sub>2</sub> coating after sodium hydroxide treatment." *Surface and Coatings Technology* 200.18-19 (2006): 5487-5492.
- [44] Li, Chang-Jiu, et al. "Phase formation during deposition of TiO<sub>2</sub> coatings through high velocity oxy-fuel spraying." *Materials transactions* 47.7 (2006): 1690-1696.
- [45] Yang, Guan-Jun, et al. "Low temperature deposition and characterization of TiO<sub>2</sub> photocatalytic film through cold spray." *Applied surface science* 254.13 (2008): 3979-3982.
- [46] Yamada, Motohiro, et al. "Cold spraying of TiO<sub>2</sub> photocatalyst coating with nitrogen process gas." *Journal of Thermal Spray Technology* 19.6 (2010): 1218-1223.
- [47] Hadi, A., Hsian Sagr, and Yasutaka Ando. "Development of a Fabrication Process Using Suspension Plasma Spray for Titanium Oxide Photovoltaic Device." *Coatings* 7.3 (2017): 40.
- [48] Popescu, Simona, et al. "Plasma column and nano-powder generation from solid titanium by localized microwaves in air." *Journal of Applied Physics* 118.2 (2015): 023302.
- [49] Ando, Yasutaka. "Titanium oxide film deposition on acrylic resin by atmospheric TPCVD." *IEEE Transactions on Plasma Science* 37.11 (2009): 2202-2206.
- [50] Hashimoto, Kazuhito, Hiroshi Irie, and Akira Fujishima. "TiO<sub>2</sub> photocatalysis: a historical overview and future prospects." *Japanese journal of applied physics* 44.12R (2005): 8269.
- [51] Sima, C., et al. "Properties of TiO<sub>2</sub> thin films deposited by RF magnetron sputtering." *Journal of optoelectronics and advanced materials* 9.5 (2007): 1446-1449.

- [52] Cimpean, Anisoara, et al. "Effects of LP-MOCVD prepared TiO<sub>2</sub> thin films on the in vitro behavior of gingival fibroblasts." *Materials Chemistry and Physics* 125.3 (2011): 485-492.
- [53] Oja, Ilona, et al. "Properties of TiO<sub>2</sub> films prepared by the spray pyrolysis method." *Solid State Phenomena*. Vol. 99. Trans Tech Publications, 2004.
- [54] Hench, Larry L., and Jon K. West. "The sol-gel process." *Chemical reviews* 90.1 (1990): 33-72.
- [55] Zhao, Xiaobing, et al. "In vitro bioactivity of plasma-sprayed TiO<sub>2</sub> coating after sodium hydroxide treatment." *Surface and Coatings Technology* 200.18-19 (2006): 5487-5492.
- [56] Ando, Yasutaka, Shogo Tobe, and Hirokazu Tahara. "Photo-catalytic TiO<sub>2</sub> film deposition by atmospheric TPCVD." *Vacuum* 80.11-12 (2006): 1278-1283.
- [57] Sanpo, Noppakun. "Solution precursor plasma spray system." *Solution Precursor Plasma Spray System*. Springer, Cham, 2014. 1-3.
- [58] Nolan, M. G., et al. "One step process for chemical vapour deposition of titanium dioxide thin films incorporating controlled structure nanoparticles." *Thin Solid Films* 515.4 (2006): 1956-1962.
- [59] Hwang, Heewon, et al. "Di (2-pyridyl) ketone stabilized titanium dioxide nanoparticles for the room temperature processed electron transporting layer in organic photovoltaics." *Organic Electronics* 28 (2016): 281-286.
- [60] Chaturvedi, Amita, et al. "Growth of anatase and rutile phase TiO<sub>2</sub> nanoparticles using pulsed laser ablation in liquid: influence of surfactant addition and ablation time variation." *Applied Surface Science* 396 (2017): 303-309.